J. Fluid Mech. (1974), *vol.* 62, *part* 3, *pp.* 465–538
Printed in Great Britain

Convection in the earth's mantle: towards a numerical simulation

By D. P. McKENZIE, J. M. ROBERTS
Department of Geodesy and Geophysics, University of Cambridge
AND N. O. WEISS
Department of Applied Mathematics and Theoretical Physics, University of Cambridge

(Received 22 December 1972 and in revised form 24 September 1973)

Plate tectonics provides a remarkably accurate kinematic description of the motion of the earth's crust but a fully dynamical theory requires an understanding of convection in the mantle. Thus the properties of plates and of the mantle must be related to a systematic study of convection. This paper reviews both the geophysical information and the fluid dynamics of convection in a Boussinesq fluid of infinite Prandtl number. Numerical experiments have been carried out on several simple two-dimensional models, in which convection is driven by imposed horizontal temperature gradients or else by heating either internally or from below. The results are presented and analysed in terms of simple physical models. Although the computations are highly idealized and omit variation of viscosity and other major features of mantle convection, they can be related to geophysical measurements. In particular, the external gravity field depends on changes in surface elevation; this suggests an observational means of investigating convection in the upper mantle.

1. Introduction

It is now generally accepted that the earth's surface consists of a number of spherical caps, or plates, in relative motion, and plate tectonics, the kinematic description of this behaviour, has recently been reviewed at some length (Le Pichon 1968; Isacks, Oliver & Sykes 1968; McKenzie 1972). The movement of plates is presumably associated with convection in the mantle but the full dynamical process that causes their displacement is still obscure. The aim of this paper is to bridge a gap between applied mathematics and earth sciences. Though the forces which maintain the plate motions appear to be governed by the equations of fluid dynamics, the form of these equations differs from those which determine the motions of the oceans and atmosphere; a new branch of geophysical fluid dynamics is necessary in order to understand convection in the earth's mantle.

We shall therefore review the geophysical data on plate tectonics and the structure of the upper mantle together with their sources, as well as relevant fluid-dynamical information. Though Turcotte & Oxburgh (1972) have recently discussed these questions they have fewer reservations than we do about the direct

relationship between surface observations and mantle motions. Recent work on oceanic heat flow (Sclater & Francheteau 1970) and the topography of ridges (Sclater, Anderson & Bell 1971) has not supported Turcotte & Oxburgh's views. A recent laboratory demonstration by Oldenburg & Brune (1972) of a ridge and transform fault pattern when the skin on cooling wax is stretched clearly demonstrates that ridges are the direct result of extension. There are therefore at present no surface observations which suggest that the position of ridges is related to major vertical motions in the mantle, and it is therefore useful to discuss the relevance of surface observations to major motions within the mantle with some care.

We also present some new fluid-dynamical results, derived from numerical experiments on various two-dimensional models of convection in the mantle. Although the equations and boundary conditions are highly simplified, and in particular assume a constant viscosity, the computations already display a wealth of complicated behaviour. The simplification is deliberate: it is more profitable to begin with a carefully planned study of idealized models than to program every detail and generate results that are neither comprehensible nor accurate. Although caution is needed in making geophysical inferences from such simple models, this systematic investigation of the fluid dynamics of viscous convection is a necessary preliminary to more elaborate computations.

The next section contains a brief review of plate tectonics for applied mathematicians, with a summary of basic concepts and of current ideas. Various dynamical mechanisms are discussed, but any treatment of convection requires some knowledge of relevant properties of the mantle. This is provided in §3, with arguments for assuming that convection is confined to the upper mantle, where the fluid may have a Newtonian viscosity whose value, with other parameters, can be estimated. The geophysical situation is then replaced by a highly simplified mathematical problem, governed by nonlinear partial differential equations which must be solved on a computer. The numerical methods of §4 are used to solve these equations in the two-dimensional case. In §5 we review previous work and present results of numerical experiments on convection produced by horizontal temperature gradients, by heating from below and by internal energy sources. These results are then analysed and explained in terms of simple boundary-layer ideas. An attempt is made, in §6, to relate these computations to the behaviour of the earth's mantle by estimating relevant measurable quantities: the surface elevation, gravity anomaly, heat flux, temperature gradient and surface velocity. Finally, we indicate the extensive further calculations that are needed to understand convection in the mantle.

2. Plate tectonics

In 1962 Hess published a speculative paper on the history of the ocean basins, and the subsequent development of his ideas has profoundly changed our understanding of the evolution of the earth's surface. The essential concept of plate tectonics, that the earth's surface is composed of rigid plates in relative motion, is simple and easily confirmed. Analysis of earthquake motions (McKenzie &

Parker 1967) and of oceanic fracture zones (Morgan 1968) shows that this hypothesis provides an accurate description of surface motions of the earth. Moreover, the theory has increased our understanding of many geological problems and, in particular, of the history of ocean basins.

The theory is constructed in terms of relative motion between the spherical caps or plates because such motion can be directly measured. The boundaries between the plates are defined by the earthquake belts of the world, which in oceanic regions are very narrow linear strips (Isacks *et al.* 1968; Barazangi & Dorman 1969). When two plates are moving apart mantle material from below wells up and cools to form new plate. Plate boundaries of this type are known as ridges, and form shallow linear features in many ocean basins, elevated 3 km above the deep ocean floor. Where two plates slide past one another the motion conserves the area of both plates. Such boundaries are called transform faults (Wilson 1965). The third and most complicated type of plate boundary is one where plate is destroyed, and is called a trench. Destruction is accomplished by one plate overriding the other and pushing it down into the mantle. In the development of the theory the boundaries between oceans and continents are ignored, and all major plates defined by the seismic belts consist of both continent and ocean. The only difference between the behaviour of continental and oceanic crust occurs in trenches. Continental rocks contain more silica than those from the oceans; they are therefore less dense and cannot sink into the mantle. Thus continental rocks remain on the surface and are generally considerably older and more deformed than those from the ocean basins. However, the oceanic crust and upper mantle are formed from the mantle below the plates. Therefore the mean chemical composition of the oceanic part of a plate is the same as that of the material below, from which it differs only by being colder. For this reason the oceanic plates are denser than the mantle below and can sink through it. The different behaviour of continental and oceanic crust must occasionally result in major rearrangements of the plate boundaries.

These rather simple ideas are important because the relative motion between two rigid spherical caps can be described by a rigid rotation about some axis through the centre of the earth. This result is a consequence of Euler's theorem applied to motions on the surface of a sphere (Goldstein 1950; Bullard, Everett & Smith 1965). It is therefore possible to describe the relative motion of two plates with three parameters – for example, the latitude and longitude of the rotation axis, and either the rotation rate or the rotation angle. An adequate description of the earth's surface motions can be obtained by using seven plates, and hence 18 free parameters. The success of plate tectonics is a direct consequence of the small number of degrees of freedom permitted by the rigid motion of large caps. Le Pichon (1968) determined 15 of the parameters, and recent redeterminations of these 15 by Chase (1972) have demonstrated that major revisions of Le Pichon's values are not required by the more extensive data now available. It is clear from the success of plate tectonics and from its general acceptance that an accurate kinematic theory now exists which can describe the surface motions of the earth. It is, however, important to realize that this success has come about only because the theory is a kinematic one. In the earlier attempts

to construct a general theory of the tectonics of the earth (Hess 1962; Runcorn 1965) surface features had been explained as direct expressions of flow throughout the mantle. These authors believed that the rising limb of the convection cell must be beneath the ridge axis and the sinking limb beneath a trench. When the details of the observed motions were worked out this view required implausibly complicated evolution of the convective flow and it has now largely been abandoned (see, for instance, Isacks *et al.* 1968; McKenzie 1969). Perhaps the major reason why surface features are no longer believed to be closely related to the flow below is because they can now be simply and accurately accounted for by the creation and destruction of plates. Though this success does not demonstrate that the earlier views were incorrect, the simplicity of the plate model is in striking contrast to the complications required to generate a ridge offset by transform faults as a result of convection in the mantle.

The major features of ridges are their elevations above the surrounding ocean basins, and the high heat flow observed through the sea floor near their axes. Both features can be explained if they are sites of the creation of plate about 75 km thick by upwelling of hot mantle from below (McKenzie 1967*a*; Sclater & Francheteau 1970; Sclater *et al.* 1971). The strength of a plate 75 km thick is sufficient to transmit stresses across distances comparable with the radius of the earth without exceeding the yield stress of the rock from which it is made, and therefore permits rigid motion of the largest plates.

The topography and large gravity anomalies of trenches are the consequence of the bending of the plate which is underthrusting beneath the island arc (Hanks 1971). If the upper 30 km of the plate behaves elastically during the bending then the details of the bathymetry of the trench can be accounted for if the shearing stress within the slab is of the order of a few kilobars (1 kilobar = 10^8 N m^{-2}).

Perhaps the most unexpected success of plate tectonics was the explanation it provided of earthquakes below a depth of 70 km beneath the island arcs. No previous theory had satisfactorily explained their existence. The earthquakes on ridges and transform faults are always at a depth of less than 70 km and may well be shallower. Beneath island arcs, however, earthquakes occur within thin planar slabs extending to depths of up to 690 km, and with thicknesses of 50 km or less (Sykes 1966; Mitronovas, Isacks & Seeber 1969). Oliver & Isacks (1967) suggested that these shocks occur within a slab of what was once part of an oceanic plate but has since been underthrust beneath an island arc. This explanation accounts for the mechanism of earthquakes beneath island arcs, and also for the low attenuation and high propagation velocity of longitudinal (P) and transverse (S) waves travelling through the slab compared with corresponding paths through the rest of the upper mantle (Isacks *et al.* 1968; Cleary 1967; Davies & McKenzie 1969).

This brief summary of the theory of plate tectonics gives little idea of the wide variety of geophysical observations for which it now accounts, or of the power of the simple kinematic theory when used to reconstruct the positions of the continents and the bathymetry of ocean basins. An account of the relationship of many seismological observations to the new theory is given by Isacks *et al.*

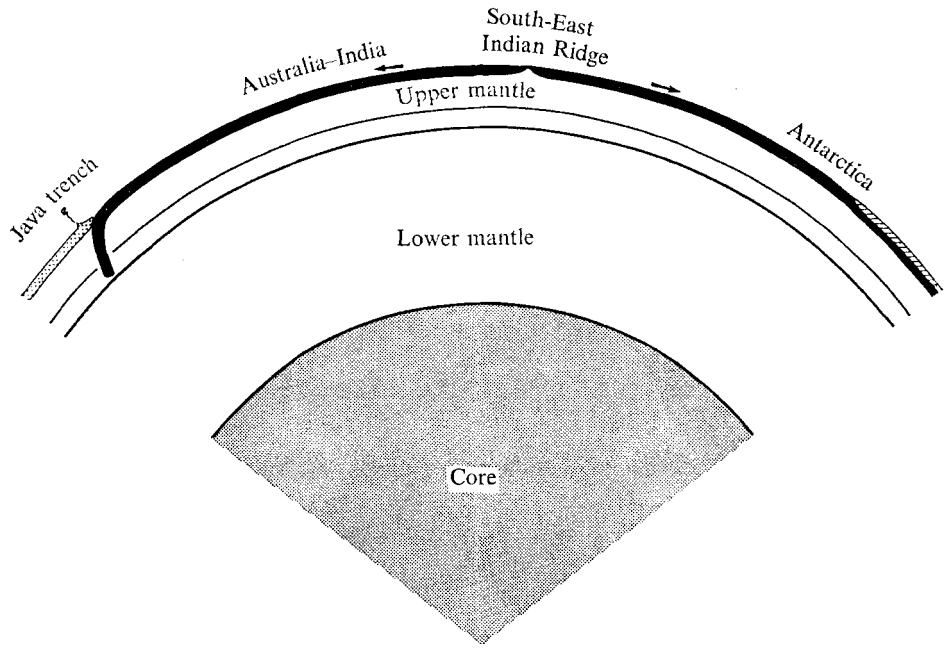

FIGURE 1. Section through the earth along 110° E from the equator to the South Pole with no vertical exaggeration. The black outer boundary layer consists of rigid plates which are created at ridges and separate from the earth's surface beneath island arcs to descend no more than 700 km.

(1968). Dewey & Bird (1971) have shown how the structure and evolution of many mountain chains is related to that of island arcs, and McKenzie & Sclater (1971) have used the concepts of plate tectonics to study the features of the floor of the Indian Ocean and its evolution during the last 80 Myr. Though opposition to the new theory remains, it is generally based on misconceptions rather than on contradictory observations.

The main features of the theory of plate tectonics are shown in figure 1, which also shows the more important horizontal boundaries in the earth's mantle discussed in this section. It represents a section across the Indian Ocean, from the Java–Sumatra Arc to the Antarctic continent along 110° E. The vertical scale of the section is not exaggerated and the great horizontal extent of the plates, compared with their thickness, is striking. In figure 2 the earth's curvature has been omitted and the vertical scale exaggerated to show the shape of ridges and trenches; the horizontal means of the density and temperature are also shown. The determination and accuracy of these estimates is discussed in § 3.

The section in figures 1 and 2 closely resembles many examples in fluid dynamics in which boundary layers are formed at the edges of the flow. The plates are, however, rather different from the thermal boundary layers formed in convecting liquids because their mechanical behaviour differs from that of the mantle below. The ridges are lines where the boundary layer is generated from the hotter material below, and the trenches mark lines where one boundary layer becomes detached from the earth's surface and is absorbed into the mantle

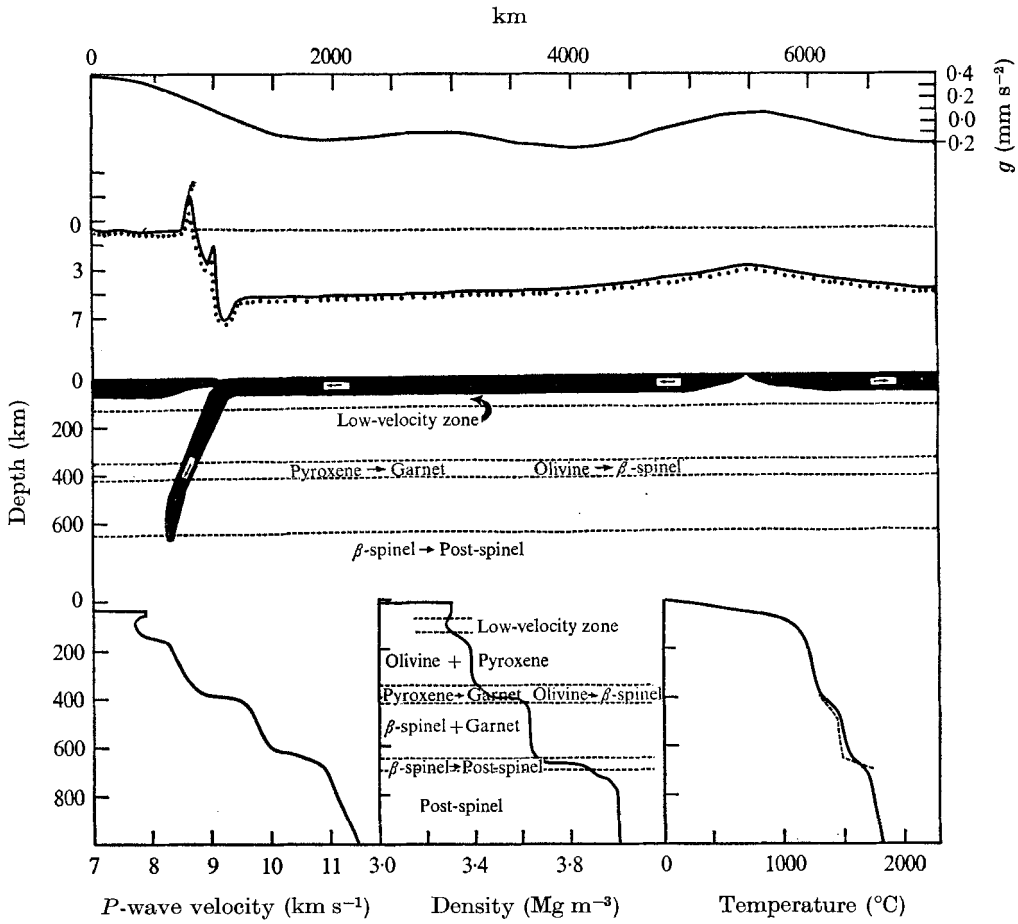

FIGURE 2. The same section as that in figure 1, ignoring the earth's curvature and showing the gravity field determined from the motion of satellites, a simplified section of the topography and the variation of P-wave velocity, density and temperature with depth. The gravity field is that of Gaposchkin & Lambeck (1971) referred to the best-fitting ellipsoid, the bathymetry is simplified from Zhivago (1966), the P-wave velocity is taken from Johnson (1967) and the density distribution from Ringwood (1972*b*). The best estimate of the temperature distribution beneath the ocean basins to a depth of 150 km is shown by the solid curve. Below 150 km the solid curve follows Ringwood's (1972*b*) estimate of the adiabatic temperature distribution: the dotted line shows the distribution expected if convection of heat is taken into account (see §6).

as it sinks. This motion convects cold material to a depth of 700 km and therefore represents a mechanism of vertical heat transfer by convection. The thermal structure of the plates which form the boundary layer is governed by the diffusion of heat vertically, or normal to the plane of a sinking slab, and by convection in directions lying in the plane.

Though plate motions must involve thermal convection it is not obvious that it is the convection which maintains the motion. For example, several authors have suggested that the earth might expand owing to a variation of G, the gravitational constant. Recently this argument has been vigorously revived by

Hoyle (Hoyle & Narlikar 1972; Hoyle 1972), who argues that $\dot{G}$ may be obtained from the variation of the length of day due to processes within the earth in the last 2×10^3 yr, and that such a variation can account for the existence of spreading ridges. Though it is by no means clear that there has been a change in the earth's moment of inertia in the last 2×10^3 yr, a change in the observed magnitude and sign would be expected in response to isostatic adjustments after the last glaciation (McKenzie 1967*b*; O'Connell 1971). There is therefore no necessity to appeal to cosmological effects to explain the observations. Hoyle's suggestion that the oceanic ridges might be produced by expansion of the earth is not consistent with the observations. Chase (1972) has calculated the rate at which sea floor is now being produced to be $2{\cdot}93\,\mathrm{km^2\,yr^{-1}}$. The uncertainty in this value is unlikely to be greater than 10%. In contrast Hoyle's larger value for $\dot{G}$ gives a figure of $1{\cdot}5 \times 10^{-2}\,\mathrm{km^2\,yr^{-1}}$, which is insignificant. There is a further important argument against any major change in the earth's radius in the last 4×10^8 yr. Bullard *et al.* (1965) were able to fit Africa to America by rigid motions, showing that the radii of curvature of both continents have not changed during the formation of the south Atlantic. Furthermore except in the Andes and Atlas mountains both continents have suffered little deformation in the last 4×10^8 yr. Therefore, though geophysical arguments cannot rule out small changes in G there is at present no evidence in their favour. Moreover any allowable changes in G are quite unable to account for plate motions which have occurred in the last 75 Myr.

Many other possible mechanisms have been suggested, but only three can satisfy the constraint imposed by the energy requirements. Since all major earthquakes are the result of plate motions, their energy release of about $5 \times 10^{18}\,\mathrm{J\,yr^{-1}}$, or $2 \times 10^{11}\,\mathrm{W}$, provides a lower bound on the rate of energy production required by the driving mechanism (McKenzie 1972). Owing to the success of the kinematic theory, few observations remain to be accounted for by a dynamic theory. Exceptions are the mean oceanic heat flow (McKenzie 1968*a*; Sclater & Francheteau 1970) of about $5{\cdot}8 \times 10^{-2}\,\mathrm{W\,m^{-2}}$, the relative motion between plates of 10–100 mm $\mathrm{yr^{-1}}$, and the long-wavelength gravity anomalies determined from the motion of satellites (Runcorn 1965; McKenzie 1969). These phenomena are not explained by the existence of plates, yet all must be the surface expressions of motion below the plates. Unlike the seismic energy release, they cannot easily be used to eliminate mechanisms. They do, however, provide conditions which any successful theory of the motion must satisfy

The three driving forces which satisfy the energetic requirements are the growth of the earth's core, tidal friction and radioactive heat generation. If the iron now in the earth's core was originally uniformly distributed throughout the mantle, then the energy released by core formation would be 10^{31} J (Tozer 1965). Provided that this energy is released at a uniform rate the process of conversion into seismic energy would only have to be 0·02% efficient to maintain the present rate of energy release throughout geological time. It is, however, very difficult to produce a non-catastrophic model of core formation (Tozer 1965), and therefore little work has been done on this problem. Another difficulty is that no iron metal has been found in rocks dredged from ridges. Therefore the part of the mantle involved in the creation of plates contains no free iron sinking

towards the core and thus cannot be providing the energy. These difficulties suggest that the other two possible mechanisms should be examined carefully before attempting to produce a model driven by sinking iron.

The total dissipation of the solar and lunar tides is about 3×10^{12} W, or 9×10^{19} J yr^{-1} (Munk & MacDonald 1960). The proportion of this energy which is dissipated in the oceans has been discussed for fifty years, but without any general agreement. The principal difficulty is that the coupling coefficients between the tides and the internal modes of oscillation of the ocean are unknown, and tidal currents in many shallow seas have not been measured (Munk 1968). Two rather uncertain arguments suggest that most of the dissipation does in fact take place in the oceans and not in the solid earth. The first is that Hendershott's (1972) numerical solution of Laplace's tidal equation requires a dissipation rate of 3×10^{12} W. Since these calculations agree reasonably well with tidal observations at island stations (Hendershott & Munk 1970), the calculated dissipation is probably reasonably accurate. The other argument involves the evolution of the lunar orbit. If the present rate of tidal dissipation is used to calculate the time of closest approach of the moon to the earth it is found to have occurred less than 2000 Myr ago (Kaula 1971). This event must have produced catastrophic tides on the earth (Munk 1968), and since reef-building organisms existed in shallow seas at that time it appears unlikely that the calculated date is accurate. The tidal dissipation in the oceans is profoundly affected by changes in the area covered by shallow seas and by changes in the geometry of ocean basins produced by plate motions. It is therefore more likely that major changes in total tidal dissipation can result if the energy loss takes place in the oceans rather than in the solid earth. Neither of these arguments is at present particularly strong, but the conversion of tidal energy into seismic energy would have to have an efficiency of 5 % to maintain the plate motions. Since considerable tidal dissipation undoubtedly occurs in shallow seas this estimate of the efficiency is undoubtedly too low, and tidal effects will therefore be ignored.

The third known energy source is the heat generated by radioactive decay of ^{40}K, ^{238}U, ^{235}U and ^{232}Th within the earth's crust and mantle. The heat flow through the deep oceans alone from these sources is about $3{\cdot}9 \times 10^{20}$ J yr^{-1}; if that through the continents is also included the total energy is about $1{\cdot}4 \times 10^{21}$ J yr^{-1}. Therefore the conversion of heat into seismic energy need only be between 1·0 and 0·3 % efficient. This requirement is not difficult to satisfy, and for this reason most work on the problem of the driving mechanism has been concerned with the manner in which the mantle, acting as a heat engine, converts thermal energy into mechanical work by some form of convection. Unfortunately the full equations which govern the motion cannot be solved at present even by numerical methods, principally because the motion is three-dimensional and the flow is dominated by nonlinear effects and boundary layers. Four different types of approach to these equations have been attempted. Hales (1936) first suggested that the mantle might be unstable to convection. Since then Runcorn (1965), Vening Meinesz (1962) and Knopoff (1964) have argued that the properties and temperature gradient within the mantle are such as to maintain a state close to marginal stability, and have therefore applied and extended the results of

Chandrasekhar (1961), governing the onset of convection in spherical shells. This approach applies to the mantle only if the mean temperature is governed by thermal diffusion and not by convection itself. For this condition to be satisfied the flow must be sufficiently slow to permit heat to diffuse across the convecting region in a time short compared with the overturn time. Since the convection extends to a depth of at least 700 km and the flow velocity at the surface is between 10 and 100 mm yr^{-1}, the time taken for a fluid element to travel in a circle of diameter 700 km is between 10 and 100 Myr. In this time heat can only diffuse through a distance of less than 150 km. This simple calculation shows that the temperature distribution within the mantle must be governed by convection of heat, and therefore marginal-stability solutions are not relevant to the geophysical problem.

The second type of approach is suggested by figure 1. The plates exist because they can transmit stresses over large distances, and are colder than the mantle below. Elsasser (1969) pointed out that a sinking slab beneath an island arc exerts a force towards the arc on the plate to which it is attached. The magnitude of the stress is between 10^8 and 10^9 N m^{-2} and is probably sufficient to move the plate on which it acts. There are, however, certain difficulties with Elsasser's suggestion (McKenzie 1969). The most important is that Africa and South America are separating at 40 mm yr^{-1} though neither has a large sinking slab attached. (A similar attempt to maintain the flow by the buoyancy forces in the boundary layer at ridge rather than at trenches has been made by Lliboutry (1969). However, his mechanism does not produce enough energy to satisfy the seismic energy requirements.)

The principal reason why Elsasser's and Lliboutry's suggestions are attractive is that they only involve buoyancy forces which are the direct result of plate motions. The convective term in the heat equation therefore involves a constant velocity, and for this reason the equation governing the temperature is linear and can be solved by the usual methods (McKenzie 1969). Both suggestions depend on the neglect of buoyancy forces in the main flow compared with those in the thermal boundary layer. If the temperature difference between the sinking slabs of thickness 70 km and the mantle is 1000 °C, then the temperature difference across regions 5000 km in extent must be much less than 15 °C if the buoyancy force of the boundary layer is to dominate. The calculations below and the magnitude of the non-hydrostatic gravity field both suggest that temperature differences in the main flow are greater than 15 °C and therefore that both viscous and buoyancy forces in the main flow must be included.

Another convective mechanism has recently been put forward by Howard, Malkus & Whitehead (1970), Whitehead (1972) and Huppert (1971). They suggested that radioactive heat generation within the continental crust was sufficient to heat the mantle beneath the continents and hence to maintain horizontal temperature gradients which would drive the flow and propel the continents themselves. The idea of convection driven by horizontal temperature gradients was proposed by Pekeris (1935) and briefly considered by Allan, Thompson & Weiss (1967) and McKenzie (1968*a*) as a possible means of producing continental drift. Since then the world-wide pattern of plate motions has been determined

in some detail and this mechanism proves inadequate. There are several large plates (the Pacific, Philippine Sea and Nasca plates) which are moving rapidly relative to each other and with respect to most other plates, though they contain no, or almost no, continental crust. So it is clear that continental radioactivity cannot maintain their motion. Furthermore, the relative velocity between plates consisting entirely or principally of oceanic lithosphere in fact appears to be more rapid than that between plates formed from continental lithosphere. Though these observations do not prove that continental radioactivity can be neglected as an energy source, they do show that there must be some other mechanism which produces more rapid motions. It is with this more powerful mechanism that this paper is principally concerned.

Convection driven by radioactive heating in the mantle is described by the velocity $\mathbf{u}$ and the temperature T. A proper theoretical investigation requires the solution of four partial differential equations, three of which contain nonlinear terms, in spherical co-ordinates. Any attempt to solve the full equations by numerical methods on present computers would lead to little understanding of the problem and consume a vast amount of time. Numerical solutions to the simpler set of equations in Cartesian co-ordinates governing two-dimensional flow in a slab may, however, easily be obtained, and can provide a physical understanding of the possible forms the flow may take. Such solutions also indicate how heat is converted into the mechanical work required to maintain the plate motions. Although laboratory experiments may be used to test the accuracy of these computations, it appears unlikely at present that the geophysical problem can be modelled with sufficient flexibility in the laboratory to make numerical experiments unnecessary. Many complicated processes are taking place in the mantle, and there is no rigorous way of deciding which affect the large-scale mass motions and which do not. Any model must therefore be chosen using arguments based on simplicity and physical intuition, and until extensive studies have been carried out disagreements about the importance of different processes are inevitable.

The equations which govern the flow within the mantle are

$$\frac{\partial u_i}{\partial t}+u_j\frac{\partial u_i}{\partial x_j}+2\epsilon_{ijk}\,\Omega_j u_k=-\frac{1}{\rho}\frac{\partial P}{\partial x_i}+\frac{\partial \Phi}{\partial x_i}+\frac{1}{\rho}\frac{\partial \tau_{ij}}{\partial x_j}, \tag{1}$$

$$\rho C_p\left[\frac{\partial T}{\partial t}+u_i\left\{\frac{\partial T}{\partial x_i}-\left(\frac{\partial T}{\partial x_i}\right)_s\right\}\right]=\frac{\partial}{\partial x_i}\left(k\frac{\partial T}{\partial x_i}\right)+H+\tau_{ij}\frac{\partial u_i}{\partial x_j}, \tag{2}$$

$$\partial(\rho u_i)/\partial x_i=0, \tag{3}$$

and the equation of state may be written in the form

$$\rho=\rho_0[1-\alpha(T-T_0)]. \tag{4}$$

In these equations ρ is the density, C_p the specific heat at constant pressure, k the thermal conductivity, H the rate of internal heat generation owing to radioactive decay, τ_{ij} the deviatoric stress tensor, $\mathbf{\Omega}$ the angular velocity of the earth, P the pressure, α the coefficient of thermal expansion and $(\nabla T)_s$ the adiabatic temperature gradient. Φ is the apparent gravitational potential in the rotating frame of reference:

$$\Phi=U+\tfrac{1}{2}|\mathbf{\Omega}\times\mathbf{r}|^2, \tag{5}$$

where U is the gravitational potential energy. A number of assumptions have already been made in deriving (1)–(4). The most important is that ρ is continuous within the mantle. This condition is probably not satisfied (Ringwood 1972*a*), and as Schubert & Turcotte (1971) have pointed out, the discontinuity in ρ may have an important influence on the circulation.

Equations (1)–(4) cannot be solved unless τ_{ij} and k can be expressed in terms of the other variables, and the form of H is known. The nature of the solutions will also depend on the numerical values assigned to other parameters (Turcotte & Oxburgh 1969), and therefore the properties of the mantle material involved in the motion must be known in some detail. All these questions depend on an accurate knowledge of the physical properties and mechanical behaviour of the rocks of the mantle. It is with these problems that the next section is concerned.

3. Properties of the mantle

3.1. *Structure and composition*

Most of what is known about the structure of the mantle has been determined by measurement of the velocity of longitudinal (P) and shear (S) waves, generated by earthquakes and by underground nuclear explosions (see recent discussions by Johnson 1967; Archambeau, Flinn & Lambert 1969). The variation of the velocities and density with depth can be obtained from the travel times of body and surface waves, and the periods of free oscillation of the earth (see Gilbert 1972). A summary of these results is contained in figure 2, which shows the variation of P velocity with depth, obtained from Johnson (1967), for oceanic regions.

A high-velocity layer above a depth of 80 km overlies a region in which the P-wave velocity is considerably reduced. The thickness of the high-velocity layer agrees with independent determinations of the thickness of oceanic plates (Sclater & Francheteau 1970); the region of reduced velocity below the plates is called the low-velocity layer and may contain a small fraction of melted material (Anderson, Sammis & Jordan 1972). When Gutenberg discovered the low-velocity zone he clearly recognized its tectonic importance, and proposed a model for the earth's deformation produced by ice loads which is very similar to our present beliefs (Gutenberg 1959). The seismic wave velocity of the mantle above a depth of 120 km is dominated by the rapid increase of temperature with depth, whereas below this depth the temperature is more nearly constant and the structure is governed by increasing pressure. The low-velocity zone is about 100 km thick and is underlain by a thicker layer with a higher seismic velocity. The dominant minerals of this layer are probably the same as those of the lower part of the plates. At a depth of 400 km there is a region in which the velocity increases rapidly over a depth range of 30–50 km. Careful high-pressure laboratory experiments by Ringwood & Major (1970) and by Akimoto & Fujisawa (1966, 1968) have shown that at pressures of $1{\cdot}1 \times 10^{10}\,\mathrm{N\,m^{-2}}$ (110 kilobars) and a temperature of 1000 °C the crystal structure of Mg_2SiO_4 changes from olivine to β spinel. The olivine form of Mg_2SiO_4 is the dominant material in the rock which forms the upper mantle, and therefore the change to a spinel structure increases the mean density of the rock as well as its seismic velocity. The pressure at a depth of

400 km is close to $1{\cdot}3 \times 10^{10}$ N m^{-2} and the temperature is about 1300 °C. Thus there is excellent agreement between laboratory observations and the structure of the mantle.

The details (Ringwood 1972*a*) of the olivine to spinel phase change are of some considerable importance to the convection problem because the thermodynamics of such a transformation can have a large effect on the possible motions. The first problem is concerned with heat energy and has been discussed by Verhoogen (1965). He was concerned with vertical motions in a mantle whose temperature variation is governed by conduction and he determined the conditions under which convection could take place. The full marginal-stability problem has recently been discussed by Busse & Schubert (1971). They considered a univariant phase change only, and therefore required the temperature to be continuous across the phase change boundary. The phase change in the mantle is not univariant because the olivine is not pure Mg_2SiO_4, but contains some Fe_2SiO_4 in solid solution. Also olivine is not the only mineral present. A better model is therefore a broad polyvariant phase change with perhaps a sharp univariant change within, corresponding to the change from spinel to modified spinel. Whether the temperature is continuous across such a transition zone depends upon the time necessary for heat to be conducted from one side to the other. The width of the zone is probably about 50 km and therefore the time required for heat to be conducted across it is $\sim$ 10 Myr. The sinking slabs beneath the island arcs are descending at a velocity of $\sim$ 50 mm yr^{-1} and therefore move through the transition zone in $\sim$ 1 Myr. Therefore the temperature across the transition zone will not be governed by conduction: the boundary conditions used by Busse & Schubert (1971) and by Schubert & Turcotte (1971) will not apply, and should be replaced by a temperature discontinuity of about 300 °C. This boundary condition cannot be generally applied, since the vertical velocities are unlikely to exceed 5 mm yr^{-1} everywhere. Only for velocities of much less than 5 mm yr^{-1} may Busse & Schubert's (1971) boundary conditions be used; the olivine–spinel phase change is an intermediate case. Within the sinking slabs, however, conduction can be ignored and the resulting equations are easily solved when written in terms of potential temperature (McKenzie 1970).

If convection can occur through a phase change the changes in density can cause a major increase or decrease in the buoyancy forces maintaining the motion (McKenzie 1968*a*). For instance, in the sinking slabs the temperature is less than in the surrounding mantle, and therefore olivine and spinel will be in equilibrium at shallower depths within the slabs than outside (Griggs 1972; Ringwood 1972*b*). If the transition occurs the density of the cold slabs and hence the driving force will increase (Griggs 1972). However, it is not yet certain whether the phase change can occur under equilibrium conditions within the slab or whether the olivine phase becomes metastable. Although the *P*-wave velocity structure of the slabs is not yet known in sufficient detail to determine the depth of the transition layer, studies by Julian (Toksöz, Minear & Julian 1971; Davies & Julian 1972) suggest that Griggs's models may produce a greater contrast than that observed, and therefore favour metastable olivine. Further work should resolve this problem. From this discussion it is clear that the olivine–spinel

phase change may have an important influence on the convective problem, whose consequences are not obvious.

The seismic velocity between 450 and 650 km shows little if any increase in P-wave velocity with increasing depth. This region is probably homogeneous, and laboratory experiments in this pressure range have not yet revealed any phase changes in likely mantle materials. At 650 km, however, there is a further phase change to a phase which it has not yet been possible to study in the laboratory. The exact arrangement of the atoms in the minerals of the mantle below 650 km is therefore still unknown. Laboratory experiments on similar materials do, however, strongly suggest that the phase change is the result of a rearrangement of the oxygen atoms surrounding the silicon. Both olivine and spinel contain silicon atoms surrounded by four oxygen atoms at the corners of a tetrahedron. High-pressure forms of related compounds contain silicon atoms at the centre of six oxygen atoms at the corners of an octahedron, and this arrangement probably also occurs in Mg_2SiO_4. This material is likely to be very much stronger than spinel, since the corresponding phase of SiO_2 (stishovite) is almost as hard as diamond. This transition, like the olivine–spinel transition, is not a univariant phase change and is therefore unlikely to form a sharp boundary.

The seismic velocity below 700 km increases steadily with depth, and the increase agrees well with that expected from simple equations of state (Birch 1952). The small variations in velocity observed by Johnson (1969) and other workers (see Hales & Herrin 1972) probably partly arise from lateral variations in upper mantle velocities which have become confused with radial variations.

Lateral variations of seismic velocity are most obvious in the plates since the rocks which form the upper half of the continental plates have slower P-wave velocity than those which form the similar part of the oceanic plates. There is also some seismic evidence (Brune & Dorman 1963) that the plate thickness beneath old continental regions is greater than that beneath the deep oceans. The only clear lateral variations yet discovered in the mantle beneath the plates are the high seismic velocities in the sinking slabs (Cleary 1967; Davies & McKenzie 1969; Toksöz *et al.* 1971; Davies & Julian 1972). Such variations arise because the slabs are colder than the surrounding mantle and have not yet provided any detailed information about the physical processes within the slabs. Careful studies of lateral variations of seismic velocities in regions distant from the sinking slabs, especially detailed studies of the depth of the transition layers, should provide information about non-hydrostatic conditions within the mantle.

At present the only direct observations of motion within the mantle below the plates come from the study of earthquakes with depths greater than 70 km. The mechanisms of these earthquakes are different from those of shallow shocks caused by plate motions, and have been discussed in some detail by Isacks & Molnar (1969, 1971). They showed that the shocks were caused by fracture within the sinking slab, and not by motion between the slabs and the surrounding mantle. They also studied the stress distribution in all slabs for which mechanisms were available, and found that the direction of greatest principal stress was parallel to the dip of the slab for most earthquakes below 350 km. The stresses present

between 70 and 350 km were found to depend on whether the deeper part of the slab reached a depth of 600 km. If it did, then the greatest principal stress was parallel to the dip. The stress state in which the greatest principal stress is parallel to the dip of the zone is often called compression, whereas if the least principal stress is parallel to the dip it is known as tension. (These terms are somewhat misleading because all earthquakes in the slabs are the result of the release of shear stresses, and all principal stresses are negative everywhere.) The observed behaviour would be expected if the resistance to the movement of the slabs is greater between 350 and 700 km than above 350 km, and if the resistance increases sharply at a depth of 600–650 km.

The close correlation between the stress state and the depth of the phase changes suggests that the resistance to deformation is different for the olivine, spinel and post-spinel phases. The deeper phase change is particularly important, since there is no convincing evidence that the detached boundary layer penetrates below 700 km anywhere within the earth. Isacks & Molnar (1971) have discussed two possible causes for the existence of this boundary. The first is that the resistance of the post-spinel phase to deformation is considerably greater than that of the spinel. Though such a difference in behaviour would be expected from the properties of stishovite, the properties of the post-spinel phase could be very different. The other explanation of the absence of earthquakes below 700 km is that the spinel to post-spinel change absorbs heat. The phase change would then occur deeper in the sinking slab than in the surrounding mantle, and the resulting buoyancy force could prevent penetration. However, most phase changes to denser forms at higher pressures give out heat, and therefore the second explanation is at present less likely than the first. Whatever the reason, the observations on sinking slabs show that even the thermal and mechanical boundary layers are unable to penetrate below 700 km, and therefore the convection which maintains the plate motions is restricted to the mantle above 700 km. If the lower mantle is strong then the appropriate boundary condition at 700 km is no slip for upper-mantle convection; if, however, the boundary is the result of the thermodynamics of the phase change the boundary condition will depend on the behaviour of the mantle below.

3.2. *Viscosity of the lower mantle*

Various authors (Macdonald 1963; McKenzie 1966) have argued that the viscosity of the lower mantle could be estimated from the magnitude of the earth's non-hydrostatic bulge. The argument depended on the gravitational energy of the non-hydrostatic bulge being considerably greater than that of other harmonics of the non-hydrostatic gravity field. Goldreich & Toomre (1969) have demonstrated that this conclusion depends on the axis used to express the spherical harmonics. They argued that the present magnitude of the non-hydrostatic bulge is the consequence of polar wandering so as to maximize the moment of inertia about the rotational axis. If polar wandering is to occur then this places an upper limit on the viscosity of the lower mantle.

The difference between these authors has not been resolved, since each model is internally self-consistent though they are mutually exclusive. If the kinematic

viscosity of the lower mantle is greater than $6 \times 10^{22}\,m^2\,s^{-1}$, polar wandering is not possible and so the gravity field cannot be related to the rotation axis. Then the magnitude of the non-hydrostatic bulge is larger than would be expected for a random choice of axis. Goldreich & Toomre have not disproved this argument by demonstrating that there exists an axis through the equator which also has a large non-hydrostatic bulge, since the rotational axis can be a special axis only if the gravity field is affected by rotation. Then, if the non-hydrostatic bulge is caused by a lag between the true figure of the earth and the equilibrium figure, the viscosity of the lower mantle must be greater than $6 \times 10^{22}\,m^2\,s^{-1}$.

If, however, the viscosity is less than $1{\cdot}5 \times 10^{21}\,m^2\,s^{-1}$ polar wandering can occur and will also result in a large non-hydrostatic bulge. So these complicated arguments only show that the viscosity of the lower mantle cannot lie between $1{\cdot}5 \times 10^{21}$ and $6 \times 10^{22}\,m^2\,s^{-1}$. This result is not very relevant to the question of convection in the lower mantle.

3.3. *Temperature gradients in the mantle*

A discussion of the variation of temperature within the upper mantle properly belongs in § 6, since the temperature variation is not required for the convection calculations but is derived from them. We include it here because there is no published account of how the temperature variation can best be determined from the geophysical observations now available. Although the temperature at the base of the plates cannot be directly measured, the vertical velocity of lava rising to the surface along the axes of oceanic ridges and into volcanic calderas such as those of Hawaii is sufficiently rapid for cooling to be neglected. This argument is supported by the remarkable constancy of the temperature (1150–1200 °C) of the tholeiitic magma erupted. This must therefore be the temperature of the mantle below the surface thermal boundary layer. The region below this is actively convecting, and so the temperature gradient will exceed the adiabatic gradient of 0·3–0·5 °C km^{-1}. This gradient has been used to extrapolate the temperature of 1150 °C from the base of the thermal boundary layer to the first phase change at a depth of about 400 km (figure 2). At this depth there are two other independent estimates available for the temperature. The first is obtained by using the phase diagrams for the olivine to spinel transition (Akimoto & Fujisawa 1966, 1968; Ringwood & Major 1970) and requiring the transition to occur at a pressure of $1{\cdot}3 \times 10^{10}\,N\,m^{-2}$. This condition gives a temperature of about 1600 °C. The second estimate is derived from the electrical conductivity of the upper mantle (Banks 1969). Though Parker (1971) has shown that Banks's observations do not permit the conductivity to be estimated with any accuracy at most depths, Parker's figure 3 shows that the conductivity at a depth of 400–500 km is well determined. Banks (1969) combined his estimates of the conductivity with estimates of the activation energy to show that the temperature was probably between 1150 and 1500 °C. Therefore both these estimates agree well with the adiabatic extrapolation in figure 2. Below a depth of 500 km there is no reliable method of estimating the temperature. The solid line in figure 2 is an estimate of the adiabatic temperature distribution, but with the present ignorance of the nature of the phase change at 650 km even the sign of the

(*a*) Values of parameters in the mantle

	Olivine	Spinel
k	4·2 W m^{-2} °C^{-1} (Fujisawa *et al.* 1968)	6·3 W m^{-2} °C^{-1}
ρ	3·3 × 10^3 kg m^{-3} (Mizutani *et al.* 1970)	3·6 × 10^3 kg m^{-3}
K_T	1·3 × 10^{11} N m^{-2} (Mizutani *et al.* 1970)	2·5 × 10^{11} N m^{-2}
C_p	1·2 × 10^3 J kg^{-1} °C^{-1}	1·2 × 10^3 J kg^{-1} °C^{-1}
α	3·3 × 10^{-5} °C^{-1} (Skinner 1966)	1·9 × 10^{-5} °C^{-1}
$\gamma = \alpha K_s/\rho C_p$	1·1	1·1

(*b*) Values used in calculations

$\kappa = k/\rho C_p$	= 1·5 × 10^{-6} m^2 s^{-1}
ρ	= 3·7 × 10^3 kg m^{-3}
C_p	= 1·2 × 10^3 J kg^{-1} °C^{-1}
g	= 10 m s^{-2}
ν	= 2 × 10^{17} m^2 s^{-1}
α	= 2 × 10^{-5} °C^{-1}

Surface heat flux, f = 5·85 × 10^{-2} W m^{-2}

d = 7 × 10^2 km

TABLE 1

temperature change at this depth may be in error. The dashed line is an estimate of the change in the mean temperature produced by vigorous convection (see §6). This change is insufficient to be observed by present geophysical methods.

3.4. *Parameters of the upper mantle*

Thermal properties. The physical properties which govern the convection in the upper mantle are those of olivine and spinel. Those of olivine have mostly been measured in the laboratory, but the spinel phase can only be synthesized at high pressure and much less is at present known about its properties. Fortunately the spinel phase of Fe_2SiO_4 is easily formed, and the corresponding properties of Mg_2SiO_4 spinel can be estimated from

$$\frac{M[Mg_2SiO_4(Sp)]}{M[Mg_2SiO_4(Ol)]} = \frac{M[Fe_2SiO_4(Sp)]}{M[Fe_2SiO_4(Ol)]},$$

where M is any physical property. The sources of the physical parameters and their values are given in table 1(*a*). Most of these difficult measurements were obtained by Akimoto and his collaborators.

The values of α and ρ are those at room temperature and pressure. The thermal expansion coefficient decreases with pressure. Therefore the value for spinel is used as representative of the mantle (table 1*b*). The major uncertainty in the value of α is caused by the olivine to spinel phase change. At depths where both phases are in equilibrium the effective value of α is about 3×10^{-4} °C^{-1}, and the phase change may therefore have a considerable effect on the nature of the convection.

The density is well determined from laboratory measurements and from seismic velocity measurements within the earth. The specific heat is best obtained from Dulong & Petit's law (Slater 1939). The uncertainties in the values of both ρ and C_p are small compared with those of α and κ.

The value of κ is dependent on the size of the olivine and spinel crystals, and

on small amounts of impurities and inclusions within the crystals. Small proportions of other minerals besides olivine and spinel may also have an important influence on the thermal diffusivity. Therefore the values in table 1 obtained by Fujisawa *et al.* (1968) may not be representative of the rocks of the mantle. Since Fujisawa *et al.* found that the diffusivity increases with pressure, a value of $1{\cdot}5 \times 10^{-6}\,\mathrm{m^2\,s^{-1}}$ is used in all the calculations below, and the temperature dependence of κ is ignored. This value is much smaller than that generally used in papers published before Fujisawa *et al.* made their measurements because the heat transfer by photons had previously been overestimated. A series of measurements on the opacity of olivine at high temperatures (Fukao, Mizutani & Uyeda 1968; Fukao 1969) has shown that the absorption of photons with wavelengths between 1·8 and 3·0 μm increases by a factor of about 100 between 300 and 1300 °K. This change is caused by the broadening of an iron absorption band with increasing temperature, and prevents radiative conductivity from dominating that due to phonons. The conductivity calculated from the absorption measurements now agrees reasonably well with that observed directly (Fukao *et al.* 1968; Kanamori, Fujii & Mizutani 1968).

Viscosity. Few problems in geophysics have generated as much controversy as the relation between the rate of deformation and the shearing stress. Perhaps the principal difficulty is that experiments cannot be carried out at either the high pressures or the low strain rates at which the mantle is being deformed and therefore all arguments must be based on an extrapolation of results obtained under very different conditions. As Goetz (1971) has remarked, extrapolation of any creep results outside the range determined by experiments is very uncertain. Despite these uncertainties there is now considerable agreement between different authors on the processes involved, and also between theory and experiment. Experiments at atmospheric pressure and high temperature on the deformation of metal oxides have been reviewed by Gordon (1965), McKenzie (1968*b*) and Sherby & Burke (1968). Since the strength of perfect crystals is two or three orders of magnitude greater than that of most solids under laboratory conditions, most deformation involves the movement of imperfections in crystals. The simplest imperfections are point defects, such as vacancies and interstitial atoms. Movement of interstitial atoms down pressure gradients or of vacancies in the opposite direction results in deformation. Deformation of this type can only take place if material can be transferred from one grain boundary to another and therefore the rate decreases with increasing grain size. In contrast, most deformation of solids depends on the motion of line defects such as screw or edge dislocations. The creep behaviour of metals at most temperatures and stresses depends on the ability of dislocations to move through crystals and has therefore been carefully investigated (see Read 1953). It is only at temperatures close to the melting point and shear stresses of about $10^5\,\mathrm{N\,m^{-2}}$ that most metals deform by diffusion of point defects. The movement of dislocations is controlled by the past history of the metal, the presence of small quantities of different crystals and many other complications. Fortunately at high temperatures the behaviour of most materials becomes relatively simple because dislocations can climb by transferring atoms either to or from the dislocation by migration of

point defects. Climb permits the dislocations to avoid obstructions to their motion such as other dislocations or impurities, and therefore at high temperatures creep is controlled by diffusion of atoms even though the displacement itself takes place by the glide of dislocations. The important difference between diffusion creep and creep produced by dislocation glide is the stress dependence of the rate of deformation. The diffusion creep rate $\dot{\epsilon}$ under a shearing stress σ is given by

$$\dot{\epsilon} = \frac{CDV_a}{k_B T a^2}\sigma, \tag{6}$$

where a is the mean radius of crystals, C a constant of order unity, k_B Boltzmann's constant, V_a the activation volume and $D(P, T)$ is a diffusion coefficient, whereas creep controlled by dislocation climb is governed by

$$\dot{\epsilon} \propto D\sigma^n, \tag{7}$$

where $n \geqslant 3$ and decreases with increasing temperature and decreasing stress. Therefore, whereas diffusion creep may be described by a Newtonian viscosity, creep controlled by dislocation climb is governed by a more complicated constitutive relationship which may be obtained from (7) (Prager 1961, p. 139). Recent papers on creep in the earth's mantle (Gordon 1965, 1971; McKenzie 1968*b*; Weertman 1970; Carter & Ave'Lallemant 1970; Ave'Lallemant & Carter 1970; Rayleigh & Kirby 1970) are in general agreement that diffusion creep occurs at low shearing stress, but as the stress is increased the line defects become mobile and govern the deformation. Both types of creep are rate-limited by diffusion (Gordon 1971). The main disagreement between these authors concerns the value σ_c required to cause the dislocation movements to dominate diffusion creep. Weertman (1970) believes that $\sigma_c \approx 10^3\,\mathrm{N\,m^{-2}}$ whereas McKenzie (1968*b*) and Rayleigh & Kirby (1970) argue that σ_c lies between 10^6 and $10^7\,\mathrm{N\,m^{-2}}$. The difference is principally the result of different choices of grain size. Weertman uses 220 mm, whereas Rayleigh & Kirby use a value of 10 mm derived from examination of pieces of upper mantle carried to the surface by basaltic lava. Rayleigh & Kirby's arguments are based wherever possible on experimental results and on direct observation, and are therefore more likely to be correct than those of Weertman. The shearing stress dividing the creep regimes will therefore be taken as $10^7\,\mathrm{N\,m^{-2}}$ for the mantle below the plates. If this value of σ_c is correct the motion of most of the mantle can be described by a viscosity. However, deformation of the plates and the sinking slabs occurs at stresses between σ_c and $10\sigma_c$ and therefore must be governed by dislocation motions. This suggestion is confirmed by the observations of Ave'Lallemant & Carter (1970), who showed that most olivine from the lowest part of the plates shows evidence of dislocation glide. Some olivine nodules in basalt lavas and in the fragmented rock which occurs with diamonds have probably come from below the plates, yet still show evidence of deformation at stresses above σ_c. These observations suggest that both deformation mechanisms are important, but for simplicity only diffusion creep described by a viscosity is considered below.

Both creep mechanisms are strongly temperature dependent, principally because both are rate-limited by vacancy diffusion. Weertman (1970) and Gordon

(1971) have discussed the variation of creep rate with depth; both agree that the minimum resistance to deformation occurs within the upper mantle, and that the plates and the lower mantle are much more resistant. This variation is therefore essential to the formation of plates, and must be included in any realistic calculations. Our calculations do not include any variation of viscosity with depth or temperature for reasons discussed below. Instead we adopt an appropriate constant value for the viscosity. The mean viscosity given in table 1 is that which O'Connell (1971) showed could best account for the response of the earth to surface loads which were imposed during the last glaciation.

In the past there has been much discussion by Jeffreys and others (see, for instance, Jeffreys 1963, 1971) on the value of the finite strength of the mantle, and on the nature of the creep which took place when this strength was exceeded. The existence of diffusion creep makes this argument irrelevant; the mantle is sufficiently hot for diffusion to be important, and therefore creep can occur at all stresses. Furthermore the expressions used by Jeffreys to describe creep apply only at low temperatures and pressures, and probably describe deformation caused by the formation of open cracks (Goetz 1971).

Radioactive heat generation. A less controversial but important question is the rate of radioactive heat generation by mantle rocks. If the heat flowing through the earth's surface is principally generated below 700 km, then the form of the flow is quite unlike that which results from heat generation solely from within the outer 700 km of the earth's mantle. The basalts erupted along the ridges are the result of partial melting of mantle, and measurements of the concentration of K, U and Th in the rocks which remain after melting show that these elements are concentrated in the melt. The radioactive heat generation of the mantle can therefore be obtained if the concentration of these three elements in oceanic basalts is known, and if the fraction of the mantle which melts beneath the ridges can be determined.

Engel & Engel (1970) and Melson & Thompson (1971) have determined the concentration of K, U and Th in oceanic basalts. Using the energy generation rates given by Wetherill (1966) the corresponding rate of heat generation is between 2·3 and $2{\cdot}8 \times 10^{-11}$ W kg^{-1}. This value is not very reliable since the concentration of all three elements is very much smaller than that in most common rocks, and is therefore difficult to measure by the usual methods. In view of the importance of the rate of heat generation by oceanic tholeiites, a detailed study of the distribution of these three elements is badly needed.

If the mean heat flow through the ocean basins of $5{\cdot}8 \times 10^{-2}$ W m^{-2} (von Herzen & Lee 1969) comes from energy generated uniformly throughout the mantle, then the rate required is 7×10^{-12} W kg^{-1}. Therefore if the mean composition of the mantle is constant oceanic basalts are the result of 25–30 % partial melting, with all the K, U and Th concentrated in the melt. If radioactivity is concentrated in the upper mantle, above 700 km, then 100 % melting is required. Most authors who have considered the origin of oceanic basalts have suggested that between 15 and 40 % partial melting has occurred (Gast 1968, 1972; Schilling 1971). In that case, approximately equal amounts of heat come from the mantle above and below 700 km.

4. Numerical formulation of the problem

In the last two sections we have reviewed both the geophysical evidence for convection in the earth's mantle and the properties of the region in which motion occurs. We are now in a position to set up a variety of simplified model problems which can be solved in order to illuminate the processes occurring in the rock of the mantle. In this section we shall first derive the partial differential equations governing the flow. These equations are nonlinear and cannot be solved by analytical techniques; we therefore describe the numerical methods that have been used to solve them. Even with the aid of a computer it is necessary to make many drastic and unrealistic assumptions. The direct relevance to plate tectonics of our numerical experiments is therefore in some doubt. However, they do provide a beginning to the systematic study of convection in a fluid with the properties of the earth's mantle.

We shall assume that motion is confined to the upper mantle, above 700 km. It can then be shown (Tozer 1965; McKenzie 1968*a*) that the Boussinesq approximation is valid. The flow is effectively incompressible and variations of density are significant only in the buoyancy force, which drives the motion against friction. Convection is then governed by the Boussinesq approximation to (1)–(5) and diffusion creep allows a relationship of the form

$$\tau_{ij} = \rho\nu\left(\frac{\partial u_i}{\partial x_j} + \frac{\partial u_j}{\partial x_i}\right) \tag{8}$$

between the deviatoric stress and the rate of strain, where ν is a kinematic Newtonian viscosity. The characteristic decay time associated with a viscosity of $10^{17}\,\mathrm{m^2\,s^{-1}}$ is only 10^{-5} s and the Reynolds number is typically 10^{-20}. For these reasons inertial and Coriolis forces are negligible and the left-hand side of (1) may be ignored. For buoyancy-driven flow this is equivalent to assuming that the Prandtl number $\rho C_p \nu/k$ is infinite.

The heat flow equation (2) includes a term $\tau_{ij}\,\partial u_i/\partial x_j$ corresponding to viscous generation of heat. This effect is in general negligible if the convecting layer is shallow compared with the temperature scale height, a necessary condition for the Boussinesq approximation to be valid. We shall therefore ignore this term, as a first step, even though the local effects of viscous heating in narrow plumes may have a significant effect on the pattern of convection.

The adiabatic temperature gradient

$$(dT/dz)_s = -g\alpha T/C_p \tag{9}$$

gives a temperature increase of about 300 °C over 700 km, which is roughly equal to the temperature difference across the thermal boundary layer in our computations. The heat flux conducted down this gradient is only 4 % of the total. We shall assume that this flux is constant. Then, if we ignore the dependence of ρ on the adiabatic temperature variation, we may drop $(\nabla T)_s$ from (2). However, the adiabatic gradient must be included in comparisons of numerical results with temperatures in the mantle.

For the remainder of this paper we shall make the simplifying assumption that

the specific heat, the internal heating rate, the coefficient of expansion, the thermal conductivity and the viscosity are all constant. (The latter is a serious restriction: the viscosity varies by at least an order of magnitude in the upper mantle and the effects of a variable viscosity have been investigated by Torrance & Turcotte (1971) and Turner (1973).) Equations (1)–(3) can then be rewritten in the form

$$\nu\nabla^2\mathbf{u} = \rho_0^{-1}\nabla P + \alpha(T - T_0)\,\mathbf{g}, \tag{10}$$

$$\partial T/\partial t = -\nabla.(T\mathbf{u}) + \epsilon + \kappa\nabla^2 T, \tag{11}$$

$$\nabla.\mathbf{u} = 0, \tag{12}$$

where the thermometric internal heating rate $\epsilon = H/C_p\rho$, the thermometric conductivity $\kappa = k/C_p\rho$ and $\mathbf{g} = \nabla\Phi$. The pressure can then be eliminated by taking the curl of (10):

$$\nu\nabla^2\boldsymbol{\omega} = \alpha\nabla T \times \mathbf{g}, \tag{13}$$

where the vorticity $\boldsymbol{\omega} = \nabla \times \mathbf{u}$. Thus the equation of motion reduces to a balance between generation of vorticity by the buoyancy torque and viscous dissipation.

Although these equations should be solved in a spherical shell, the earth's curvature can probably be ignored if convection does not extend below 700 km or 10 % of the earth's radius. Moreover Hsui, Turcotte & Torrance (1972) have solved the same equations (10)–(12) in spherical co-ordinates and have obtained results similar to those discussed below. Thus it is possible to consider a plane horizontal layer, and calculations are considerably simplified by adopting Cartesian rather than spherical co-ordinates. The gravitational acceleration $\mathbf{g}$ may then be assumed to be constant, acting in the negative-z direction. Such a plane layer adequately represents small-scale convection but spherical geometry may have a major influence on the large-scale flow associated with plate motions.

In order to reduce the computing time needed to solve a problem we shall further simplify the calculation by assuming that the flow is restricted to the x, z plane and independent of the y co-ordinate. From (12), the velocity can then be described by a stream function ψ such that

$$\mathbf{u} = (u, 0, w) = (-\partial\psi/\partial z, 0, \partial\psi/\partial x); \tag{14}$$

then the vorticity

$$\boldsymbol{\omega} = (0, \omega, 0) = (0, -\nabla^2\psi, 0) \tag{15}$$

and (13) reduces to

$$\nabla^2\omega = (g\alpha/\nu)\,(\partial T/\partial x). \tag{16}$$

The simplest boundary conditions are obtained by confining the flow to a rectangular region $0 < x < L$, $0 < z < d$ such that the normal velocity and the tangential stress both vanish on the surfaces $z = 0, d$, and assuming that the stream function is an odd function of x and periodic, with period $2L$. Then

$$\psi = 0, \quad \omega = 0 \quad (z = 0, d) \tag{17}$$

and

$$\psi = 0, \quad \omega = 0, \quad \partial T/\partial x = 0 \quad (x = 0, L). \tag{18}$$

We shall assume that the temperature is fixed on the upper boundary and that either the temperature or the vertical temperature gradient is prescribed at the

lower boundary. The assumption of free (slippery) boundaries is computationally convenient, though fixed boundary conditions ($\mathbf{u} = 0$) at $z = 0$ would be more realistic if the post-spinel phase is effectively solid.

It is preferable to use physical, dimensional, variables when relating the numerical experiments to geophysics; and we use throughout the values listed in table 1. However, it is more convenient to carry out the computations with equations in dimensionless form. All lengths should clearly be measured in terms of the depth d; temperatures and times can be expressed in terms of characteristic quantities T_1 and τ respectively. From (16) a typical velocity is

$$U = g\alpha T_1 d^2/\nu \tag{19}$$

and we define τ as the turnover time:

$$\tau = d/U = \nu/g\alpha T_1 d. \tag{20}$$

We now introduce dimensionless (primed) variables as follows:

$$(x', z') = d^{-1}(x, z), \quad t' = t/\tau, \quad T' = (T - T_0)/T_1, \tag{21}$$

where T_1 is arbitrarily chosen to be 1 °C and T_0 is the mean temperature of the upper boundary. Then the dimensionless conductivity

$$\kappa' = \kappa\nu/g\alpha T_1 d^3 = k\nu/\rho C_p g\alpha T_1 d^3, \tag{22}$$

the energy generation rate

$$\epsilon' = \epsilon\nu/g\alpha T_1^2 d = H\nu/\rho C_p g\alpha T_1^2 d \tag{23}$$

and the normalized cell width

$$\lambda = L/d. \tag{24}$$

We shall use these *dimensionless* quantities, suppressing primes, for the rest of this section *only*.

In order to investigate convection we have then to solve a single time-dependent equation

$$\partial T/\partial t = -\nabla.(T\mathbf{u}) + \epsilon + \kappa\nabla^2 T \tag{25}$$

over the region $0 \leqslant x \leqslant \lambda$, $0 \leqslant z \leqslant 1$, where the velocity $\mathbf{u}$ is derived, using (14), from a stream function satisfying the biharmonic equation

$$\nabla^4\psi = -\partial T/\partial x, \tag{26}$$

subject to boundary conditions (17) and (18).

The partial differential equations (25) and (26) are solved by finite-difference methods, using techniques developed by Moore, Peckover & Weiss (1974) for studying time-dependent two-dimensional convection. The variables T and ψ are represented on a grid with uniform spacing $\Delta x = \Delta z = h$; let $x_j = jh$, $z_k = kh$ and $t^n = n\Delta t$, where $j = 0, 1, \ldots, N_x$ and $k = 0, 1, \ldots, N_z$, and put $T^n_{j,k} = T(x_j, z_k, t^n)$, etc. Then (25) becomes

$$\begin{aligned} T^{n+1}_{j,k} = T^n_{j,k} + \frac{\Delta t}{4(h^2 + 2\kappa\Delta t)} [&(\psi^{n+\frac{1}{2}}_{j+1,k+1} - \psi^{n+\frac{1}{2}}_{j+1,k-1})\, T^{n+\frac{1}{2}}_{j+1,k} \\ &- (\psi^{n+\frac{1}{2}}_{j-1,k+1} - \psi^{n+\frac{1}{2}}_{j-1,k-1})\, T^{n+\frac{1}{2}}_{j-1,k} - (\psi^{n+\frac{1}{2}}_{j+1,k+1} - \psi^{n+\frac{1}{2}}_{j-1,k+1}) T^{n+\frac{1}{2}}_{j,k+1} + (\psi^{n+\frac{1}{2}}_{j+1,k-1} \\ &- \psi^{n+\frac{1}{2}}_{j-1,k-1}) T^{n+\frac{1}{2}}_{j,k-1} + 4\epsilon h^2 + 4\kappa(T^{n+\frac{1}{2}}_{j+1,k} + T^{n+\frac{1}{2}}_{j-1,k} + T^{n+\frac{1}{2}}_{j,k+1} + T^{n+\frac{1}{2}}_{j,k-1} - 4T^n_{j,k})]. \end{aligned} \tag{27}$$

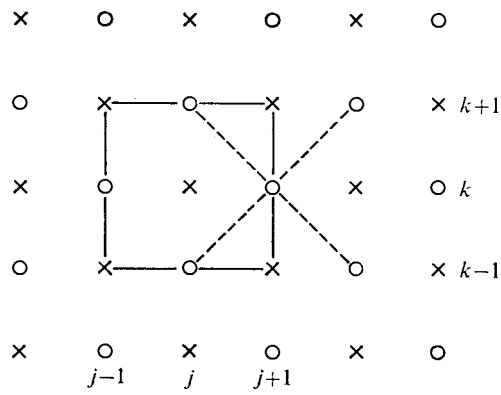

FIGURE 3. The mesh for numerical integration. ×, points with $j+k$ even, at which T^n, $\omega^{n+\frac{1}{2}}$ and $\psi^{n+\frac{1}{2}}$ are calculated; ○, points with $j+k$ odd, at which $T^{n+\frac{1}{2}}$, ω^n and ψ^n are calculated (where n is an integer). The temperature $T^{n+1}_{j,k}$ is obtained from (27), which is derived by considering the fluxes at time $t^{n+\frac{1}{2}}$ across the box centred on (x_j, z_k). This is used to estimate $\partial T/\partial x$ at the circles, whence $\omega^{n+1}_{j+1,k}$, etc., are obtained from (29), which relates values at points connected by the broken lines; $\psi^{n+1}_{j+1,k}$, etc., can then by calculated similarly from (30). These values are then used to give $T^{n+\frac{3}{2}}_{j+1,k}$ and so $\omega^{n+\frac{3}{2}}_{j,k}$ and $\psi^{n+\frac{3}{2}}_{j,k}$.

The difference equation uses the leapfrog scheme on a staggered mesh (Roberts & Weiss 1966); it is centred in space and time and has second-order accuracy. The values of T required for (27) are defined on a staggered mesh: at integral time levels ($n = 0, 1, 2, \ldots$) $T^n_{j,k}$ is only defined at points with $j+k$ even; at intermediate times ($n = \frac{1}{2}, \frac{3}{2}, \ldots$) $T^n_{j,k}$ is defined on the interlocking mesh of points with $j+k$ odd, as depicted in figure 3. These values of the temperature suffice to calculate T explicitly for $n = \frac{1}{2}, 1, \frac{3}{2}, \ldots$, provided that the stream function is also known.

The boundary conditions on the velocity make it convenient to solve (26) as two coupled Poisson equations

$$\nabla^2\omega = \partial T/\partial x, \quad \nabla^2\psi = -\omega \tag{28}$$

with homogeneous Dirichlet boundary conditions on ψ and ω. These equations are expressed in the form

$$\omega_{j+1,k+1}+\omega_{j+1,k-1}+\omega_{j-1,k+1}+\omega_{j-1,k-1}-4\omega_{j,k} = h(T_{j+1,k}-T_{j-1,k}), \tag{29}$$

$$\psi_{j+1,k+1}+\psi_{j+1,k-1}+\psi_{j-1,k+1}+\psi_{j-1,k-1}-4\psi_{j,k} = -2h^2\omega_{j,k}. \tag{30}$$

The stream function ψ is obtained by successively solving the implicit equations (29) and (30) using fast Fourier analysis in the x direction and tridiagonal elimination in the z direction; the boundary conditions on the vorticity can be applied without synthesizing ω from its Fourier components. This process yields values of ψ at points adjacent to those where T is defined (see figure 3) and inspection of (27) shows that these are precisely the values required to describe the advection of temperature.

The accuracy of these difference schemes is analysed in detail elsewhere (Moore, Peckover & Weiss 1974). In fact the overall accuracy of the solution to the biharmonic equation is comparable with that of the interpolated solution discussed

by Moore *et al.*, though the error is more anisotropic, since certain circulatory modes are preferentially enhanced. It is essential to ensure that the mesh used for differences has adequate resolution. The horizontal boundary layers are generally thinner than the vertical (Moore & Weiss 1973). Hence we use the horizontally averaged temperature field $\overline{T}$ to define the boundary-layer thickness as the distance across which 90 % of the change in $\overline{T}$ occurs. Investigations by Moore & Weiss (1973) show that computations are only reliable (in the sense that the overall heat flux is accurate to within 1 %) provided that there are at least three mesh intervals across any boundary layer.

5. Results of the numerical experiments

Thermal conduction could only carry a small fraction of the heat transported through the mantle; the mathematical problem is thoroughly nonlinear. Although linearized solutions of (1)–(4) have been studied in some detail and various interesting nonlinear problems have been solved, there has not yet been a systematic investigation of different forms of convection in a layer with infinite Prandtl number. In this section we survey the fluid dynamics of two-dimensional convection between free boundaries. Since there is now extensive understanding of Rayleigh–Bénard convection, which has been reviewed by Brindley (1967) and by Spiegel (1971), we make use of the existing knowledge of this type of convection for comparison with our results.

Most published work has concentrated on the behaviour of a fluid heated uniformly from below. In the present work we have used several computational models all of which use (10)–(12). In the simplest, convection is driven by an imposed horizontal temperature gradient; in others, the temperature or temperature gradient is fixed at the lower boundary and the fluid is heated either from below or uniformly within. These models are undoubtedly too simple to reproduce the major features of plate motions. Nevertheless, they can behave in remarkably complicated ways and the results are a necessary preliminary to a proper physical understanding of fluid dynamics in the mantle

5.1. *Convection driven by horizontal temperature gradients*

In the simplest models that we studied, convection was driven by an imposed horizontal variation of temperature, using (10)–(12) with $\epsilon = 0$. Since $\partial T/\partial x \neq 0$ equation (16) shows that motion must occur: there is no static equilibrium state. In addition to (17) and (18), the boundary conditions were

$$T = \begin{cases} \Delta T \cos \pi x/L & (z = d), \\ 0 & (z = 0). \end{cases} \tag{31}$$

This configuration can be described by a dimensionless Rayleigh number

$$R_H = g\alpha \Delta T d^3/\kappa\nu. \tag{32}$$

For $R_H \ll 1$ advection of heat is negligible and T is therefore harmonic (Allan *et al.* 1967):

$$T = \Delta T \cos \eta x \, (\sinh \eta z/\sinh \eta_1), \tag{33}$$

where $\eta = \eta_1/d = \pi/L$. The equations are all linear and can be solved to give

$$\psi = \left(\frac{g\alpha\Delta T}{\nu}\right)\frac{\sin\eta x}{8\eta^2\sinh\eta_1}[\eta(z^2-d^2)\sinh\eta z - (2\eta_1\coth\eta_1+1)(z\cosh\eta z - d\coth\eta_1\sinh\eta z)] \quad (34)$$

(Peckover 1972).

The model permitted a range of results to be obtained, showing the effect of convection of heat on the form of the solution. This sequence is shown in figure 4 for increasing values of the Rayleigh number. The first two cases (figures 4*a*, *b*) show the isotherms and streamlines for $\Delta T = 0{\cdot}01$ and $0{\cdot}1\,^\circ\mathrm{C}$ ($R_H = 4{\cdot}58$ and $45{\cdot}8$). These are both very similar to the linear solution; only the $T = 0$ isotherm is distorted by the motion. As the horizontal temperature difference is increased to $1{\cdot}0\,^\circ\mathrm{C}$ convection of heat becomes important and by $10\,^\circ\mathrm{C}$ a sinking plume appears beneath the cold region. When the temperature difference reaches $100\,^\circ\mathrm{C}$ thermal boundary layers develop and these become thinner as ΔT is further increased. The main flow occupies a nearly isothermal region with a mean temperature $T_M < 0$. The streamlines are less interesting: solving the biharmonic equation is an effective smoothing operation. Since the bottom boundary is maintained at $T = 0$ the fluid gains heat from below and a weak rising plume forms on the left-hand side of the box. This feature of the circulations shows most clearly in the vorticity field.

To eliminate this effect, we also studied a modified version of the same problem with the boundary condition

$$\partial T/\partial z = 0 \quad (z = 0)$$

so that no heat flux crosses the lower boundary. This model compares better with convection caused by internal heating, as described below. Once again, when $R_H \ll 1$ the equations are linear and

$$T = \Delta T\cos\eta x\,(\cosh\eta z/\cosh\eta_1), \quad (35)$$

$$\psi = \left(\frac{g\alpha\Delta T}{\nu}\right)\frac{\sin\eta x}{8\eta^3\cosh\eta_1}\{\eta^2 z(2d-z)\cosh\eta z + [\eta_1^2\coth\eta_1 - \eta(z-d)]\sinh\eta z\}. \quad (36)$$

As can be seen from figure 5, the rising plume vanishes while the sinking sheet is thin and colder than T_M. These features remain unchanged as the horizontal temperature variation is increased though the thickness of the boundary layers and the sinking sheet becomes smaller. Since the Prandtl number is infinite, shear instabilities are suppressed. A steady-state solution was found for all values of ΔT that were investigated.

Qualitatively, the significant results of this set of experiments are the formation of a thin thermal boundary layer at the upper (active) boundary but not at the lower (passive) one, together with a cold sheet falling from the active boundary. The contrast between the upper and lower thermal boundary conditions destroys any symmetry in the solution.

Two features of the temperature field when $R_H \geqslant 20000$ are of particular interest. Figure 6 shows the horizontally averaged temperature as a function of

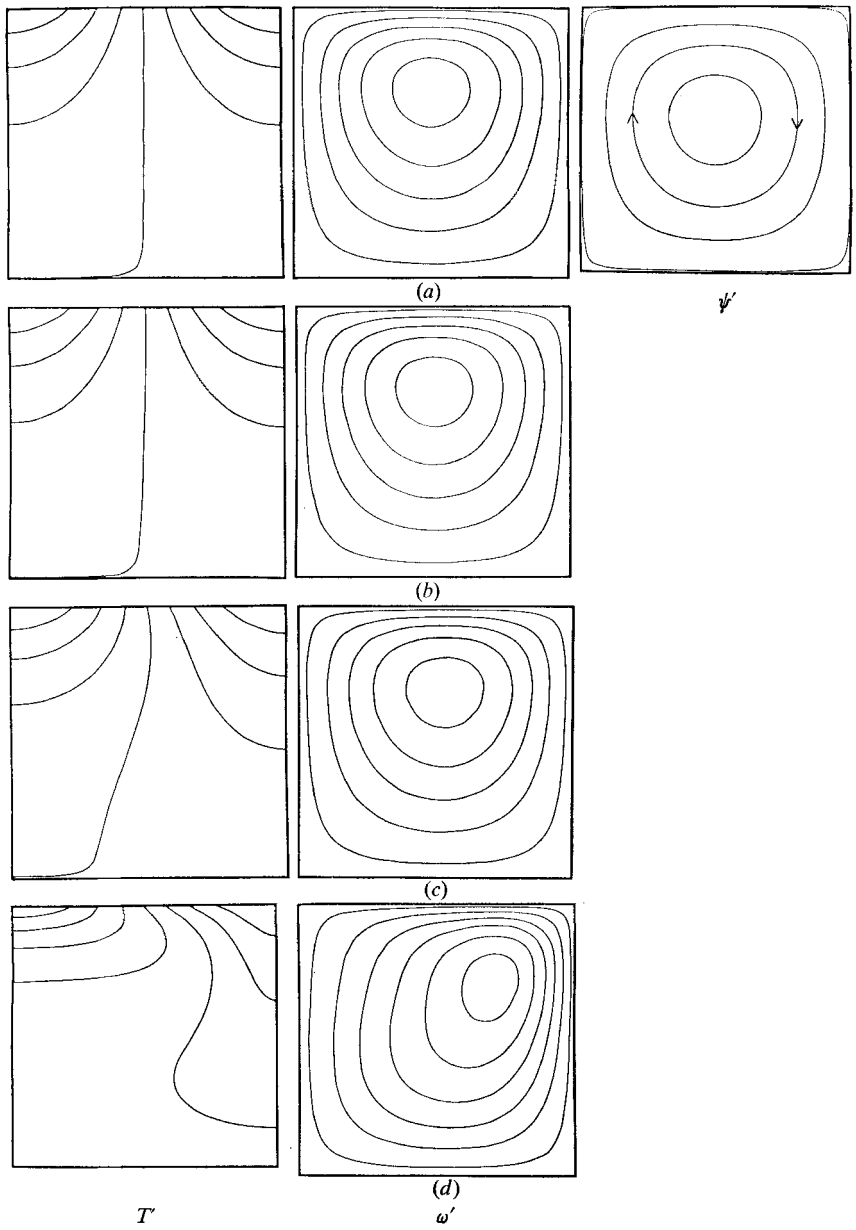

FIGURES 4(*a*)–(*d*). For legend see facing page.

height. Except in the boundary layers the mean temperature gradient is positive everywhere even though the motion is maintained by the release of gravitational potential energy. The other related feature of figure 6 is that the mean horizontally averaged temperature is strongly modified by the convection. The mean temperature of most of the fluid is negative when convection is actively transporting heat.

These results may be compared with those of Beardsley & Festa (1972) by noting that the governing equations are invariant if ψ, z and T are replaced by

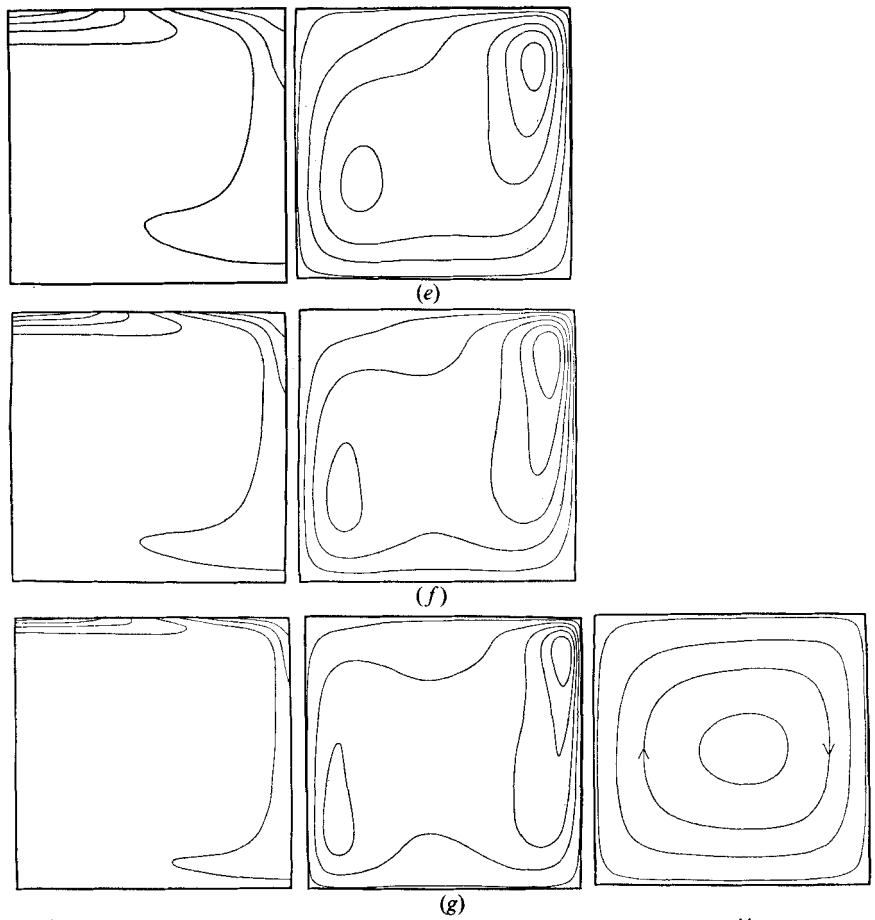

FIGURE 4. Flow driven by a horizontal temperature variation imposed on the upper boundary [equation (31)] and with $T' = 0$ at the lower boundary. All boundaries are stress free and the dimensionless width is unity. Contours of T' are uniformly spaced with interval $\frac{1}{4}\Delta T'$.

	$\Delta T'$	R_H	t'	Contour intervals for ω'		
(*a*)	0·01	4·58	31·7	$1{\cdot}07 \times 10^{-4}$	$(1{\cdot}11 \times 10^{-4})$	$5{\cdot}53 \times 10^{-4}$
(*b*)	0·1	45·8	187·9	$1{\cdot}07 \times 10^{-3}$	$(1{\cdot}11 \times 10^{-3})$	$5{\cdot}53 \times 10^{-3}$
(*c*)	1·0	458	171·4	$1{\cdot}05 \times 10^{-2}$	$(1{\cdot}11 \times 10^{-2})$	$5{\cdot}51 \times 10^{-2}$
(*d*)	10	4580	183·4	0·0319	(0·0728)	0·3959
(*e*)	100	45800	91·4	0·083	(0·392)	2·044
(*f*)	300	137000	12·7	1·155	(0·962)	5·002
(*g*)	1000	458000	6·1	0·433	(2·585)	10·773

Contour intervals for ψ'

(*a*)	$0{\cdot}028 \times 10^{-5}$	$(0{\cdot}737 \times 10^{-5})$	$2{\cdot}239 \times 10^{-5}$
(*g*)	0·0184	(0·0959)	0·3061

The value of t' gives the dimensionless time taken to reach the steady state ($t' = 1$ is equivalent to 45·5 Myr). The numerical experiments were carried out in the order (*a*)–(*d*) on a 24×24 mesh, with each steady-state solution used as the initial temperature distribution for the next run; (*e*) was started from the conductive solution with $\Delta T' = 100$, on a 48×48 mesh and again successive steady-state solutions were used as initial temperature distributions for (*f*) and (*g*).

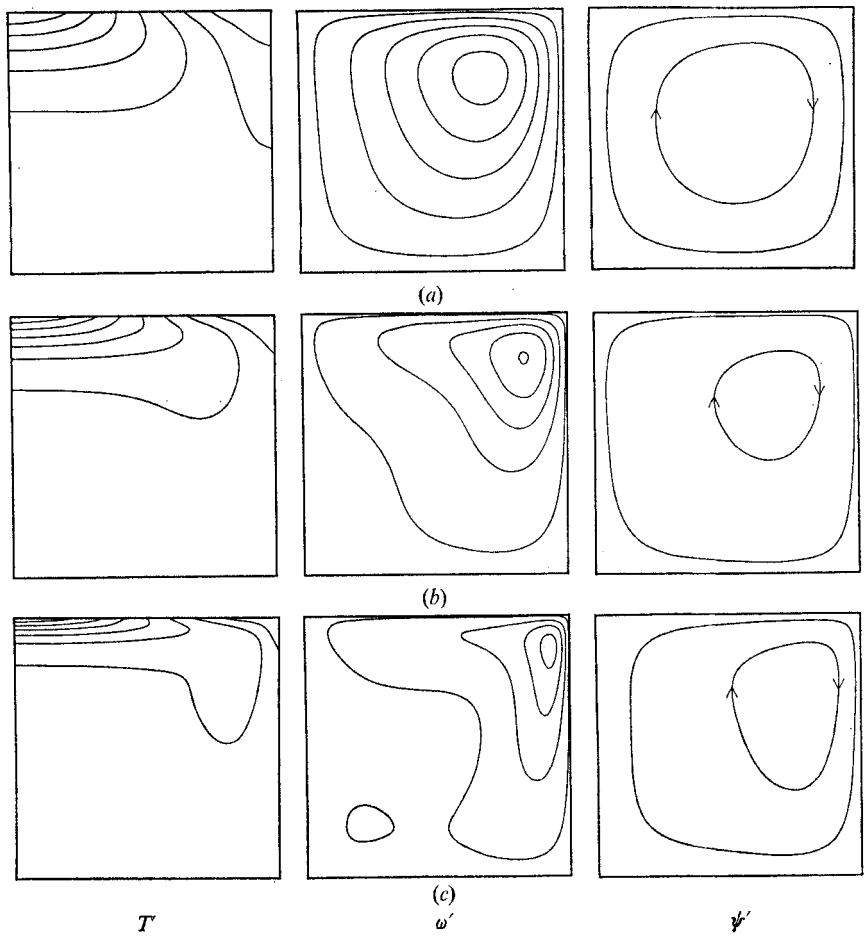

FIGURE 5. Boundary conditions as for figure 4 but with $\partial T/\partial z = 0$ at $z = 0$.

	$\Delta T'$	R_H	t'	Contour intervals for ω'		
(*a*)	10	4580	80·14	0·032	(0·073)	0·324
(*b*)	100	45800	310·8	0·084	(0·392)	1·652
(*c*)	1000	458000	32·37	0·50	(2·59)	8·27

Contour intervals for ψ'

(*a*)	0·00217	(0·0060)	0·00817
(*b*)	0·0039	(0·0223)	0·0262
(*c*)	0·019	(0·047)	0·066

Run (*a*) was started from the appropriate conductive solution and the resulting steady state used to give initial values for (*b*); both were on a 24×24 mesh. Run (*c*) was started from the conductive solution on a 48×48 mesh.

$-\psi$, $-z$ and $-T$. Thus if figures 4 and 5 are looked at upside-down the streamlines and the isotherms are those for a fluid heated non-uniformly from below. A detailed comparison between our results and those of Beardsley & Festa is not feasible since they used $\mathbf{u} = 0$ as a boundary condition on all but one boundary. The same remark applies to Somerville's (1967) calculations, for he used

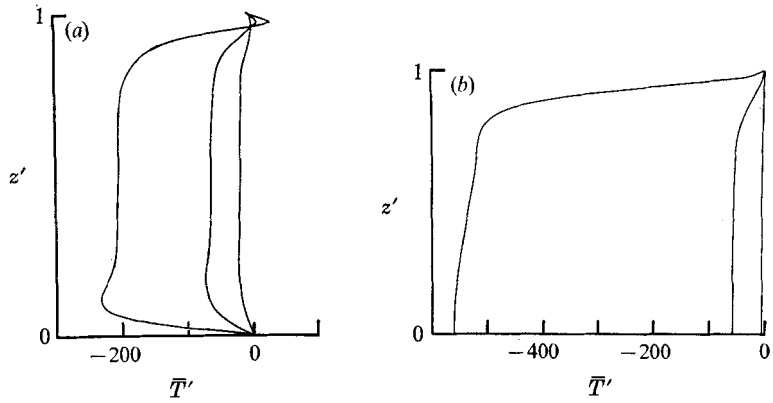

FIGURE 6. The mean horizontal temperature as a function of height (*a*) for the convection in figure 4 and (*b*) for figure 5.

a box with a dimensionless width of ten and different temperature boundary conditions. Despite these differences all numerical experiments show the development of a thermal plume, the asymmetry of the streamlines and the growth of a nearly isothermal region.

5.2. *Convection in a layer uniformly heated from below*

Rayleigh–Bénard convection has been intensively studied for many years. The Rayleigh number R can be defined in terms of the heat flux $E = \rho C_p F$ that would be carried in the absence of convection:

$$R = g\alpha F d^4/\kappa^2 \nu. \tag{37}$$

For the classical thermal boundary conditions:

$$T = \begin{cases} 0 & (z = d), \\ \Delta T & (z = 0), \end{cases} \tag{38}$$

the thermometric flux $F = \kappa \Delta T/d$ and the Rayleigh number

$$R = g\alpha \Delta T d^3/\kappa \nu. \tag{39}$$

A static equilibrium solution exists and is stable for $R < R_c$; when $R = R_c = \frac{27}{4}\pi^4$, convection first occurs in rolls with a normalized cell width $\lambda_c = L/d = \sqrt{2}$ (Chandrasekhar 1961).

The critical Rayleigh number R_c is independent of the Prandtl number p and numerical investigations of finite Prandtl number convection have been made over the range $0{\cdot}01 < p < 100$ for $R/R_c \leqslant 1000$ (Fromm 1965; Veronis 1966; Moore & Weiss 1973). Numerical experiments with an infinite Prandtl number are discussed by Straus (1972) and Moore & Weiss (1973). The efficiency of convection is measured by the Nusselt number N, which is the ratio of the total flux carried to that which would have been carried in the absence of convection: in a steady state,

$$N = \frac{d}{\kappa \Delta T}\left[\overline{wT} - \frac{d\overline{T}}{dz}\right], \tag{40}$$

where the bars denote horizontal averages. For viscously dominated convection Moore & Weiss (1973) found that

$$N \approx 1{\cdot}96\,(R/R_c)^{\frac{1}{3}}. \tag{41}$$

This dependence can be obtained by a simple boundary-layer argument (Turcotte & Oxburgh 1967). The computations show that the bulk of the fluid is isothermal with a temperature $T_M \approx \frac{1}{2}\Delta T$. This isothermal region is contained between two horizontal boundary layers of thickness δ, with temperature gradients T_M/δ; on either side it is bounded by rising and falling plumes also of thickness δ, within which generation of vorticity is balanced by viscous dissipation. Within the horizontal boundary layers the horizontal convection of heat is balanced by the vertical diffusion; thus

$$u(\partial T/\partial x) \approx \kappa(\partial^2 T/\partial z^2), \tag{42}$$

whence $u \approx \kappa d/\delta^2$. In the vertical plumes,

$$\frac{\partial^2 \omega}{\partial x^2} \approx \frac{g\alpha}{\nu}\frac{\partial T}{\partial x}, \tag{43}$$

so that $\omega \approx g\alpha\delta\Delta T/\nu$. But in the centre of the box T = constant, so that $\nabla^2\omega \approx 0$ and we may take $u \approx w \approx \omega d$. Thence we obtain

$$w \approx R^{\frac{2}{3}}\kappa/d, \quad \delta \approx R^{-\frac{1}{3}}d, \quad N \approx R^{\frac{1}{3}} \tag{44}$$

in agreement with the computed results.

Contours of T, ω and ψ for several Rayleigh numbers are included in figures 7–11. The symmetric boundary conditions ensure that these all have point symmetry about the centre of the cell when appropriate intervals are chosen. The boundary layers become narrower as the Rayleigh number is increased.

All the results so far have asssumed that the tangential stress vanishes at the boundary, a condition that has only once been realized in an experiment (Goldstein & Graham 1969). The more realistic case of rigid boundaries, where $\mathbf{u} = 0$, has been extensively studied both theoretically (Chandrasekhar 1961; Fromm 1965; Schlüter, Lortz & Busse 1965; Busse 1967; Plows 1968) and in experiments (Rossby 1969; Krishnamurti 1970*a*, *b*; Willis & Deardorff 1970; Busse & Whitehead 1971). We shall discuss some of these results later in this section.

5.3. *Convection in a fluid heated from within*

The most extensive numerical experiments were carried out on a fluid layer heated from below or within ($\epsilon \neq 0$ in (11)), but with the heat flux rather than the temperature held constant on the lower boundary. The free boundary conditions (17) and (18) still apply but (38) must be replaced by

$$\left.\begin{aligned} T &= 0 \qquad (z = d), \\ \partial T/\partial z &= -f/\kappa \quad (z = 0), \end{aligned}\right\} \tag{45}$$

where f is the thermometric flux through the lower boundary. Then the total heat flux

$$E = \rho C_p F = \rho C_p(f + \epsilon d) \tag{46}$$

and the corresponding Rayleigh number is, from (37),

$$R = (g\alpha d^4/\kappa^2\nu)(f+\epsilon d). \tag{47}$$

As in the previous example, there is always a static equilibrium solution with

$$T = \kappa^{-1}(d-z)[f+\tfrac{1}{2}\epsilon(d+z)]; \tag{48}$$

since only the temperature gradient enters the linearized equations, it is more appropriate to define a mean temperature gradient in terms of the notional temperature difference

$$\Delta T = \kappa^{-1}d(f+\tfrac{1}{2}\epsilon d) \tag{49}$$

together with a modified Rayleigh number

$$R_1 = g\alpha\Delta T d^3/\kappa\nu = (1-\tfrac{1}{2}\mu)R, \tag{50}$$

where the ratio of heat produced internally to the total heat flux is

$$\mu = \epsilon d/(\epsilon d+f). \tag{51}$$

The perturbation equations can be derived in the usual way (Sparrow, Goldstein & Jonsson 1964; Roberts 1967). The critical Rayleigh numbers for fixed boundaries and thermal boundary conditions (38) and (45) were obtained by Sparrow *et al.* (1964) and Roberts (1967) respectively; these values together with the critical wavenumber $a = \pi/\lambda$ are listed in table 2(*a*). We have computed critical Rayleigh numbers as functions of $\mu\,(0 \leqslant \mu \leqslant 1)$ for various boundary conditions, using the method of Sparrow *et al.*, and these results are also shown in table 2. The critical Rayleigh number depends on the boundary conditions and is least for free boundaries with a constant flux, when the constraints are weakest. Although the critical value of R depends on μ, the corresponding value of the modified Rayleigh number R_1 changes only slightly and in one case (free boundaries at fixed temperatures) by less than 1 %. For given boundary conditions, the stability criterion is mainly determined by the average temperature gradients; this is consistent with Krishnamurti's (1968*a*) result, that for $\mu \ll 1$ the critical values of R_1 are approximately $657{\cdot}5-2{\cdot}0\mu^2$ and $1707{\cdot}7-2{\cdot}7\mu^2$ with free and fixed boundaries, at constant temperatures, respectively.

A sequence of two-dimensional numerical experiments was carried out using a square box ($\lambda = 1$), in order to compare results for $\mu = 0$, 0·5 and 1·0 with Rayleigh–Bénard convection carrying the same heat flux. Unless stated otherwise all models were started by introducing a temperature perturbation that produced a single convection roll occupying the whole box; shorter wavelength rolls could only develop by instabilities of this single roll. Contours of the temperature, the vorticity and the stream function for five different values of the mean flux through the upper surface are shown in figures 7–11. Details of the appropriate Rayleigh numbers are provided in table 3; the last column gives the ratio R/R_c that would be needed to give the same flux in the Rayleigh–Bénard problem and so allows a better estimate of the boundary-layer thickness. It can be seen that the Rayleigh number R defined by (47) exaggerates the nonlinearity of the problem; in fact the corresponding Rayleigh–Bénard parameter is proportional to $R^{\frac{3}{4}}$.

The calculations were carried out on grids with 24×24 or 48×48 intervals and integrations were continued until a steady state had been attained. For all

	$z = 0$					
	Constant temperature			Constant flux		
μ	a	R	R_1	a	R	R_1
	(*a*) Both boundaries fixed					
0	3·12	1707·7	1708	2·55	1295·8	1296
1·0	3·13	3390·0	1695	2·63	2772·3	1386
	(*b*) Upper boundary free, lower boundary fixed					
0	2·68	1100·7	1101	2·22	816·7	817
0·2	2·68	1211·8	1091	2·22	906·8	816
0·4	2·68	1347·6	1078	2·23	1018·8	815
0·6	2·68	1517·1	1062	2·23	1162·1	814
0·8	2·68	1734·6	1040	2·24	1351·5	811
1·0	2·68	2022·9	1011	2·26	1612·6	806
	(*c*) Both boundaries free					
0	2·22	657·5	658	1·76	384·7	385
0·1	2·22	692·1	658	1·76	407·5	387
0·2	2·22	730·5	657	1·76	433·1	390
0·3	2·22	773·4	657	1·76	462·1	393
0·4	2·22	821·6	657	1·76	495·3	396
0·5	2·22	876·2	657	1·77	533·7	400
0·6	2·22	938·4	657	1·77	578·4	405
0·7	2·22	1010·4	657	1·77	631·1	410
0·8	2·22	1093·4	656	1·78	694·4	417
0·9	2·23	1191·5	655	1·78	771·6	425
1·0	2·23	1308·5	654	1·79	867·8	434

TABLE 2. Critical Rayleigh numbers for marginal stability (upper boundary at constant temperature)

the results in figures 7–11 adequate resolution was achieved by ensuring that there were at least three intervals across every boundary layer. The accuracy of the coarser grid for $R \lesssim 10^6$ was confirmed by comparison with the finer mesh.

Consider first the models in which the flux is entirely from below ($\mu = 0$). The isotherms are inclined to the lower boundary but as the Rayleigh number is increased the thickness of the thermal boundary layer diminishes. Whether the temperature or the flux is specified on the lower boundary has rather little effect on the flow at all Rayleigh numbers. What differences there are are more apparent in the vorticity field. In the fixed-flux experiments the temperature at the centre of the rising plume is greater than in the Rayleigh–Bénard cases; hence the horizontal temperature gradient and the vorticity are both greater in the lower left-hand than in the upper right-hand parts of the boxes.

The main features of the flow can again be understood by applying a simple boundary-layer analysis. The argument is similar to that for Rayleigh–Bénard convection, except that the temperature difference ΔT across the plumes must be related to the total heat flux.

$$w\Delta T\delta \approx fd. \tag{52}$$

Figure	Flux (W m^{-2})	Rayleigh number R	Heated below R/R_c	Half within, half below R_1	Half within, half below R/R_c	Heated within R_1	Heated within R/R_c	Fixed temperature R/R_c
7	10^{-3}	$2{\cdot}4 \times 10^4$	62	$1{\cdot}8 \times 10^4$	45	$1{\cdot}2 \times 10^4$	28	9·0
8	3×10^{-3}	$7{\cdot}2 \times 10^4$	190	$5{\cdot}4 \times 10^4$	140	$3{\cdot}6 \times 10^4$	83	20
9	10^{-2}	$2{\cdot}4 \times 10^5$	620	$1{\cdot}8 \times 10^5$	450	$1{\cdot}2 \times 10^5$	280	50
10	3×10^{-2}	$7{\cdot}2 \times 10^5$	1900	$5{\cdot}4 \times 10^5$	1400	$3{\cdot}6 \times 10^5$	830	120
11	10^{-1}	$2{\cdot}4 \times 10^6$	6200	$1{\cdot}8 \times 10^6$	4500	$1{\cdot}2 \times 10^6$	2800	280
14, 16–20	$5{\cdot}85 \times 10^{-2}$	$1{\cdot}4 \times 10^6$	3600	$1{\cdot}1 \times 10^6$	2600	$7{\cdot}0 \times 10^5$	1600	190

TABLE 3. Rayleigh numbers for the numerical experiments

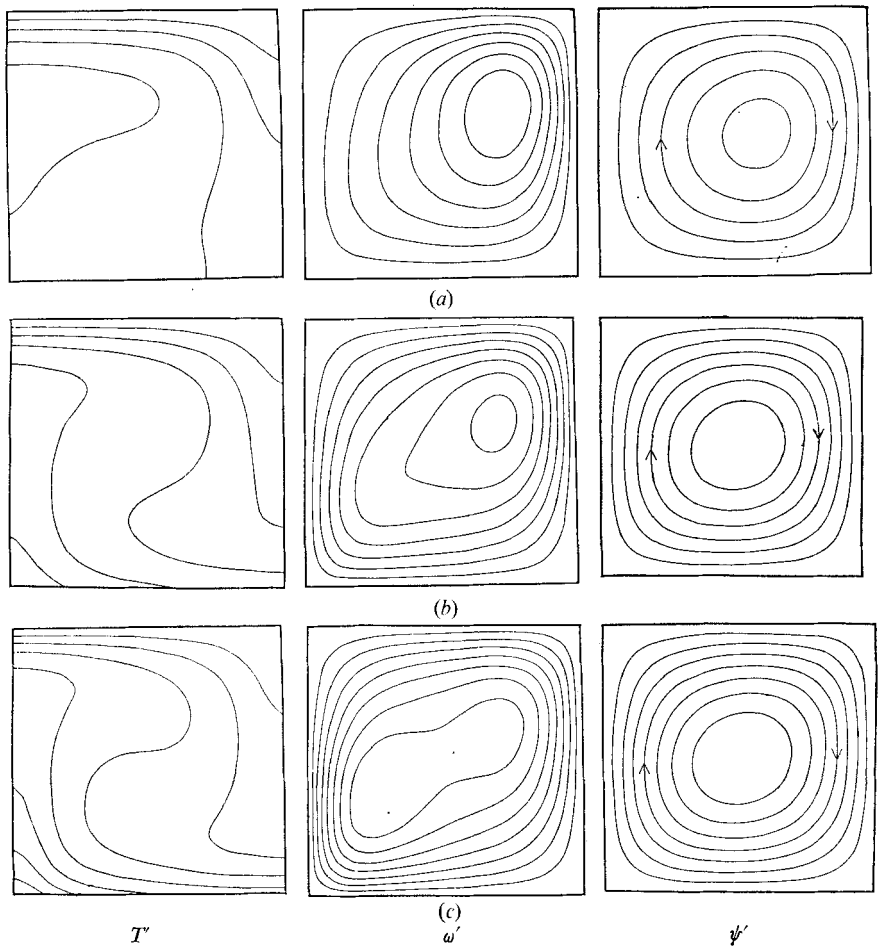

FIGURE 7. Convection in a region whose dimensionless width is unity with insulating sides. The heat flux per unit area is fixed at the lower boundary, the temperature at the upper, and all four boundaries are stress free. The mean flux through the upper surface is 10^{-3} W m^{-2} in all three cases. (*a*) All the heat is generated uniformly within the fluid and no heat enters through the lower boundary. (*b*) Half the heat lost through the upper surface enters through the bottom, the other half is generated uniformly within the region. (*c*) All the flux enters through the lower boundary. The dimensionless times required to establish these steady flows were (*a*) 270, (*b*) 182 and (*c*) 151. (1 unit of dimensionless time is equivalent to 45·5 Myr.) The initial temperature distribution was that for figure 4(*c*) with a linear vertical variation superimposed to give a temperature of 20 at $z = 0$. The calculations were carried out on a 24×24 mesh. Contour intervals: T', 0 (4·34) 30·38; ω', 0 (0·122) 0·854; ψ', 0 (0·00698) 0·0489.

Then, from (42), (43) and (52), we find that

$$\left.\begin{aligned} w &\approx R^{\frac{1}{2}}\kappa/d, \quad \delta \approx R^{-\frac{1}{4}}d, \\ \Delta T &\approx R^{-\frac{1}{4}}(Fd/\kappa) = R^{\frac{3}{4}}(\kappa\nu/g\alpha d^3). \end{aligned}\right\} \tag{53}$$

The apparent differences between (44) and (53) are only a consequence of dif-

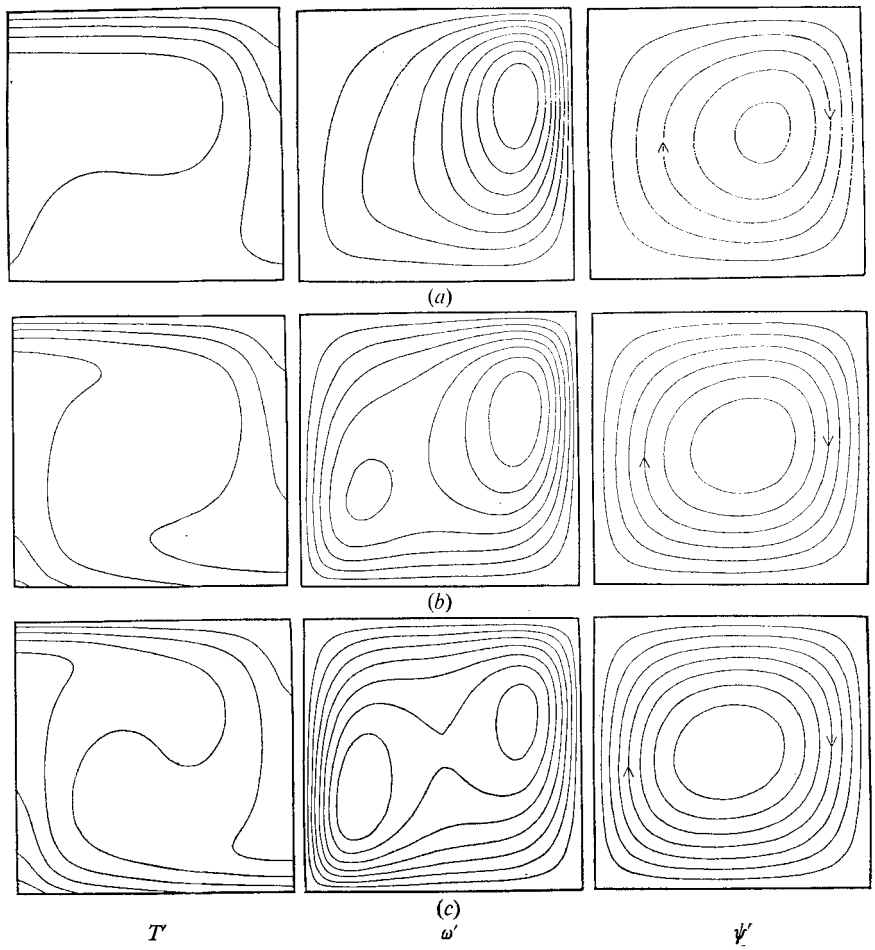

FIGURE 8. Boundary and initial conditions as for figure 7, but with a 3×10^{-3} W m^{-2} mean flux through the upper boundary and corresponding increases in flux through the lower boundary and internal heating rate. The dimensionless times required were (*a*) 197, (*b*) 179 and (*c*) 128. Calculations were carried out on a 24×24 mesh. Contour intervals: T', 0 (9·72) 68·04; ω', 0 (0·22) 1·54; ψ', 0 (0·0118) 0·0826.

ferent definitions of the Rayleigh number. The efficiency of convection can best be measured by defining a modified Nusselt number

$$M = [(1 - \tfrac{1}{2}\mu) Fd]/\kappa \Delta \bar{T}, \tag{54}$$

where $\Delta \bar{T}$ is the mean temperature difference across the layer; M is the ratio of the temperature difference that would be necessary to carry the flux in the absence of convection to that which is actually found (Thirlby 1970). From (53), $M \propto R^{\frac{1}{4}}$ when the flux is entirely from below. The maximum values of the dimensional variables T, u and w are plotted logarithmically against E in figure 13. From the slopes we find that $T \propto R^{0.74}$, $u \propto R^{0.50}$ and $w \propto R^{0.55}$ in good agreement with the predictions of (53). The Nusselt number

$$M = 1{\cdot}58(R/R_c)^{\frac{1}{4}}. \tag{55}$$

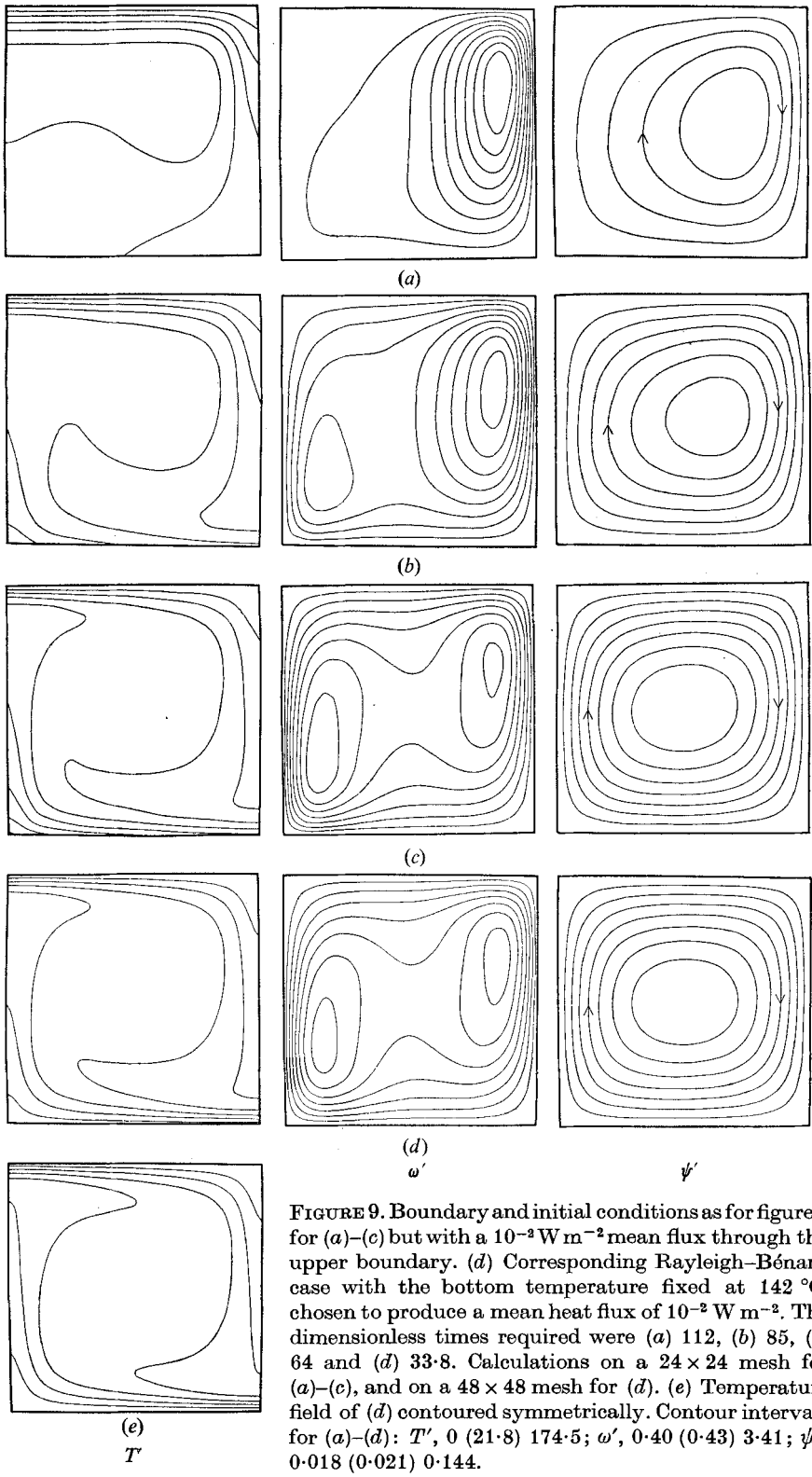

FIGURE 9. Boundary and initial conditions as for figure 7 for (*a*)–(*c*) but with a 10^{-2} W m^{-2} mean flux through the upper boundary. (*d*) Corresponding Rayleigh–Bénard case with the bottom temperature fixed at 142 °C, chosen to produce a mean heat flux of 10^{-2} W m^{-2}. The dimensionless times required were (*a*) 112, (*b*) 85, (*c*) 64 and (*d*) 33·8. Calculations on a 24×24 mesh for (*a*)–(*c*), and on a 48×48 mesh for (*d*). (*e*) Temperature field of (*d*) contoured symmetrically. Contour intervals for (*a*)–(*d*): T', 0 (21·8) 174·5; ω', 0·40 (0·43) 3·41; ψ', 0·018 (0·021) 0·144.

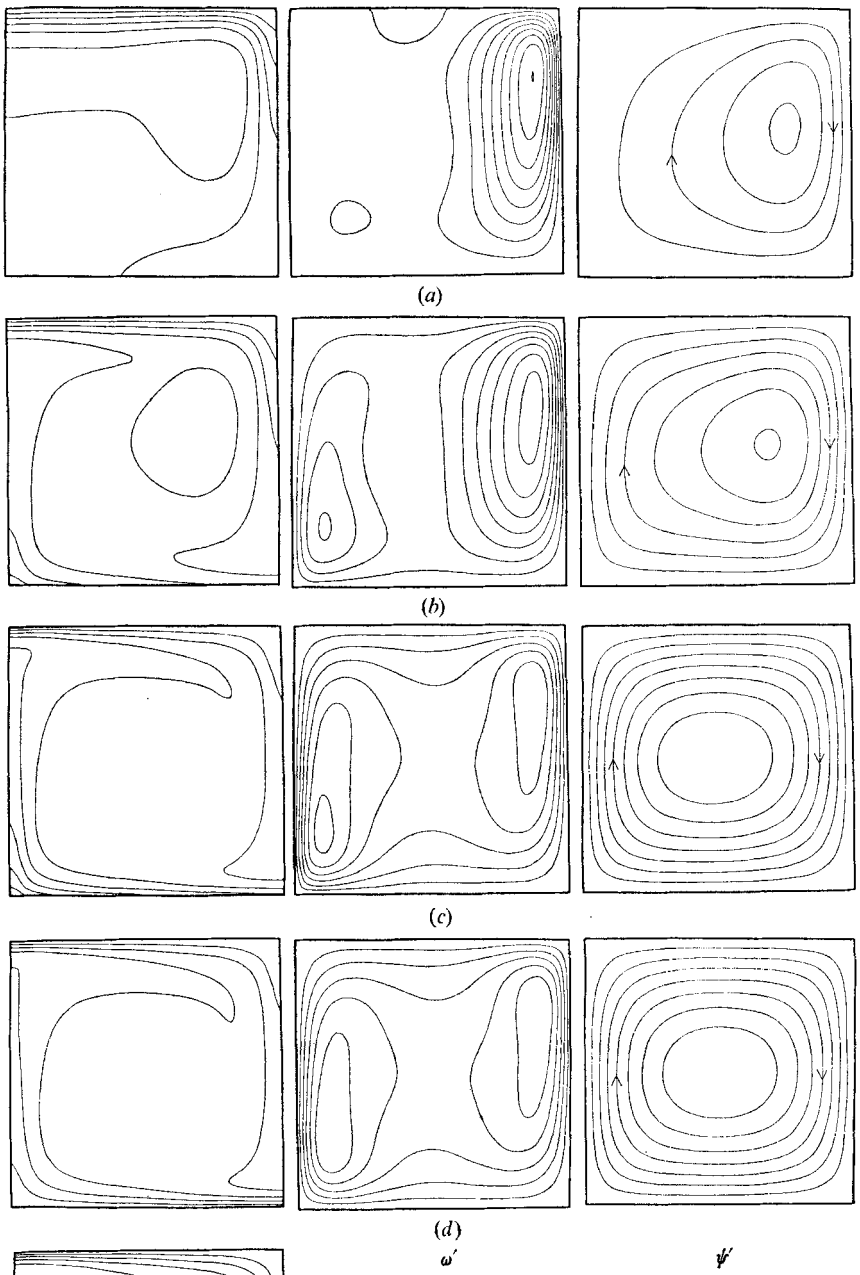

FIGURE 10. Boundary conditions as for figure 9 but with initial temperature distribution that of figure 4(*c*) superimposed on a linear variation with $T' = 200$ at $z = 0$. The mean flux through the upper boundary is 3×10^{-2} W m^{-2}. The bottom temperature for (*d*) is 324 and the initial temperature distribution is that in figure 9(*d*). The dimensionless times were (*a*) 87, (*b*) 75, (*c*) 58 and (*d*) 17·3. The calculations for (*a*)–(*c*) were carried out on a 24×24 mesh until a steady state was reached, and then were interpolated onto a 48×48 mesh. Contour intervals for (*a*)–(*d*): T', 0 (57·0) 399·0; ω', 0·02 (0·97) 7·78; ψ', 0 (0·034) 0·24. (*e*) Same temperature distribution as (*d*) but contoured symmetrically.

For comparison with geophysical measurements it is convenient to use dimensional quantities:

$$\left.\begin{aligned} \log_{10}\hat{T} &= 0{\cdot}74\log_{10}E + 3{\cdot}76, \\ \log_{10}\hat{u} &= 0{\cdot}50\log_{10}E + 1{\cdot}91, \\ \log_{10}\hat{w} &= 0{\cdot}55\log_{10}E + 2{\cdot}13, \\ \log_{10}(\delta/d) &= -0{\cdot}24\log_{10}E - 1{\cdot}57, \end{aligned}\right\} \tag{56}$$

where $\hat{T}$, $\hat{u}$ and $\hat{w}$ are the maximum temperature and horizontal and vertical component of the velocity, measured in °C and mm yr^{-1}, and E is the energy flux in W m^{-2}. The other comparison which can be made is with the computed velocity field. The streamlines near the centre of the cell are indeed circular, as would be the case if ω were constant.

The other extreme case is when all the heat is generated within the layer and $\partial T/\partial z = 0$ at $z = 0$ ($\mu = 1$). Internal heating produces a quite different temperature and flow field. This difference is especially pronounced at high Rayleigh numbers, and is the result of heat being uniformly generated throughout the fluid, yet being lost only from the upper surface. When the heat flux is solely from below, heat can be transported to the upper surface by the rapid motion of a thin sheet of fluid in the plumes and thermal boundary layers, leaving the temperature of most of the fluid in the centre of the cell constant. This type of flow is not possible if heat is generated everywhere because the flow must bring all parts of the fluid close to the upper surface to permit them to lose heat by conduction. There are two ways in which the motion can satisfy this condition. The fluid can rise into the upper boundary layer everywhere except where the cold vertical plume leaves the upper surface, or the flow can become unsteady. The experiments we have carried out suggest that both types of flow occur, but that the time-dependent modes may be suppressed by the symmetry conditions when the flow takes place in a square box. The flow in figures 9–11 shows the development of a broad rising region and a narrow sinking sheet when the box is square. At the highest Rayleigh number (figure 11) the initial single roll was unstable and the flow changed to a double roll by the development of an instability in the upper boundary layers as described in § 5.4 below.

The most striking feature of the isotherms is the detachment of the thermal boundary layer from the upper (active) boundary to give a narrow cold plume, through which all the fluid circulates. This resembles the pattern found when convection was driven by horizontal temperature gradients. The asymmetry in $\partial T/\partial x$ dominated the vorticity and even the stream function. Throughout most of the cell fluid is slowly rising and the vorticity is small. As the Rayleigh number increases, fluid can more readily enter the boundary layer if the cell is attenuated. Thus we should expect the preferred cell width to be a decreasing function of R such that the ratio of the plume's thickness to the cell width is approximately constant. This is confirmed by the development of two cells in our calculations when $R \approx 10^6$, though the detailed behaviour is more complicated.

The simple physical model must take account of the fact that there is no rising boundary layer, so that it is no longer possible to assume that ω is

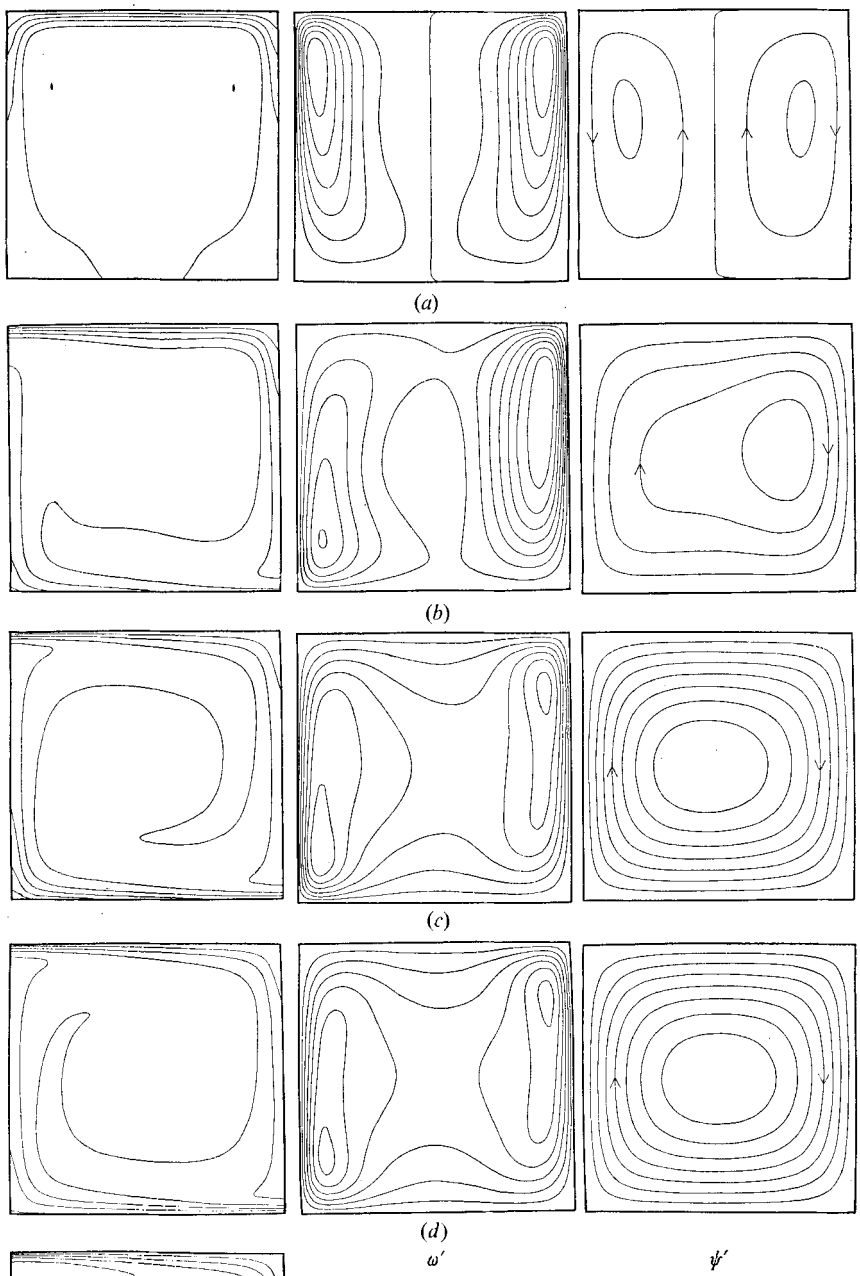

FIGURE 11. Boundary conditions as for figure 9 and initial conditions for (*a*)–(*c*) as for figure 10. The mean flux through the upper boundary is 0·1 W m^{-2}, and the bottom temperature for (*d*) and (*e*) is fixed at 800. The initial temperature distribution for (*d*) was that for figure 10(*d*). The dimensionless times were (*a*) 55, (*b*) 41, (*c*) 29·5 and (*d*) 10·6. The calculations for (*a*)–(*c*) and for (*d*) were carried out in the same way as for figure 10. Contour intervals for (*a*)–(*d*): T', 0 (132·0) 924·0; ω', −10·44 (1·74) 12·18; ψ', −0·122 (0·061) 0·427. (*e*) Same temperature distribution as (*d*) but contoured symmetrically.

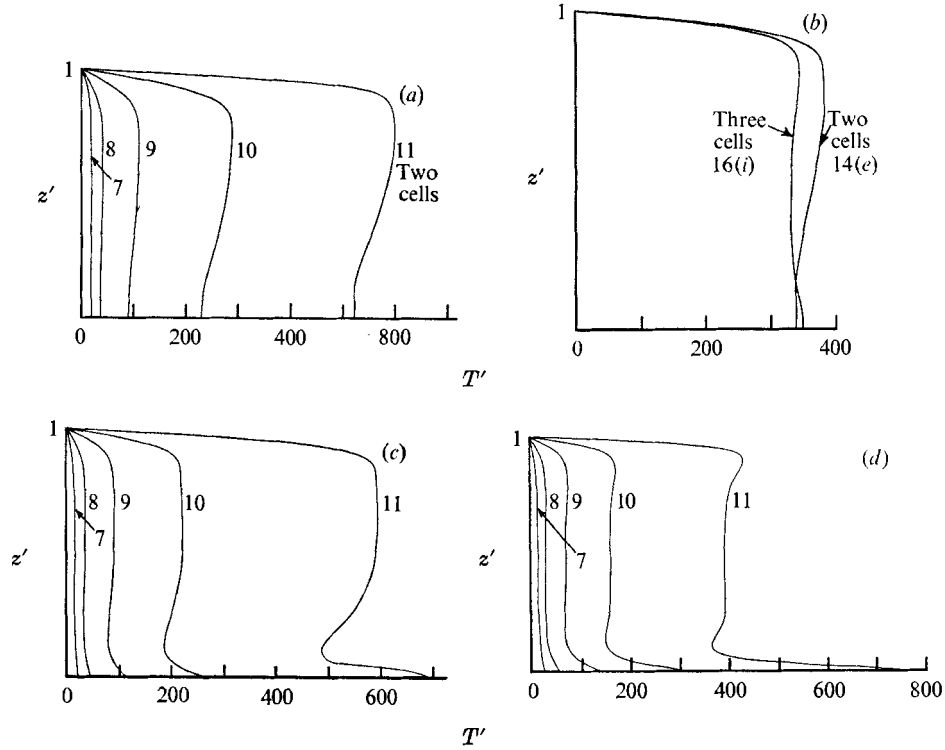

FIGURE 12. Mean horizontal temperature as a function of z'. The number against each curve refers to the figure showing the relevant isotherms. (*a*), (*b*) All heat generated within the fluid. (*c*) Half generated within, half conducted through the lower boundary. (*d*) All conducted through the lower boundary.

approximately constant throughout the main flow. Instead, we must consider a sinking plume of thickness δ and velocity w, together with a rising main flow which carries the heat upwards and moves with a velocity W. Conservation of mass then requires that

$$Wd \approx w\delta. \tag{57}$$

Conservation of energy then demands that the total flux be carried upwards by the main flow and lost by conduction through the horizontal boundary layer at the top of the box, so that

$$W\Delta Td \approx \kappa\Delta Td/\delta \approx \epsilon d^2. \tag{58}$$

Finally, from (43)

$$w/\delta^2 \approx g\alpha\Delta T/\nu. \tag{59}$$

Combining (57)–(59), we then obtain

$$\left.\begin{aligned} w \approx R^{\frac{2}{3}}\kappa/d, \quad \delta \approx R^{-\frac{1}{3}}d, \\ \Delta T \approx R^{-\frac{1}{3}}\epsilon d^2/\kappa = R^{\frac{1}{3}}(\kappa\nu/g\alpha d^3), \end{aligned}\right\} \tag{60}$$

so that the Nusselt number $M \propto R^{\frac{1}{3}}$. The difference between (60) and (53) is caused by the lack of symmetry in the convection. From the results plotted in

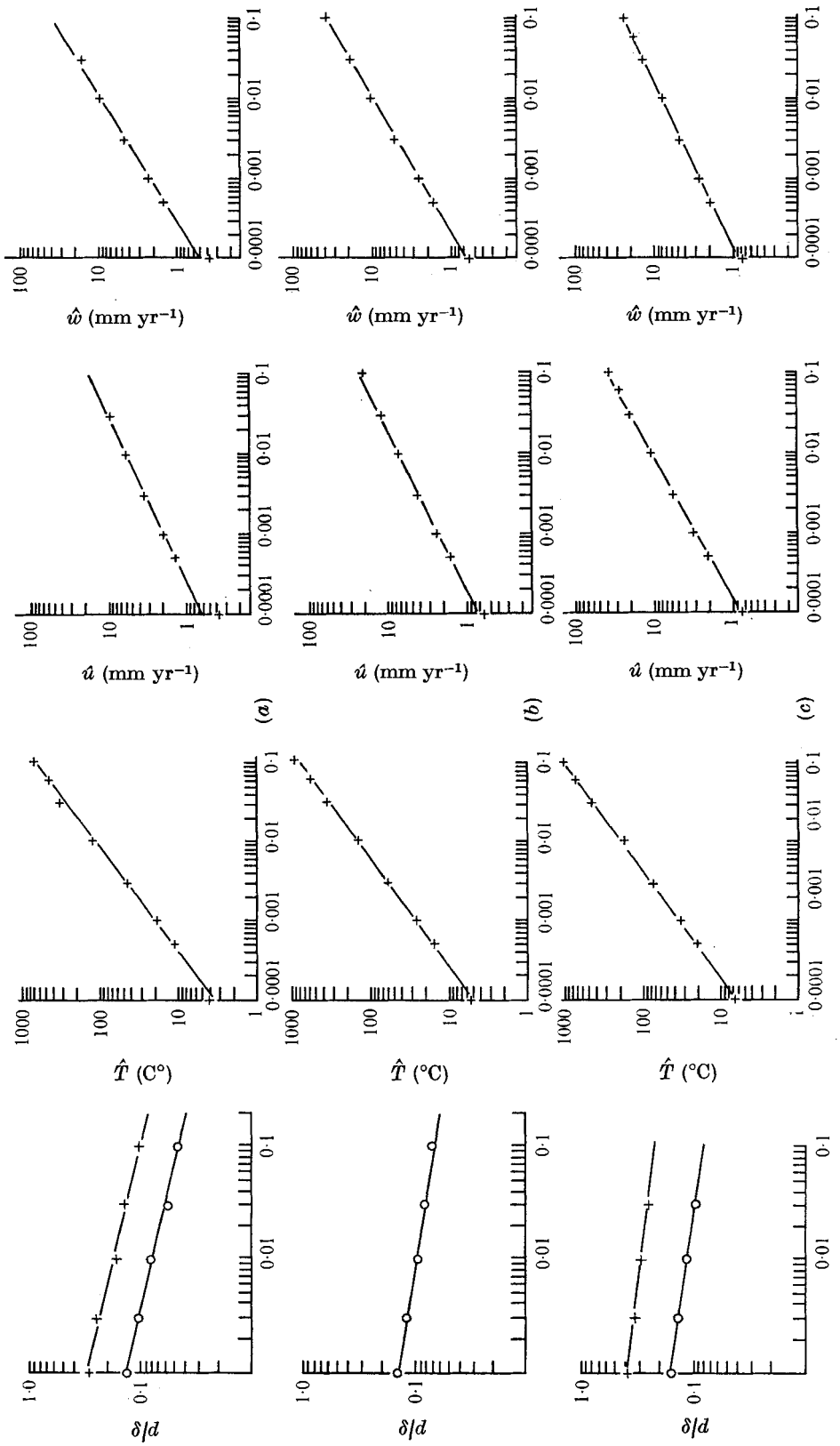

FIGURES 13 (*a*)–(*c*). For legend see next page.

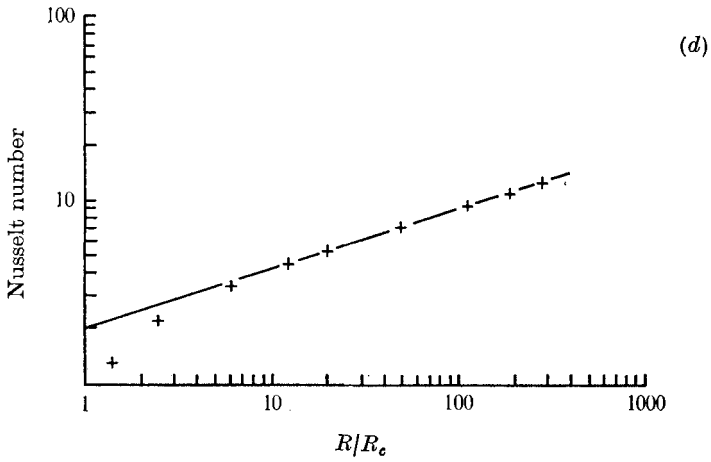

FIGURE 13. Log–log plots of δ/d, $\hat{T}$, $\hat{u}$ and $\hat{w}$ as functions of E for (*a*) all heat supplied internally, (*b*) half supplied internally, half from below and (*c*) all supplied from below. The straight lines are the least-squares best fits given in (56), (61) and (62). Two lines are shown for δ/d for (*a*) and (*c*): ×, values for the depth at which the maxima of the mean temperature in figure 12 occurs; ○, values of δ/d obtained from $\bar{T}_{\max} = -(d\bar{T}/dz)_{z=d}(\delta/d)$. The lines fitted to the circles are given in (56), (61) and (62). (*d*) Nusselt number as a function of R/R_c for the Rayleigh–Bénard cases.

figure 13 we find that $\hat{T} \propto R^{0.76}$, $\hat{u} \propto R^{0.54}$, $\hat{w} \propto R^{0.65}$ and $\delta \propto R^{-0.15}$. Except that for δ, these exponents are in fact closer to the predictions of (53) than to those of (60). The best fit to the numerical results is obtained with

$$\left.\begin{aligned} \log_{10}\hat{T} &= 0{\cdot}76\log_{10}E + 3{\cdot}58, \\ \log_{10}\hat{u} &= 0{\cdot}54\log_{10}E + 1{\cdot}85, \\ \log_{10}\hat{w} &= 0{\cdot}65\log_{10}E + 2{\cdot}28, \\ \log_{10}(\delta/d) &= -0{\cdot}15\log_{10}E - 1{\cdot}25. \end{aligned}\right\} \tag{61}$$

The intermediate case with half the heat supplied from below and half generated internally has features in common with both the other models. The rising plume is less important than the sinking one and the flow carries all the fluid into the upper boundary layer, but at a slower rate than when the energy is generated within. Contours of T, ω and ψ are shown in figures 7–11 and the results are in good agreement with the predictions from the simple model in (53). The best-fitting straight lines give

$$\left.\begin{aligned} \log_{10}\hat{T} &= 0{\cdot}75\log_{10}E + 3{\cdot}71, \\ \log_{10}\hat{u} &= 0{\cdot}49\log_{10}E + 1{\cdot}80, \\ \log_{10}\hat{w} &= 0{\cdot}59\log_{10}E + 2{\cdot}18, \\ \log_{10}(\delta/d) &= -0{\cdot}16\log_{10}E - 1{\cdot}33. \end{aligned}\right\} \tag{62}$$

One feature of the temperature field which is not apparent in figures 7–11 is the mean temperature profile, given by

$$\bar{T}(z) = \frac{1}{L}\int_0^L T(x,z)\,dx,$$

which is shown in figure 12. Malkus (1954) argued that the mean vertical temperature gradient had to be negative everywhere within a convecting region. Though physically plausible his rule does not appear to be obeyed in the numerical experiments described here, nor in those with finite Prandtl numbers (Veronis 1966; Moore & Weiss 1973). Indeed, wherever the flow is dominated by vertical plumes the mean vertical temperature gradient is positive. The physical explanation of this phenomenon is clear from the two-dimensional flow structure in figures 7–11. When the heating is from below the lowest mean temperature occurs just above the bottom boundary layer because the sinking sheet of cold fluid spreads out horizontally and so contributes more to the horizontal average than where the sheet is vertical. The rising sheet shows the same behaviour and therefore the mean temperature gradient is negative away from the boundaries. The cause of the similar behaviour in the internally heated case is more obvious because the cold sinking fluid spreads over the bottom of the box and gradually warms as it rises, becoming hottest before entering the upper horizontal boundary layer. Though these physical explanations of the positive mean temperature gradient are particular to the experiments carried out above, the phenomenon appears to be a general and surprising feature of convection dominated by the nonlinear terms.

Convection driven by internal heating has been investigated in laboratory experiments by Tritton & Zarraga (1967), using water containing dissolved zinc sulphate, with a Prandtl number of 5·5, and heated internally by ohmic dissipation. They found polygonal cells, dominated by descending plumes, whose size *increased* with R. These experiments were repeated by Schwiderski & Schwab (1971), who explained the increased cell widths as a consequence of the variation of electrical conductivity with temperature, which results in non-uniform heating. This conclusion is supported by Roberts' (1967) theoretical treatment and by a careful computational investigation by Thirlby (1970), which indicated that the cell width should decrease, as predicted by our numerical experiments. Thirlby studied two-dimensional convection in water, with *rigid* boundary conditions, for $3000 \leqslant R \leqslant 52000$ $(1 < M < 3)$ and also computed three-dimensional results for $4000 \leqslant R \leqslant 20000$. From the results of these three-dimensional numerical experiments he concluded that convection cells would in fact be three-dimensional provided that the Prandtl number was greater than 2·5.

5.4. *Time-dependent behaviour*

Owing to the limited class of perturbations permitted by the periodic boundary conditions, the existence of steady convection in a square box does not imply that square rolls in a layer of infinite horizontal extent would necessarily be stable at the same Rayleigh numbers. The only instability found in experiments with a square box occurred with internal heat generation. For $R = 2{\cdot}4 \times 10^6$, a single roll developed into two cells (figure 11). The same instability of the single roll occurred with $R = 1{\cdot}4 \times 10^6$ and was studied in detail using this value of the Rayleigh number because the boundary layer was thicker and therefore the errors in the numerical scheme were reduced. This investigation showed both the

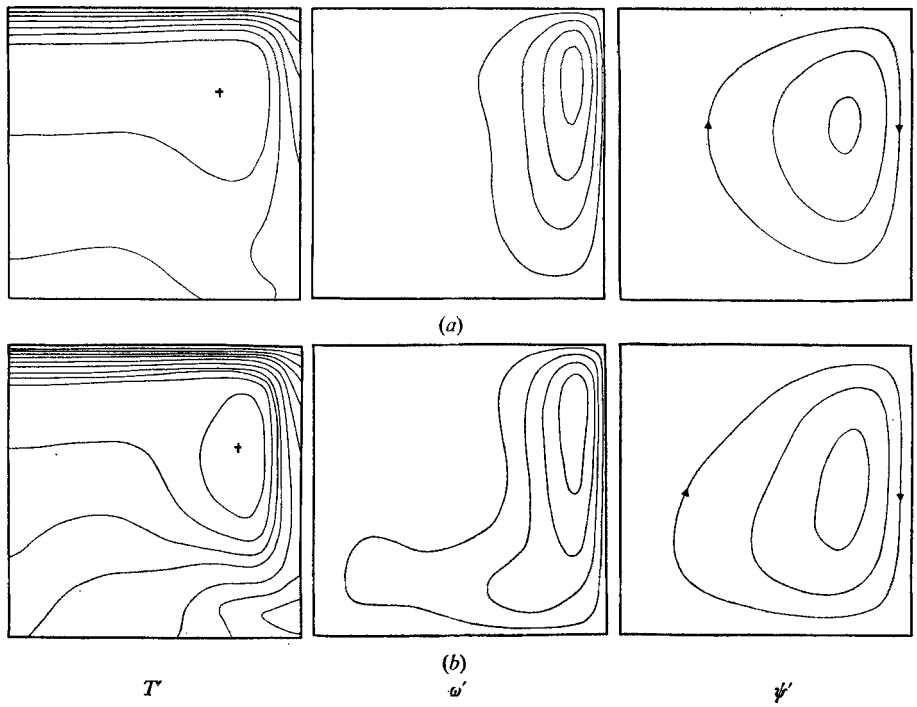

FIGURES 14 (*a*) and (*b*). For legend see facing page.

influence of the periodic boundary conditions and the finite grid size on the development of short-wavelength instabilities.

As in all experiments on a square box the convection was started by perturbing the temperature to form one roll. The flow quickly settled down to a single roll. The temperature and flow fields are shown in figure 14 and closely resemble those in figure 10. The temperature increases steadily in the flow below the boundary layer and the mean temperature gradient is positive except in the upper boundary layer. The isotherms in figure 14 show that the horizontal boundary layer is the only unstably stratified part of the convecting region and therefore we should expect any instabilities to grow there. The local Rayleigh number R_b for the boundary layer is

$$R_b = g(\alpha\delta^3\Delta T/\kappa\nu). \tag{63}$$

Substitution from (60) gives

$$R_b \approx R^{\frac{1}{3}} \tag{64}$$

whereas (53) would give

$$R_b \approx 1. \tag{65}$$

Therefore internal heating, unlike heating from below, tends to produce a boundary layer which becomes more unstable with increasing Rayleigh number. The same argument was used by Busse (1967) to suggest that Rayleigh–Bénard convection between rigid boundaries would become unstable as the Rayleigh number was increased. In our experiments this instability of the boundary layer did not develop until the temperature of the main body of the fluid had increased to a critical value. The experiment was first carried out on a 24×24 mesh with

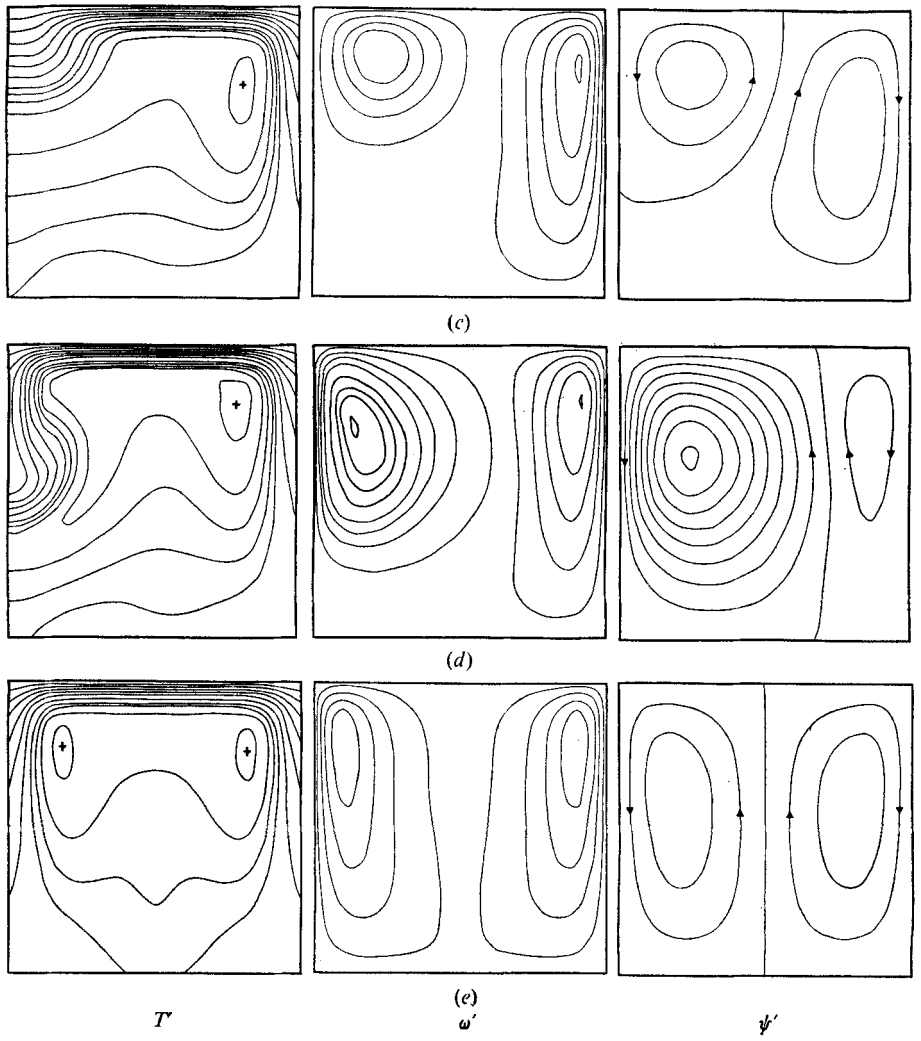

FIGURE 14. The formation of two cells from one on a 24×24 mesh when the mean flux through the upper boundary is $5{\cdot}85 \times 10^{-2}$ W m^{-2} and is all generated within the fluid. Initial temperature distribution that for figure 4(*c*) but with a linear temperature variation $T' = 400(1-z')$ superimposed. (*a*) $t' = 6{\cdot}38$, (*b*) $t' = 16{\cdot}64$, (*c*) $t' = 19{\cdot}14$, (*d*) $t' = 19{\cdot}34$, (*e*) $t' = 147{\cdot}6$. Contour levels: T', 0 (50·0) 350·0 (25·0) 450·0; ω', $-9{\cdot}0$ (2·0) 17·0; ψ', $-0{\cdot}12$ (0·04) 0·32.

the result shown in figure 14. Instability of the boundary layer produced a cold blob of fluid which sank along the left-hand edge of the box, and after the flow had settled down two cells remained. Before the cold blob shown in figure 14 had been produced, several instabilities of the boundary layer had already occurred, but had been swept to the right by the main flow before they had reached a sufficient depth to break up the roll. When these perturbations reached the sinking sheet on the right they produced a considerable increase in the vertical velocity. The kinetic energy as a function of time is shown in figure 15, where the

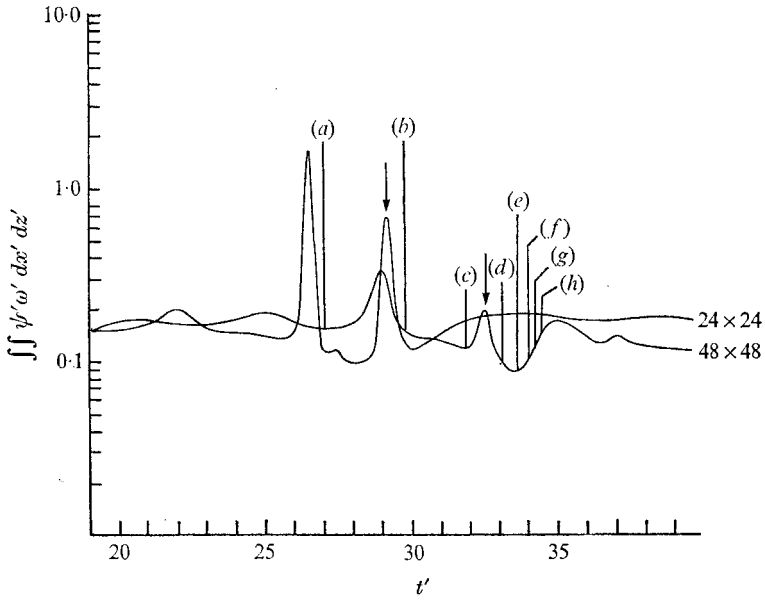

FIGURE 15. $\int_0^1 \int_0^\lambda \omega'\psi'\,dx'\,dz'$ (= $A \times$ kinetic energy, where A is a positive constant) for figure 14 (marked 24×24) and figure 16 (marked 48×48). Initial values of T' for both cases from figure 4(c) with $T' = 200(1-z')$ superimposed. This condition was also used for the calculations in figure 16 but not for figure 14. The instability which breaks the circulation into 2 and 3 cells respectively is marked by an arrow. Vertical lines labelled (a)–(h) correspond to figures 16(a)–(h). The difference between the two curves is the result of inadequate resolution of small-scale temperature variations on the 24×24 mesh. ($t' = 1$ is equivalent to 45·5 Myr.)

time-dependent behaviour before the formation of two rolls is striking. The large peak for both meshes which occurs before the formation of two and three cells is the result of a sinking blob of cold fluid being swept into the sinking sheet before it had penetrated to a sufficient depth to rearrange the circulation.

The experiment was repeated on a 48×48 mesh and the corresponding development together with the kinetic energy as a function of time are shown in figures 16 and 15. The kinetic energy shows similar oscillations but they do not occur at the same time. Furthermore when the instability does develop the blob sinks at some distance from the left-hand edge and the final state has three, and not two, rolls in the square box. The difference in behaviour is the consequence of the importance of the boundary layers in controlling the loss of heat and instabilities. With a 24×24 mesh only the upper two of each column of 24 points lie within the boundary layer. The error analysis of Moore *et al.* (1974) shows that such short-wavelength disturbances are not accurately represented. The representation of the convective terms is less accurate than that of the diffusive, and the combined result of both is equivalent to a higher value of the diffusion coefficient and thus a lower Rayleigh number for short-wavelength disturbances. Although the difference between the results from the 24×24 and 48×48 meshes depends on the detailed treatment of two-dimensional short-

wavelength disturbances, which cannot be represented simply by changing the Rayleigh number, the discrepancy between the two experiments is not surprising. Nevertheless, the qualitative behaviour of the 24×24 mesh is the same as that at higher resolution except that the final state consists of two rather than three rolls. This difference is the consequence of the exact position at which the blob falls, combined with the limitations imposed on further instabilities by the reflexional symmetry. Once a two- or three-roll flow has developed it cannot easily be changed.

These experiments show that square rolls are not stable at Rayleigh numbers above $1{\cdot}3 \times 10^6$. It is desirable to discover the preferred width of rolls at all Rayleigh numbers, but this information appears to require numerical experiments in very wide boxes. Malkus (1954) suggested that the flow in the Rayleigh–Bénard problem is such as to maximize the convective heat transport for a given temperature difference. The corresponding principle, if the mean heat flux is fixed, is the minimization of the maximum temperature of the fluid. This criterion is easy to apply but it does not seem to agree with the experimental observations. Busse (1967) studied Rayleigh–Bénard convection with rigid boundary conditions and showed that the wavenumber of the rolls for which the heat flux was greatest increased from 3·117 at the critical Rayleigh number to approximately 3·8 at $R/R_c = 5{\cdot}85$. The width of the stable rolls should therefore decrease with increasing Rayleigh number. Krishnamurti (1970*a*) has carried out experiments with the same boundary conditions as Busse used, and has found that the width of the rolls increases as the Rayleigh number is increased. Busse & Whitehead (1971) carried out a series of elegant experiments which strongly supported Busse's (1967) theory, and also studied the interaction between rolls of different widths. They showed that wide rolls generally grew at the expense of narrower ones even if the larger rolls were themselves unstable. The numerical experiments described below show the same phenomenon. It is clear from these experiments that Malkus's (1954) criterion does not provide an accurate method of determining the preferred aspect ratio of an individual roll, which can only be discovered by carrying out experiments in boxes containing many cells (Foster 1969).

Furthermore, numerical experiments by Lipps & Somerville (1971) showed that it is essential to permit three-dimensional disturbances to be present if the Nusselt number obtained from the numerical calculations is to agree with that observed even though the resulting flow is two-dimensional. This result is of interest because it demonstrates that two-dimensional calculations will not show the increase in λ with increasing Rayleigh number observed in laboratory experiments. The manner in which three-dimensional motions achieve this change in the form of the flow is more clearly displayed by the laboratory experiments of Willis, Deardorff & Somerville (1972). Though these results show the importance of three-dimensional motions in the evolution of two-dimensional flows, they do not suggest that the small values of λ found in the internal-heating experiments described here are a result of the restriction of the flow to two dimensions. Neither the numerical nor the laboratory experiments suggest that the existence of three-dimensional transient motions can produce a steady

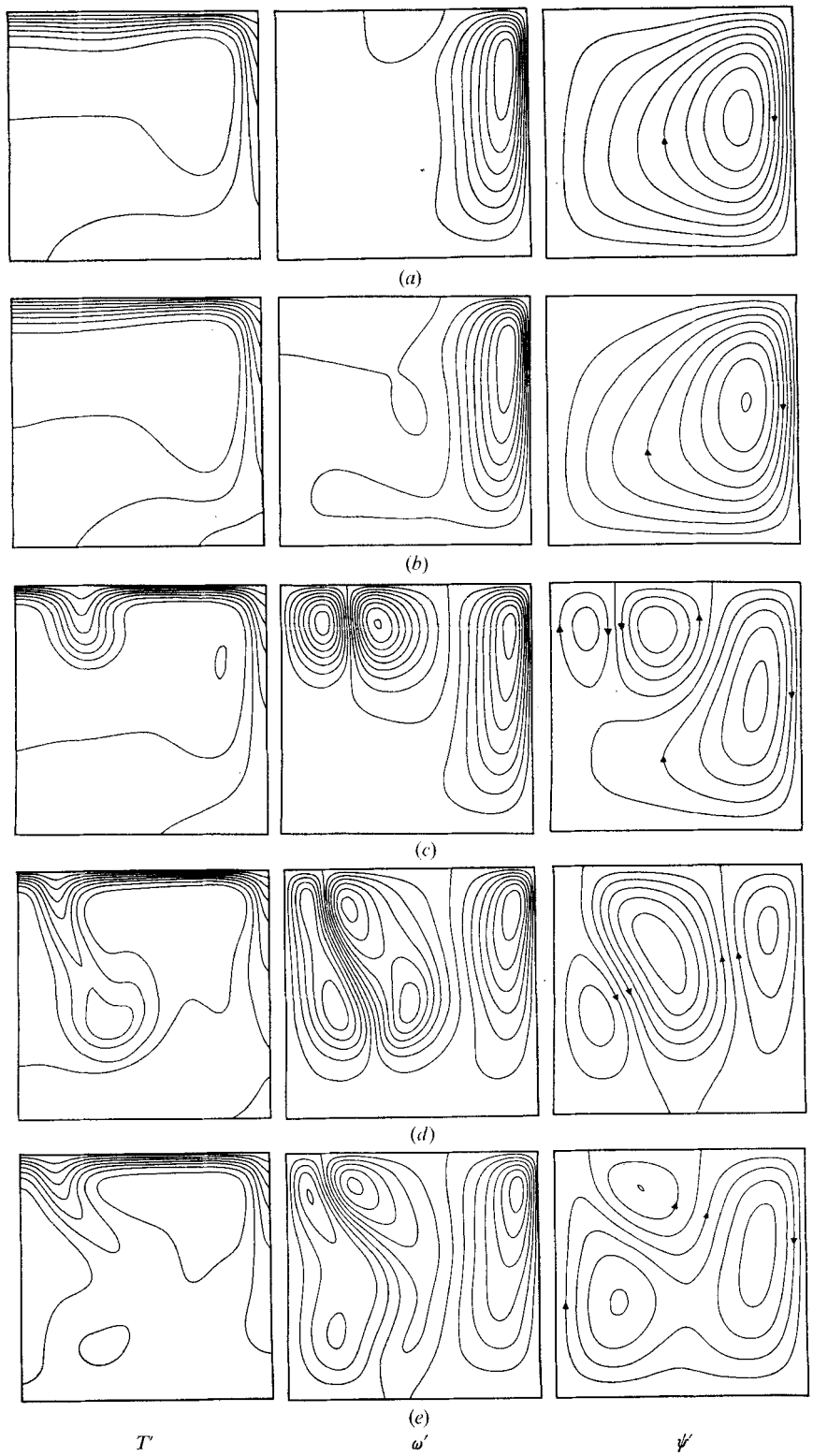

FIGURES 16 (a)–(e). For legend see facing page.

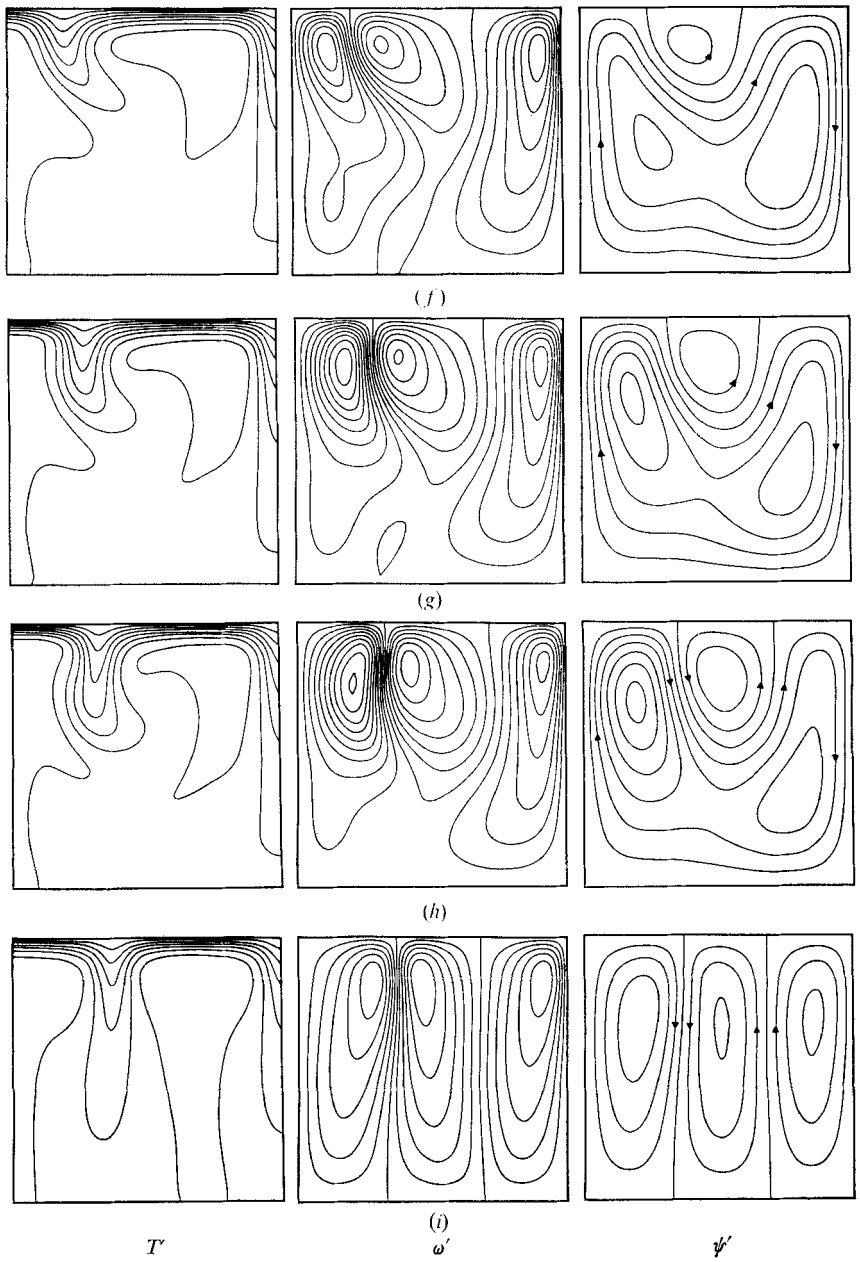

FIGURE 16. Boundary conditions as for figure 14, initial values of T' from figure 4(*c*) with $T' = 200(1-z')$ superimposed. Calculations carried out on a 48 × 48 mesh. (*a*) $t' = 27{\cdot}16$, (*b*) $t' = 29{\cdot}77$, (*c*) $t' = 32{\cdot}05$, (*d*) $t' = 32{\cdot}80$, (*e*) $t' = 33{\cdot}61$, (*f*) $t' = 34{\cdot}01$, (*g*) $t' = 34{\cdot}25$, (*h*) $t' = 34{\cdot}41$, (*i*) $t' = 53{\cdot}77$. Contour intervals: T', 0 (61·5) 492·0; ω', $-10{\cdot}4$ (1·3) 11·7; ψ', $-0{\cdot}095$ (0·019) 0·150.

two-dimensional flow which is itself unstable to two-dimensional disturbances: indeed such a result would be very surprising.

An attempt was made using a 48×24 mesh to investigate the flow in a box whose width was twice its height, containing two square cells and with a Rayleigh number of $1{\cdot}4 \times 10^6$. Judging by the results from the square box at the same value of the heat flux, the behaviour of such an experiment is likely to be qualitatively correct, though the resolution will be insufficient to describe accurately the temperature field in particular. The experiment was first carried out with all the heat generated internally, starting the convection as usual with one roll in the box. The flow was unstable and broke down into two rolls with both sinking plumes at the vertical boundaries of the box. The subsequent behaviour is shown in figure 17. As was expected from the experiments on a square box at the same Rayleigh number the boundary layer becomes unstable and forms a cold sinking blob, followed by the formation of four rolls. Since the blob does not fall exactly in the middle of the box two of these rolls are larger than the other two. The larger rolls grow at the expense of the smaller until the sinking sheet which was formed by the blob joins one of the sinking sheets at the edge of the box. The velocities increase for a short time when this happens, but the flow and temperature fields soon return to a pattern which resembles that which existed before the instability developed. However, this state is unstable, a new blob forms and the whole cycle is repeated. Since the dimensionless repeat time τ_r is governed by the time taken to eliminate the two smaller rolls, and since this in turn depends sensitively on the exact position at which the cold blob sinks, the oscillation is not periodic and observed values of τ_r covered the range $3 < \tau_r < 4$. Various initial conditions were tried, to determine if the time-dependent behaviour was the result of an attempt to find a steady state not compatible with the starting conditions. The behaviour of the fluid was the same whether the experiment was started with two, three or four rolls, in the box, though the time taken for it to become established was not. This experiment is barely within the resolving power of the numerical scheme used, as the experiments with a square box and different mesh sizes showed. The development of the sinking blob is, however, the critical event, and it reproduces the behaviour found in a square box. For this reason we believe that the time-dependent behaviour may be a feature of the solution of the nonlinear equations and not just an artifact of the numerical scheme. This belief should, however, be checked using a finer mesh. If a steady state were attained, the time taken to reach it would be the thermal time for the box,

$$\tau_\kappa = L^2/\pi^2\kappa, \tag{66}$$

which is far greater than the turnover time $\tau = d/V$. (For the earth, $\tau \sim 10^7$ yr but $\tau_\kappa \approx 4 \times 10^9$ yr, which is comparable with the age of the earth.)

Time-dependent flow did not occur with $R = 7{\cdot}2 \times 10^5$ and a normalized cell width $\lambda = 2$. This difference could either have been caused by the existence of a steady solution for an infinite layer, or by the suppression owing to reflexional symmetry of the instabilities which would have produced time-dependent behaviour. Experiments with $\lambda = 2$ and $R = 1{\cdot}4 \times 10^6$, but with half or all the

flux coming from below, also showed time-dependent behaviour. However, because the horizontal velocities at the upper surface were more rapid than for the internal-heating experiments, the boundary-layer instabilities were carried into the sinking sheet before they could form two rolls.

These results should be compared with Krishnamurti's (1970*b*) careful experiments at large Rayleigh number, and with the ideas and calculations of Howard (1966) and Foster (1971). The Rayleigh number required to maintain the same heat flux in a Rayleigh–Bénard experiment is $1{\cdot}2 \times 10^5$, which is almost two orders of magnitude less than that believed by Foster (1971) to be necessary for time-dependent flow. Foster, however, used the mean-field equations to establish this limit, and since these equations assume that both the flow and any disturbances to it have a single horizontal wavenumber, the class of disturbances by which time dependence is produced in a box with $\lambda = 2$ is suppressed by the mean-field equations. Clearly Krishnamurti's (1970*b*) experiments permit instability to a yet wider class of disturbances, and particularly three-dimensional forms. It is therefore not surprising that she finds that time-dependent behaviour for three-dimensional flow occurs when $R/R_c = 34$. Furthermore, her experiments were carried out in a fluid confined between rigid walls, and as Busse (1967) has pointed out, the boundary layers for such flows are less stable than those formed with the free boundary conditions used here.

Recently Kulacki & Goldstein (1972) have carried out a series of experiments on an internally heated layer confined between rigid isothermal plates. They observed time-dependent behaviour very similar to that described above but at considerably lower Rayleigh number ($R/R_c \approx 10$). This difference is not surprising since the upper boundary layer in their experiments is likely to be more unstable than that in our numerical experiments because three-dimensional perturbations are permitted and the rigid boundary condition results in a thicker layer. Despite these differences in experimental conditions the form of the instabilities of the upper boundary layer, the growth of the larger cells at the expense of the smaller and the lack of steady flows described by Kulacki & Goldstein are strikingly similar to figure 17.

5.5. *Validity of the numerical results*

The computations described above were all two-dimensional and assumed periodic boundary conditions in the x direction. This symmetry applies both to the main flow and to any perturbations which affect it. The most significant limitation of these models is that the resulting solutions may well be unstable if a wider class of disturbances is admitted.

The discussion of time-dependent behaviour indicates that the solutions we have obtained may be unstable to two-dimensional disturbances which do not possess the imposed reflexional symmetry. Though the importance of this limitation can be reduced by increasing the width of the box, programming and computing considerations limited our work to models with $\lambda \leqslant 2$.

The problem of the stability of the solutions obtained below to three-dimensional perturbations, or two two-dimensional perturbations in a plane different

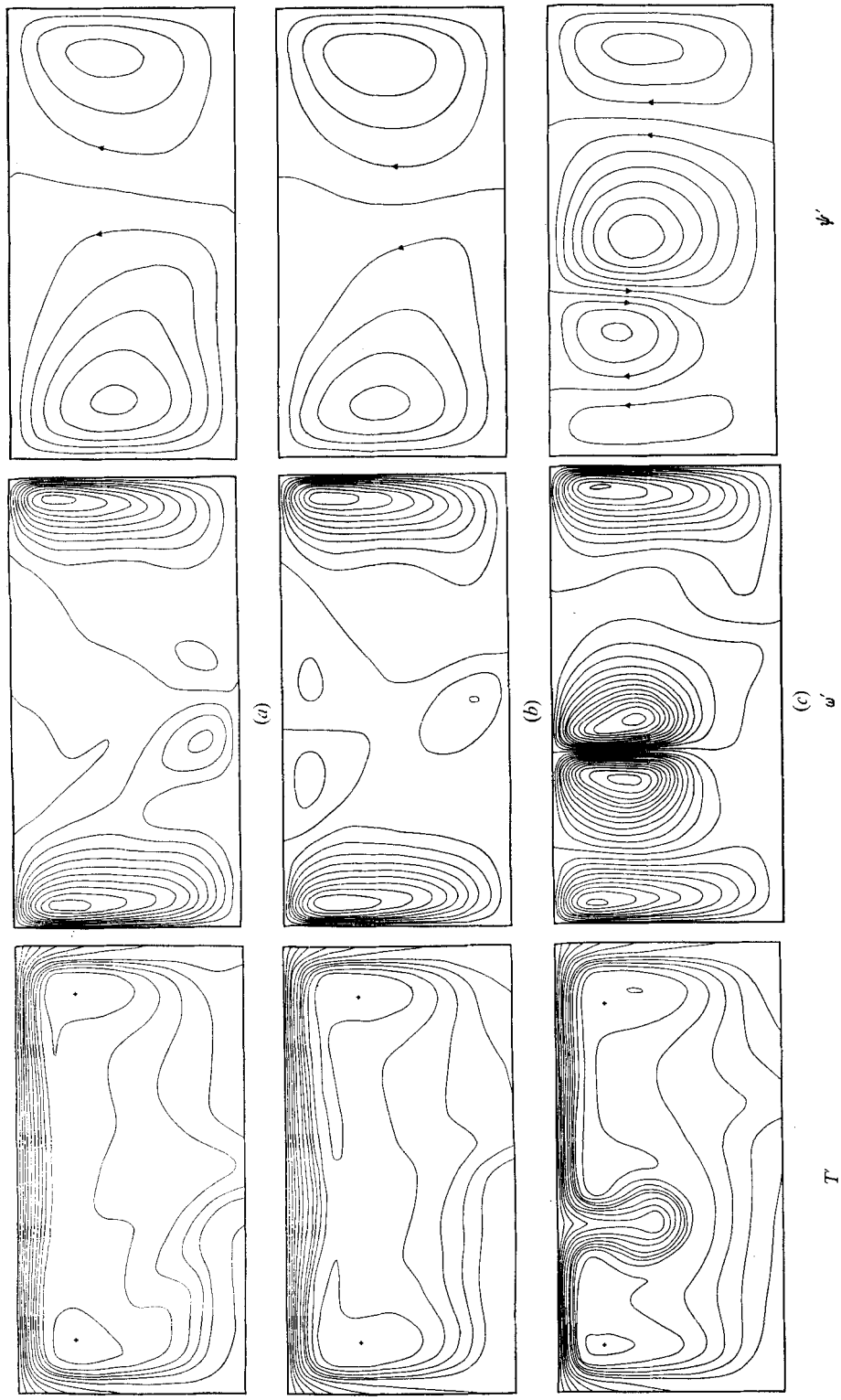

FIGURES 17 (*a*)–(*c*). For legend see page 518.

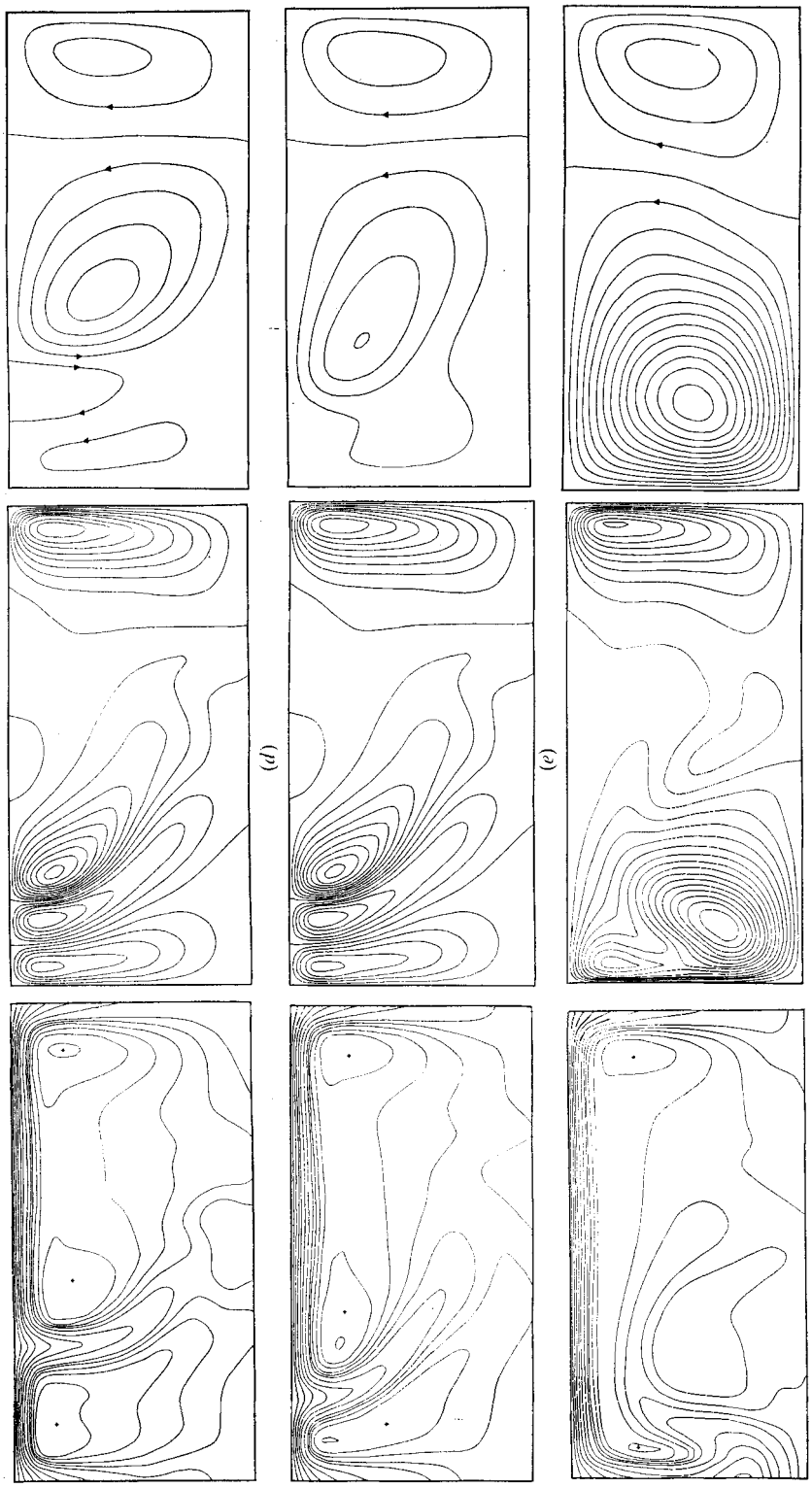

FIGURES 17 (*d*)–(*f*). For legend see page 518.

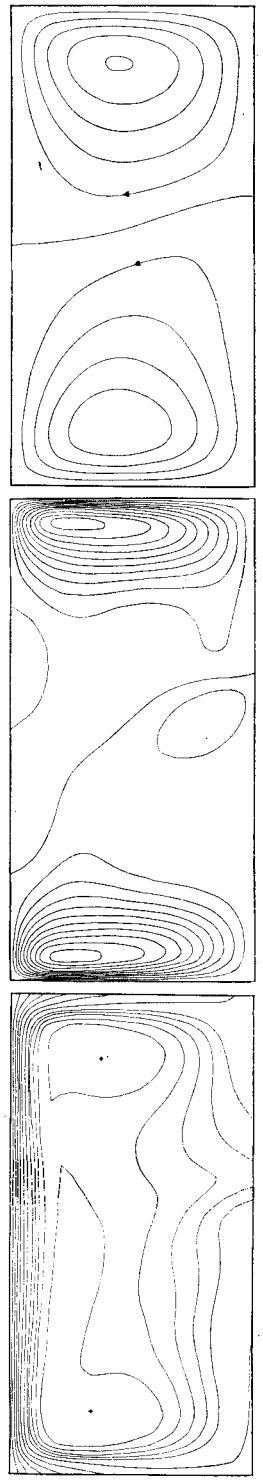

FIGURE 17. Time-dependent behaviour of a fluid heated only from within, in a box with $\lambda = 2$. Initial conditions:

$$T' = \cos(\pi x'/\lambda)\sinh(\pi z'/\lambda)/\sinh\tfrac{1}{2}\pi + 400\,(1-z');$$

other boundary conditions as for figure 14. Calculations carried out on a 48×24 mesh with square cells. (*a*) $t' = 38{\cdot}70$, (*b*) $t' = 39{\cdot}49$, (*c*) $t' = 40{\cdot}70$, (*d*) $t' = 41{\cdot}74$, (*e*) $t' = 42{\cdot}79$, (*f*) $t' = 43{\cdot}69$, (*g*) $t' = 45{\cdot}48$. Contour intervals: T', 0 (50·0) 350 (25·0) 475·0; ω', $-15{\cdot}0$ (1·0) 10·0; ψ', $-0{\cdot}52$ (0·04) 0·12.

from that of the main flow, can obviously not be tested by the present numerical scheme. The stability of Rayleigh–Bénard convection between rigid boundaries has been extensively studied both theoretically (Schlüter *et al.* 1965; Busse 1967) and experimentally (Rossby 1969; Krishnamurti 1970*a*, *b*; Willis & Deardorff 1970; Busse & Whitehead 1971). The agreement between theoretical and experimental results is impressive, and both show that for $R \lesssim 9R_c$ the only stable form of convection is in two-dimensional rolls. For $9R_c < R \lesssim 13R_c$ both rolls and certain other forms of convection are stable, whereas for $R \gtrsim 13R_c$ rolls of all wavelengths are unstable to three-dimensional perturbations and are replaced by a bimodal form of convection (Busse & Whitehead 1971). The transitions, which occur at higher Rayleigh numbers, to time-dependent three-dimensional flow and to turbulence have been studied experimentally (Rossby 1969; Krishanmurti 1970*b*; Willis & Deardorff 1970) but have not yet been described by any satisfactory theory.

The corresponding problem when convection is driven by internal heat sources has been much less studied. Krishnamurti (1968*a*, *b*) investigated an equivalent problem at Rayleigh numbers close to the critical value. She discussed the behaviour of a layer of fluid bounded by horizontal surfaces at uniform temperatures when the average of the upper and lower temperatures changed at a rate η. This corresponds to heating from within and below, with $\mu = -\eta/(1-\frac{1}{2}\eta)$. Krishnamurti showed both theoretically (1968*a*) and experimentally (1968*b*) that rolls were the preferred form of instability at the critical Rayleigh number only when $\eta \approx 0$. When $|\eta| > 0{\cdot}1$ hexagons are stable and rolls are not. Moreover, the hexagons have a rising region in the centre if $\eta < 0$ (up-hexagons) and a sinking region if $\eta > 0$ (down-hexagons). As the Rayleigh number is further increased, the hexagons become unstable and are replaced by rolls. Thus her study shows that for a fluid heated entirely from within ($\eta = -2$) there is a region close to the critical Rayleigh number where up-hexagons should exist.

The agreement between experiment and theory so strikingly demonstrated by Krishnamurti is less satisfactory at higher Rayleigh numbers. Roberts (1967) used the mean-field equations to examine the stability of rolls and hexagons to small perturbations. He found that rolls are marginally stable at all Rayleigh numbers. Up-hexagons are always unstable and down-hexagons are stable only for $R \gtrsim 3R_c$. The one wavenumber for which marginally stable rolls exist increases slowly with increasing R. Thirlby (1970) concluded from his numerical experiments that the cells would always be three-dimensional. Near the critical Rayleigh number, they are rectangular, developing into hexagons for $R \gtrsim 4R_c$. The flow is always downwards at the centre of the cells. The experiments of Tritton & Zarraga (1967) and Schwiderski & Schwab (1971) also gave down-hexagons, though the horizontal wavenumbers disagreed with theory. Further experiments are required to investigate the differences between the Rayleigh–Bénard case and convection driven by internal heating.

The calculations described here are only two-dimensional. Both Busse (1967) and Roberts (1967) have shown that, as R is increased, rolls first become unstable to perturbations which cannot be represented in our numerical model. These instabilities will therefore be suppressed. Though such instabilities can probably

only develop where the mean temperature is unstably stratified and rolls will be stabilized by free boundaries, it would nevertheless be desirable to carry out an analysis similar to that of Busse (1967) on the models computed here.

The restriction on the planform of permitted instabilities is the major limitation of this study. Therefore even though the solutions obtained here are good approximations to the exact solutions of the governing nonlinear equations it does not necessarily follow that they are stable solutions, nor that any instabilities they may show are in fact instabilities which apply to the full solutions. The solutions do, however, illustrate the physical processes which must govern convection at high Rayleigh numbers. In particular they show how boundary layers are developed and the possibility that they may become gravitationally unstable. The understanding of convection at high Rayleigh numbers gained with the help of these numerical experiments will now be used to investigate some features of convection in the mantle.

Apart from the geometrical limitations discussed above it must be remembered that our model is undoubtedly too simple to reproduce the major features of plate motions. The two most important effects which are omitted are the variation of viscosity with temperature and the shear-stress heating. Without the first plates could not exist, and simple order-of-magnitude calculations suggest that the second may govern the temperature structure in critical parts of the boundary layers. Furthermore, we have only considered zero-stress conditions at the lower boundary. Nevertheless, despite its simplicity, the model we have used can, we believe, be related to geophysical measurements on the earth. Moreover, the complicated behaviour of this simple model illustrates the difficulties likely to be encountered in producing a realistic model of convection in the mantle.

6. Geophysical implications for mantle convection

There is at present no means by which the streamlines or the temperature structure of convection in the earth's mantle can be observed. The few known phenomena which are directly related to the flow have been discussed in §2, and it is with these that the numerical experiments should be compared. If surface observations of long-wavelength gravity anomalies, regional changes in the elevation and heat flow are to be related to the models obtained in the previous section, corresponding values must be calculated from the flow and temperature fields. The methods by which these quantities were obtained are discussed in the appendix. The calculation of the gravity field is less straightforward than that of the other two, and to avoid errors due to the concentration of mass at the mesh points it was evaluated 35 km above the upper surface of the boxes.

The variation of the heat flow, surface elevation and gravity field for three models is shown in figures 18–20. For these calculations the mean heat flux through the surface of the boxes has been fixed at $5{\cdot}85 \times 10^{-2}\,\mathrm{W\,m^{-2}}$ and three cases are investigated. In figure 18 all the heat flux is from below, in figure 19, $3{\cdot}0 \times 10^{-2}\,\mathrm{W\,m^{-2}}$ is from below and the rest from within, and in figure 20 all

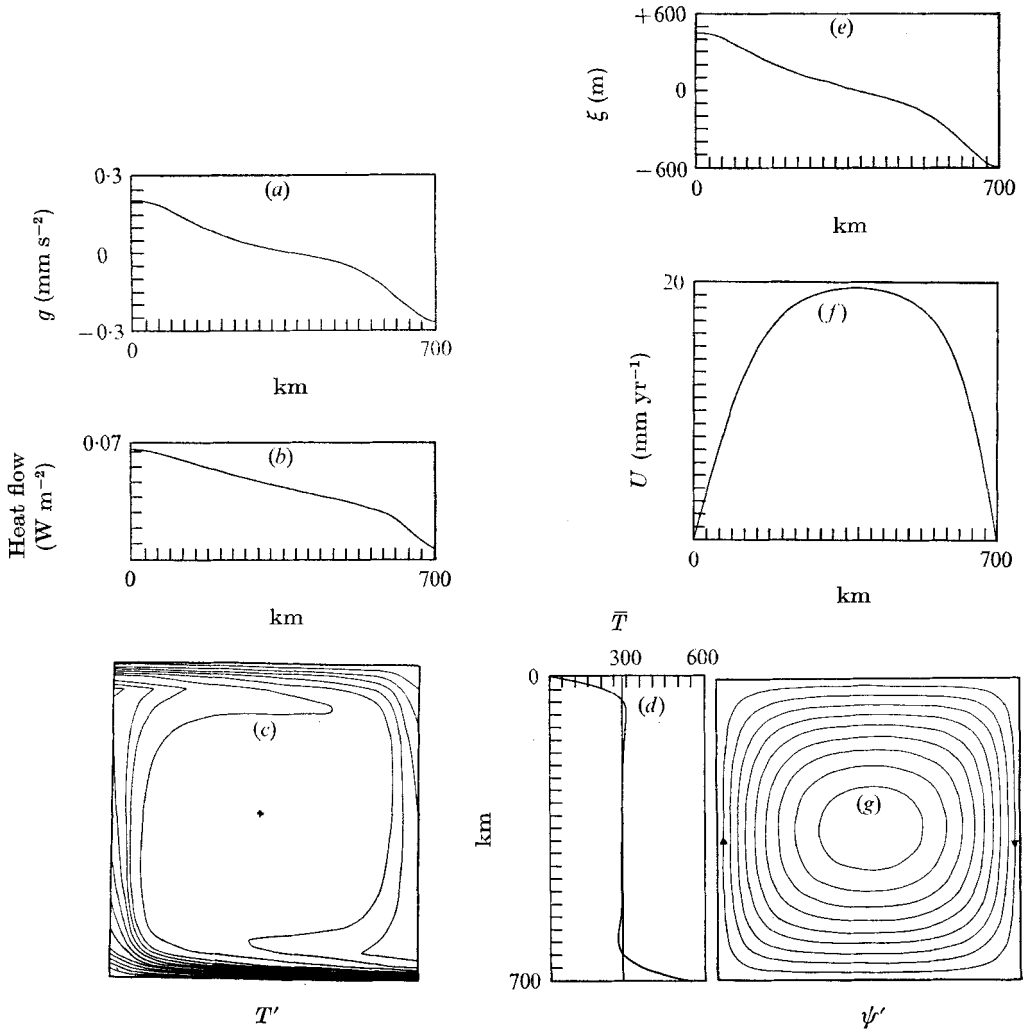

FIGURE 18. (*b*) The surface heat flow, the perturbation (*a*) to the gravity field and (*e*) to to the upper surface, (*f*) the horizontal velocity at the upper surface, (*c*) the temperature distribution, (*d*) its horizontal mean as a function of depth and (*g*) the streamlines obtained by fixing the flux at $5{\cdot}85 \times 10^{-2}$ W m^{-2} at the lower boundary, and supplying no heat internally. The initial temperature distribution was the same as for figures 10(*a*)–(*c*) on a 24×24 mesh and calculations continued until $t' = 39{\cdot}85$, to give the various fields shown. Contour intervals: T', 0 (50·0) 350·0 (25·0) 600·0; ψ', 0·0338 (0·04) 0·3538.

the heat is generated within the fluid. As explained in § 3 the results in figure 19 most closely resemble the earth's mantle if present estimates of the degree of partial melting beneath ridges are correct.

The most striking feature of figures 18–20 is the positive gravity anomaly over rising parts of the flow. The total gravity anomaly is produced partly by the upward deformation of the surface over a rising current, and partly by the higher temperature of the rising material. These effects act in opposite directions [appendix, equation (85)] and are of the same order of magnitude. Various authors,

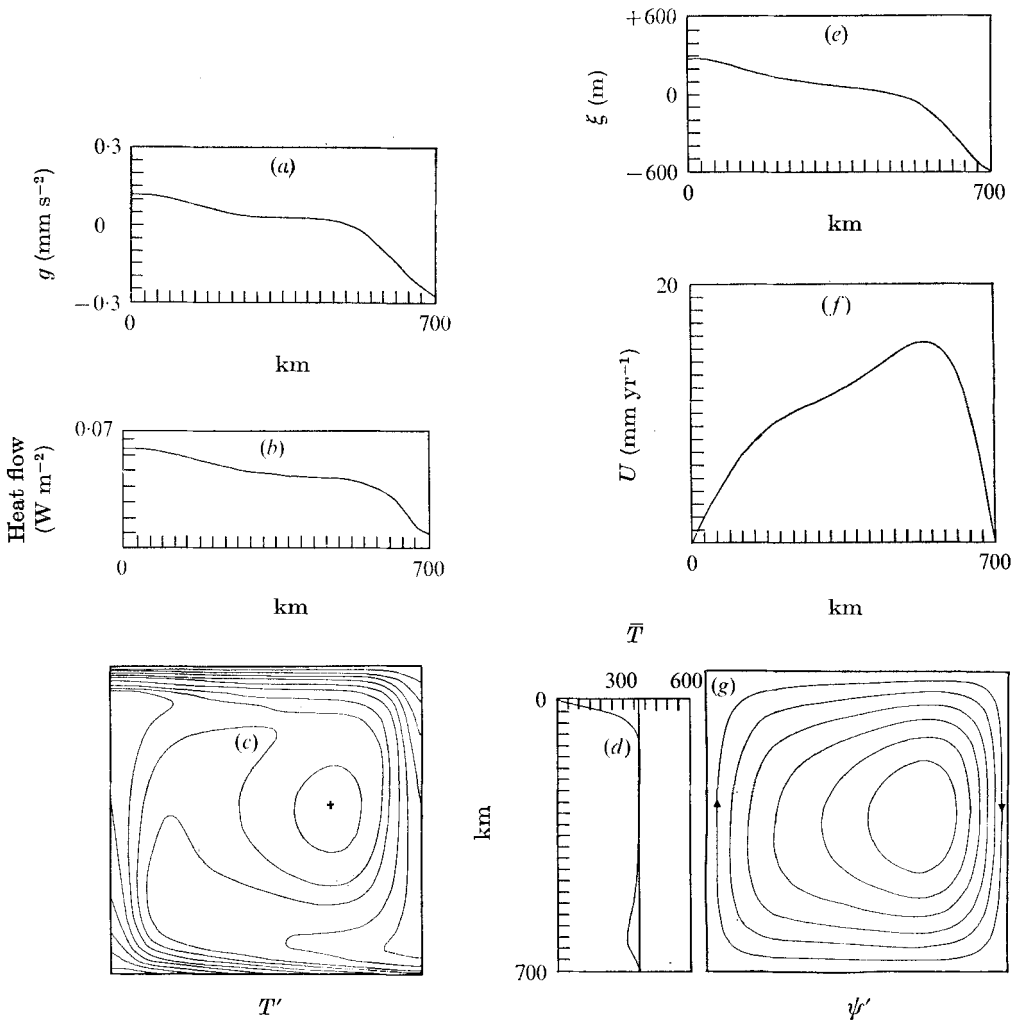

FIGURE 19. As for figure 18 but with 3×10^{-2} W m^{-2} supplied from below and $4{\cdot}07 \times 10^{-8}$ W m^{-3} supplied uniformly from within to give a mean surface heat flow of $5{\cdot}85 \times 10^{-5}$ W m^{-2}. Starting conditions on a 24×24 mesh as for figure 18, and calculation continued until $t' = 63{\cdot}7$. Contour levels: T', 0 (50·0) 350 (25·0) 500·0; ψ', 0·0338 (0·04) 0·2338. Of figures 18–20 this most resembles the probable conditions within the earth's mantle.

notably Runcorn (1965), have argued that the gravity anomaly should be negative over a hot rising current, but calculations by Pekeris (1935) and by McKenzie (1968*a*) on simple flows driven by horizontal temperature gradients applied to the upper surface showed that the effect of surface deformation dominated the gravity field caused by changes in density within the fluid, and the gravity anomaly was therefore positive over rising regions. Both authors used flows in which the conduction of heat dominated its convection. McKenzie (1968*a*) attempted to extend the results to flows in which the convection of heat was important and suggested that the gravity anomaly should change sign. The

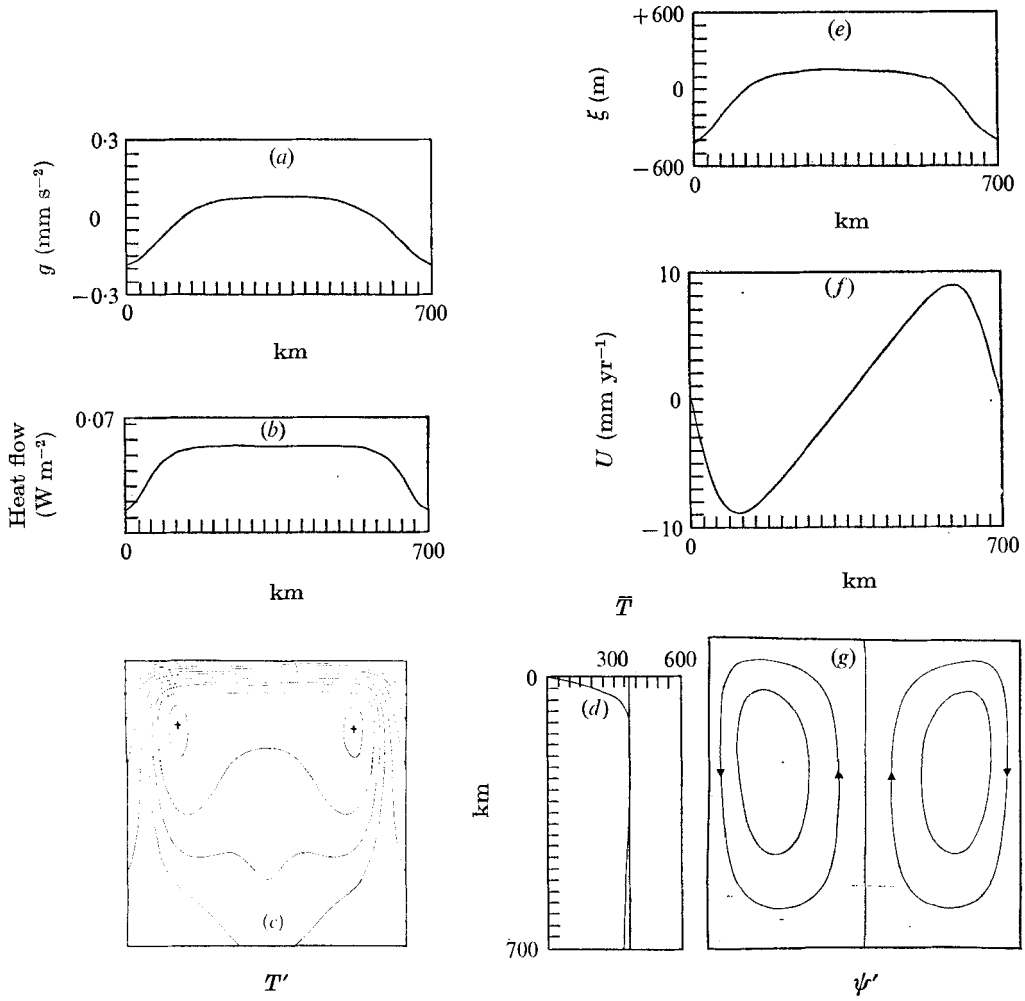

FIGURE 20. Geophysically important quantities for figure 14(*e*). For details see figure 18. All heat generated internally at a rate of $8{\cdot}36 \times 10^{-8}$ W m^{-3}. Contour levels: T', 0 (50·0) 350·0 (25·0) 400·0; ψ', −0·08 (0·04) 0·08; $t' = 147{\cdot}6$.

results of the present calculations show that McKenzie's argument is not correct since the gravity anomaly is dominated by the surface deformation at all Rayleigh numbers. Only results from steady-state solutions at a single value of the heat flux are shown in figures 18–20, but the gravity anomalies were calculated for all the models discussed in the previous section, and without exception their behaviour was the same.

The principal difference between the three cases is in the variation between the sinking and rising regions. When all the flux comes from below the rising region convects as much heat and has the same shape as the sinking sheet. Therefore the heat flux, surface elevation and gravity do not show a pronounced asymmetry between rising and sinking regions. In the other two cases the rising region occupies most of the box, and above it the gravity, surface elevation and heat

flow vary to only a small extent. The sinking sheet, however, remains thin and produces a marked minimum in all three quantities above it.

The correspondence between the results of the calculations above and corresponding measurements on the earth's surface is unlikely to be close because of the simplifications made to the governing equations. The most serious difference is probably the neglect of the temperature dependence of the viscosity. Without such dependence there is no difference between the mechanical properties of the fluid in the cold boundary layers and in the rest of the flow, and therefore the boundary layers do not correspond to plates on the earth's surface. Certain features of figures 18–20 are, however, of geophysical relevance. The uniformity of heat flow through the upper surface of the boxes in figures 19 and 20 may explain the uniformity of oceanic heat flow in the deep ocean basins. The heat flux in these regions is not the result of the cooling of young plates, as it is locally near the ridges. Another explanation of this uniformity suggested by these experiments is that the convection is time-dependent in the manner described in the last section. Provided that the characteristic time for geometry of the sinking sheets to change is less than the thermal time constant of the plates (~ 30 Myr) the heat flowing through the sea floor will be constant. The flow in the experiments described above satisfies this condition.

The values of the horizontal velocities on the upper surfaces of the boxes in figures 18–20 should be compared with the half spreading rates determined from the oceanic magnetic lineations. The observed rates vary between about 5 and 120 mm yr^{-1}, and the calculated values lie in the middle of this range. Unlike the observed values the calculated velocities are not constant over large regions because plates cannot be formed unless the viscosity depends on temperature. Similar results were obtained from a simple cellular model (Turcotte & Oxburgh 1967; Oxburgh & Turcotte 1968).

From a geophysical point of view the most important result of these experiments is the relationship between a positive gravity anomaly and upward deformation of the surface. This is not only a somewhat unexpected result; it can also be tested using observations of the elevation and gravity field. There are various difficulties which must be overcome before such a test can be carried out. The major variations of elevation are associated with active mountain belts and continent–ocean boundaries. These changes in height are compensated and are not maintained by convection in the mantle. They are also not associated with long-wavelength gravity anomalies. The smaller variations of elevation due to forces on the base of the plates can be separated from other effects only over regions where the crust and upper mantle do not have large lateral changes in density, or where the lateral changes are known and their effect can be removed.

On the continents the only areas where these conditions are satisfied are the Pre-Cambrian shields. Woollard (1969) has collected the observations for various regions and determined for each of these the best-fitting straight lines relating the means of the free-air gravity anomaly and elevation evaluated over 3° squares. The relationships he found are given in table 4, together with that obtained from the convection experiments. Apart from one relationship for Africa all areas

	Δg (mm s^{-2})
Eastern and Central Canada	$7{\cdot}4 \times 10^{-4}\,h - 0{\cdot}33$
Central and North Africa	
0–400 m	$-8{\cdot}5 \times 10^{-4}\,h + 0{\cdot}29$
above 400 m	$8{\cdot}6 \times 10^{-4}\,h - 0{\cdot}45$
South Africa, above 700 m	$5{\cdot}0 \times 10^{-4}\,h - 0{\cdot}36$
India south of 22° N	$10{\cdot}1 \times 10^{-4}\,h - 0{\cdot}70$
All convective models give values close to	$4{\cdot}5 \times 10^{-4}\,h$

TABLE 4. Free-air gravity anomalies and elevation (h in m). The relations for the geophysical areas are those given by Woollard (1969) for 3° × 3° squares

show an increasing free-air gravity anomaly with increasing elevation, in agreement with the convection experiments. The observed slopes do not, however, agree particularly well with that calculated.

The other type of region in which the crustal thickness is approximately constant is the ocean basins. A correction must, however, be applied to take account of the time-dependent temperature structure of the plates. When a new plate is formed along the world's rift system its temperature is that of the mantle, and as it moves away it gradually cools and shrinks. Since the heat is lost by vertical conduction the temperature distribution within the plate, and hence the depth of the ocean, depends only on age. Thus the ocean depth can easily be calculated (Langseth, Le Pichon & Ewing 1966; McKenzie & Sclater 1969). Comparison of the theoretical elevation with observations shows a striking agreement between the two (Sclater *et al.* 1971). Any observations of ocean depth must first be corrected for this effect before being compared with the gravity field.

The appropriate value of the gravity anomaly is rather less easy to obtain. It is clear that the comparison should be made only with the non-hydrostatic part of the gravity field, but because of the uncertainties associated with the origin of the earth's non-hydrostatic bulge discussed in §3, it is not obvious whether this term should be included. However, all other harmonics of the external gravity field determined by Gaposchkin & Lambeck (1971) are clearly non-hydrostatic and should be used. Unlike satellite observations, those from surface ships show short- as well as long-wavelength anomalies. Trenches especially have huge negative gravity anomalies which were for many years believed to be maintained by convection in the mantle. Recently it has been generally recognized that elastic forces within the plates themselves are sufficient to maintain such anomalies (McKenzie 1967*a*), and Lambeck (1972) has even suggested that the same forces could maintain the shortest wavelength anomalies observed by satellites. Therefore, only those gravity anomalies whose wavelength exceeds about $2{\cdot}5 \times 10^3$ km should be used for such a comparison. Another contribution to the gravity field has been discussed by Lambeck (1972). He calculated the gravity anomaly to be expected over a ridge from the temperature structure suggested by Sclater & Francheteau (1970), and showed that the effect was as

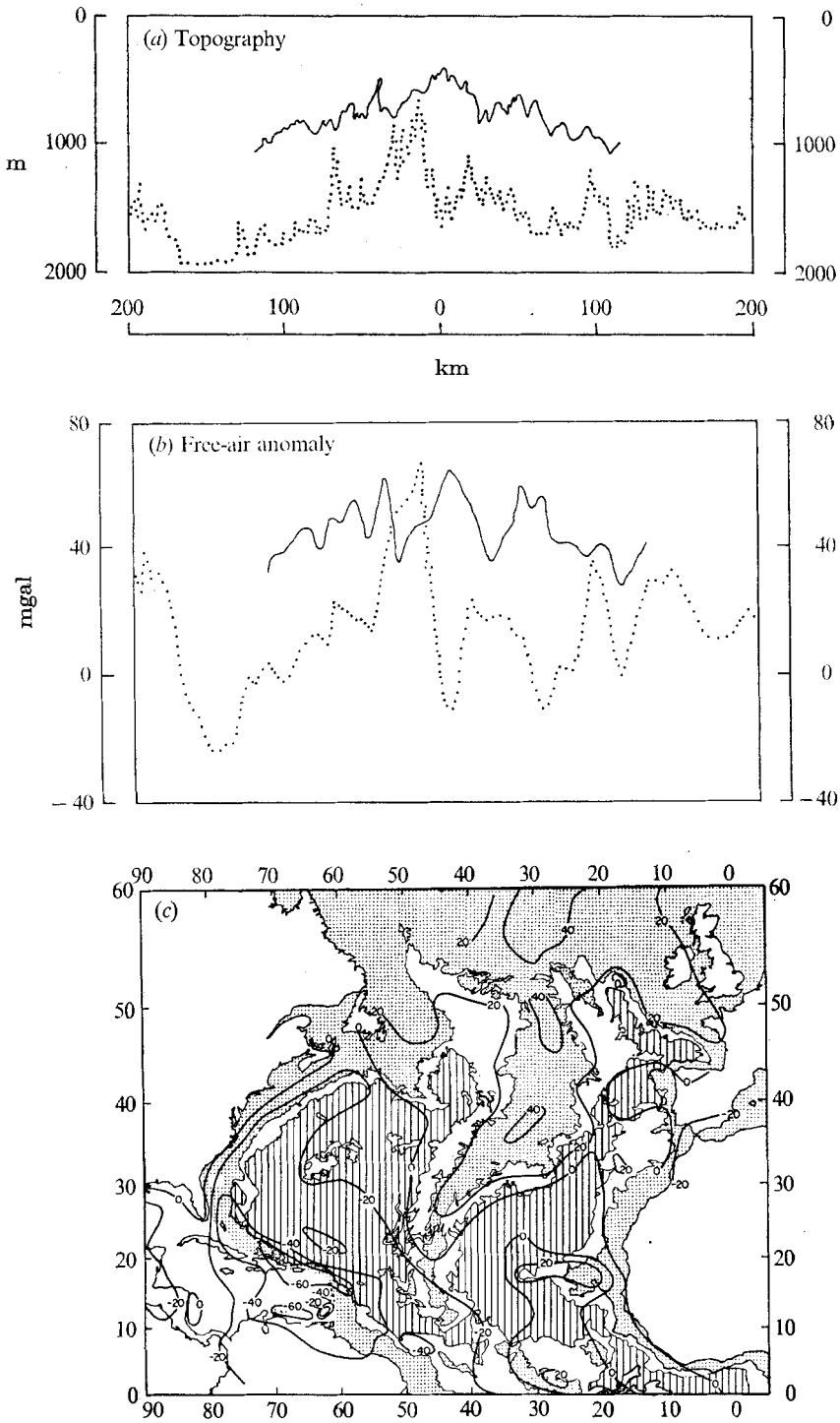

FIGURE 21. (*a*), (*b*) Profiles and (*c*) contour charts from the North Atlantic to show the correlation between surface elevation and gravity anomaly. (*a*) Section across the Reykyanes ridge (solid line) and at 30° N (dotted line). (*b*) Corresponding gravity profiles in milligals from Talwani *et al.* (1971). (*c*) Contours of the gravity field in the North Atlantic in milligals. Areas with depths less than 2000 fathoms are stippled, areas with depths greater than 2500 fathoms are indicated by vertical lines (from Talwani & Le Pichon 1969). (100 milligals is equivalent to 1 mm s^{-2}, 1 fathom is equivalent to 1·8 m.)

large as $0{\cdot}4\,\mathrm{mm\,s^{-2}}$ over ridges spreading at a half-rate of $10\,\mathrm{mm\,yr^{-1}}$, but decreased to $0{\cdot}1\,\mathrm{mm\,s^{-2}}$ when the half-rate was $50\,\mathrm{mm\,yr^{-1}}$. However, Anderson, McKenzie & Sclater (1973) failed to find a correlation between the value of the gravity anomaly over a ridge and its spreading rate, and it appears that this effect does not influence the satellite gravity field. Despite the various effects on both the gravity field and depth which are unrelated to convection in the mantle, this discussion clearly suggests that long-wavelength gravity anomalies should be correlated with regional variations of elevation.

Such a correlation has in fact been remarked by Talwani & Le Pichon (1969) and by Talwani, Windisch & Langseth (1971) in the North Atlantic. Figure 21 shows the regional gravity field over the North Atlantic, together with two profiles across the ridge axis at different latitudes. The correlation between gravity anomaly and depth in this region is striking. A similar result was obtained by Anderson *et al.* (1973), who compared the depth of the ridge axes of the world with the gravity anomaly obtained from the satellite gravity field of Gaposchkin & Lambeck (1971). They used the depth to the ridge axis because it could be directly compared with the gravity field without any corrections being applied, and showed that the slope m of the best-fitting line

$$\Delta g = md + C \tag{67}$$

(where Δg is the gravity anomaly in $\mathrm{mm\,s^{-2}}$ and d is the difference between the mean and the observed depth of the ridge in metres), obtained from oceanic observations agrees excellently with that, $3{\cdot}0 \times 10^{-4}$, obtained from the calculations above when allowance is made for the fact that sea water rather than a vacuum overlies the convecting region. These comparisons suggest that the regional elevation of both the continents and the oceans is affected by movements below the plates, and that both the calculated and observed gravity anomalies are positive over rising flows.

Perhaps the most important difference between the numerical experiments and the type of convection required to move the plates is in the cell width required. The largest plate is the Pacific plate, with a horizontal extent of about $10^4\,\mathrm{km}$. If the flow is to maintain its motion then the normalized cell width must be about 14. The experiments described here suggest that such a flow is unstable if the viscosity is constant. Unfortunately, the only numerical experiments as yet carried out on a fluid with temperature-dependent viscosity (Torrance & Turcotte 1971) were not sufficiently extensive to show whether the resulting flows had large cell widths. A useful model for mantle convection must possess stable solutions of this type, and it remains to be seen whether Torrance & Turcotte's model does behave in this manner.

The last problem of geophysical interest in these results is the behaviour of the mean temperature. There is at present some confusion among geophysicists about the relationship between the temperature variation with depth and the existence and vertical extent of convection in the mantle. The confusion is best illustrated by the variation of mean temperature with depth when all the heat is generated within the fluid (figure 12). It is clear that a layer of fluid with this temperature profile would be stable to any perturbations which did not move

the surface boundary layer, and it would therefore be supposed that convection could not occur. This argument is clearly false, since the temperature profile which must be tested for stability is not that in figure 12 but the profile obtained when the velocity is zero. Such a temperature structure is certainly unstable. The difficulty arises because major changes in the mean temperature structure are caused by convection. This argument shows that it is useless to test whether the observed structure of the mantle is marginally stable if in fact it is the result of vigorous convection. Since the sinking slabs beneath island arcs convect up to a third of all the heat lost by the earth, the mantle is certainly convecting and therefore probably has a mean temperature gradient which is subadiabatic away from the boundaries (figure 2).

Another confusion arises from the same cause and concerns the influence of phase changes within the mantle on convection. The marginal-stability condition is again not satisfied between the surface and a depth of 700 km, since the sinking slabs convect heat to this depth. The temperature structure of the mantle will therefore be very close to the adiabatic, defined in the correct way to include phase changes. As material moves through the region in which phase changes occur its entropy will remain constant, and its temperature will change to satisfy this condition. Difficulties only occur if rapid changes in temperature occur over a small depth range (McKenzie 1970).

The profile of mean temperature as a function of depth in figure 12 is in general similar to the best available estimates for the earth's mantle (figure 2). There is, however, one important difference. In figure 2 the temperature at the base of the surface boundary layer is about 1200 °C, whereas the corresponding value from figure 19 is 380 °C. This difference is presumably caused by the neglect of the variation of viscosity with temperature in the calculations. Inclusion of this effect increases the thickness of the surface boundary layer and produces better agreement with the observations (Torrance & Turcotte 1971). Below the boundary layer the best estimate of the temperature in the earth was obtained by requiring the gradient to be adiabatic. Figure 12 shows that convection will modify the temperature gradient, making it subadiabatic throughout much of the convecting region and producing a boundary layer at its base. The resulting profile is shown in figure 2, but the difference between it and the adiabatic profile is too small to be measured by present geophysical techniques.

An unexpected feature of the calculations described above was the time taken for the temperature field to reach its final state, irrespective of whether this was a steady state or time-dependent flow. In all cases of geophysical interest the time required was comparable with the age of the earth. Realistic geophysical calculations must therefore examine the time dependence of the flow.

7. Conclusion

The two-dimensional numerical experiments described in §5 can be understood in terms of a simple boundary-layer theory. At large Rayleigh numbers the flow develops thermal boundary layers, and their behaviour and stability determine the cell width and time dependence of the resulting flow. At Rayleigh

numbers comparable with that of the earth's mantle steady-state solutions were found only when the experiments were carried out in square boxes, and required times comparable with the age of the earth to lose their time dependence. Furthermore, no steady-state solutions were found for convection in boxes with a normalized width $\lambda = 2$. It is therefore likely that convection in the earth's mantle is unsteady.

Few geophysical observations are directly related to flow in the mantle. The gravity field obtained from the numerical experiments shows that the gravity anomaly is positive over the rising part of the flow because the contribution from the deformed surface dominates that from the temperature field within the fluid. The magnitude of the gravity and elevation anomalies agrees well with the gravity field obtained from the orbits of satellites and with the regional variations in ocean depth. Also the results of Talwani & Le Pichon (1969) and of Anderson *et al.* (1973) show that the correlation between gravity and elevation agrees with that predicted from this numerical experiment. The magnitudes of the horizontal velocities on the surface of the convecting layer are within the range determined from oceanic magnetic lineations. These results show that there is no reason to believe that convection in the upper 700 km of the earth's mantle cannot account for those features of the earth which can be shown to have a dynamic origin.

Two features are not accounted for. The horizontal extent of the largest plates requires ordered flow with $\lambda = 15$. Also the temperature difference between the top and bottom of the boundary layer at the earth's surface is about four times greater than that in the numerical experiments. Both these differences are probably consequences of the neglect of the variation of viscosity with temperature in the calculations in §5. Its inclusion should suppress the type of boundary-layer instability observed in the present experiments, and hence permit the flow to develop with a large cell width and also thicker boundary layers. The numerical experiments of Torrance & Turcotte (1971) on fluids with variable viscosity were carried out with the bottom temperature rather than the heat flux prescribed, and used only small cell widths. These experiments do not therefore reveal whether the variation of viscosity with temperature can indeed explain the differences observed above. Further experiments with Torrance & Turcotte's model and with a fixed lower boundary are planned, and some effects of shear-stress heating will also be included. None of these effects were included in the present calculations because we wished first to study the behaviour of the simplest possible system of equations. The behaviour of the numerical experiments was more complicated than had been expected, even though the simple two-dimensional model that we used suppressed many forms of instability observed in experiments on real fluids at lower Rayleigh numbers.

The relevance of these and other calculations to Wilson's (1963) and Morgan's (1971) suggestions about the velocity and temperature distribution within the convecting mantle will be examined in a later paper.

This research was supported by a grant from the Natural Environmental Research Council and the calculations were principally carried out on the IBM 360/44 computer at the Institute of Theoretical Astronomy. We wish to thank Dr D. R. Moore for his advice and, in particular, for adapting his convection program to solve the problems described here. In addition, we are grateful to Dr R. S. Peckover and Dr K. V. Roberts for their collaboration in the initial stages of this study, and to Sir Edward Bullard for his comments.

Appendix. Evaluation of the external gravity field

For comparison with geophysical observations the variation of the heat flux, surface elevation and gravity on the upper surface of the convecting layer must be obtained from the flow and temperature fields calculated in § 5. The heat flux $E(x_j)$ is the easiest to obtain, since to a first approximation it is given by

$$E_j = -k\left(\frac{\partial T}{\partial z}\right)_{z=d} \simeq \frac{kT_1}{d}\frac{T_{j,N_z-1}}{\Delta z}. \tag{68}$$

This value is, however, the heat carried by conduction across a plane at a depth of $\frac{1}{2}\Delta z$ below the upper surface. Since the vertical velocity is not zero on this plane the value on this surface must include the heat convected across it as well as the heat generated within the fluid above it:

$$E_j = \frac{T_1}{d}\left[\frac{kT_{j,N_z-1}}{\Delta z} + \frac{T_{j,N_z-1}(\psi_{j-1,N_z-1} - \psi_{j+1,N_z-1})}{8\Delta x} + \tfrac{1}{2}\epsilon\Delta z\right]. \tag{69}$$

The surface deformation is less easy to calculate. It must be obtained from the boundary condition on the normal stress τ_{zz} on the deformed upper surface:

$$\tau_{zz} = -P + 2\rho\nu\,(\partial w/\partial z) = 0. \tag{70}$$

The pressure P consists of a hydrostatic component

$$P_0 = \rho_0 g d(1 - z') \tag{71}$$

and a component P_1 due to the flow which vanishes if $\mathbf{u} = 0$. The deformation of the surface is assumed to be small compared with the thickness of the thermal boundary layer, and therefore to first order in αT_1 only the value P_0 changes between $z' = 1$ and $z' = 1 + \alpha T_1 \xi'$, where ξ' is the dimensionless deformation. The values for ξ in figures 18–20 show that this approximation is justified. P_1 must be obtained from the equation governing the conservation of momentum. Writing

$$P_1 = \rho_0 g d\alpha T_1 P_1', \quad U_1 = g d\alpha T_1 U_1', \tag{72}$$

the momentum equation becomes

$$0 = \nabla'^2\mathbf{u}' - \nabla' P_1' + \nabla' U_1' + T'\mathbf{a}_z. \tag{73}$$

If the wavelength of the disturbance is short compared with the radius of the earth

$$\nabla' P_1' \gg \nabla' U_1' \tag{74}$$

and $\nabla' U_1'$ may be neglected (McKenzie 1968*a*). Hence

$$\frac{\partial P_1'}{\partial x'} = \nabla'^2 \frac{\partial \psi'}{\partial z'} = -\frac{\partial \omega'}{\partial z'} \tag{75}$$

or on the upper surface

$$[P_1']_{z'=1} = -\int \left(\frac{\partial \omega'}{\partial z'}\right)_{z'=1} dx' + f(1). \tag{76}$$

The constant term may be omitted since it is the variation of ξ' with x' that is of interest. Evaluation of (70) on the deformed surface then gives

$$\xi' = 2\left[\frac{\partial^2 \psi'}{\partial x' \, \partial z'}\right]_{z'=1} - \int \left(\frac{\partial \omega'}{\partial z'}\right)_{z'=1} dx', \tag{77}$$

which is easily evaluated.

The variation of the gravity field depends on both the variation of density, and hence of temperature, throughout the convecting region and on the surface deformation. The gravitational potential due to these causes at $\mathbf{r}_0$ is

$$U_1(\mathbf{r}_0) = \rho_0 \alpha T_1 G \left[\int_S \frac{\xi d' \, dx \, dy}{|\mathbf{r} - \mathbf{r}_0|} - \int_V \frac{T' \, dx \, dy \, dz}{|\mathbf{r} - \mathbf{r}_0|}\right]. \tag{78}$$

However, what is measured is

$$\begin{aligned} \partial U_1 / \partial z_0 &= g \alpha T_1 g_1' \\ &= \tfrac{4}{3} \pi a \rho_0 \bar{\rho} \alpha T_1 g_1', \end{aligned} \tag{79}$$

where a is the radius of the earth and $\rho_0 \bar{\rho}$ is its mean density.

Substitution and evaluation of the integral over y gives

$$g_1' = -\frac{3d}{4\pi a \bar{\rho}} \left\{ \int_0^1 \int_{-\infty}^{\infty} \frac{(z - z_0) \, T \, dx \, dz}{(x - x_0)^2 + (z - z_0)^2} - \int_{-\infty}^{+\infty} \frac{\xi (1 - z_0) \, dx}{(x - x_0)^2 + (1 - z_0)^2} \right\}, \tag{80}$$

where all variables under the integral signs are dimensionless. The periodic boundary conditions require that

$$T(x, z) = T(2n\lambda - x, z) = T(2m\lambda + x, z), \tag{81}$$

where λ is the normalized width of the box in which convection is occurring and n and m are integers. Hence

$$\begin{aligned} \int_{-\infty}^{\infty} \frac{T \, dx}{(x - x_0)^2 + (z - z_0)^2} = \int_0^{\lambda} T \, dx \sum_{m=-\infty}^{\infty} \{(x - x_0 + 2m\lambda)^2 + (z - z_0)^2\}^{-1} \\ - \int_0^{\lambda} T \, dx \sum_{n=-\infty}^{\infty} \{(x + x_0 + 2n\lambda)^2 + (z - z_0)^2\}^{-1} \end{aligned} \tag{82}$$

but

$$\sum_{j=-\infty}^{\infty} \{(j + u)^2 + v^2\}^{-1} = \frac{\pi \sinh 2\pi v}{v(\cosh 2\pi v - \cos 2\pi u)} \tag{83}$$

(Jolley 1961, equation 858), whence (82) becomes

$$\frac{\pi \sinh\frac{\pi(z-z_0)}{\lambda}}{2\lambda(z-z_0)}\int_0^\lambda T(x,z) \times\left\{\frac{2\left[\cosh\frac{\pi(z-z_0)}{\lambda}-\cos\frac{\pi x}{\lambda}\cos\frac{\pi x_0}{\lambda}\right]}{\cosh^2\frac{\pi(z-z_0)}{\lambda}-2\cosh\frac{\pi(z-z_0)}{\lambda}\cos\frac{\pi x}{\lambda}\cos\frac{\pi x_0}{\lambda}+\frac{1}{2}\left(\cos\frac{2\pi x}{\lambda}+\cos\frac{2\pi x_0}{\lambda}\right)}\right\}dx. \tag{84}$$

Equation (80) therefore gives

$$g_1' = \frac{3d}{2a\lambda\bar{\rho}}\left\{\int_0^\lambda \xi(x)\,G(x_0,z_0,x,1)\,dx-\int_0^1 dz\int_0^\lambda T(x,z)\,G(x_0,z_0,x,z)\,dx\right\}, \tag{85}$$

where

$$G(x_0,z_0,x,z) = \frac{\sinh\frac{\pi(z-z_0)}{\lambda}\left[\cos\frac{\pi(z-z_0)}{\lambda}-\cos\frac{\pi x}{\lambda}\cos\frac{\pi x_0}{\lambda}\right]}{\cosh^2\frac{\pi(z-z_0)}{\lambda}-2\cosh\frac{\pi(z-z_0)}{\lambda}\cos\frac{\pi x}{\lambda}\cos\frac{\pi x_0}{\lambda}+\frac{1}{2}\left(\cos\frac{2\pi x}{\lambda}+\cos\frac{2\pi x_0}{\lambda}\right)}. \tag{86}$$

Evaluation of (85) was carried out for $z_0 = 1{\cdot}05$ and the results were checked by comparison with McKenzie's (1968*a*) calculations.

REFERENCES

Akimoto, S. & Fujisawa, H. 1966 Olivine–Spinel transition in system Mg_2SiO_4–Fe_2SiO_4 at 800 °C. *Earth Planet. Sci. Lett.* **1**, 237–240.

Akimoto, S. & Fujisawa, H. 1968 Olivine–Spinel solid solution equilibrium in the system Mg_2SiO_4–Fe_2SiO_4. *J. Geophys. Res.* **73**, 1467–1479.

Allan, D. W., Thompson, W. B. & Weiss, N. O. 1967 Convection in the Earth's Mantle. In *Mantles of the Earth & Terrestrial Planets* (ed. S. K. Runcorn), p. 507. Wiley.

Anderson, D. L., Sammis, C. & Jordan, T. 1972 Composition of the Mantle and Core. In *The Nature of the Solid Earth* (ed. E. C. Robertson), p. 41. McGraw-Hill.

Anderson, R. N., McKenzie, D. P. & Sclater, J. G. 1973 Gravity, bathymetry and convection within the earth. *Earth Planet. Sci. Lett.* **18**, 391–407.

Archambeau, C. B., Flinn, E. A. & Lambert, D. G. 1969 Fine structure of the upper mantle. *J. Geophys. Res.* **74**, 5825–5865.

Ave'Lallemant, H. G. & Carter, N. L. 1970 Syntectonic recrystallization of Olivine and modes of flow in the Upper Mantle. *Bull. Geol. Soc. Am.* **81**, 2203–2220.

Banks, R. J. 1969 Geomagnetic variations and the electrical conductivity of the upper mantle. *Geophys. J. Roy. Astr. Soc.* **17**, 457–487.

Barazangi, M. & Dorman, J. 1969 World seismicity maps compiled from ESSA Coast and Geodetic survey epicenter data, 1961–1967. *Bull Seism Soc. Am.* **59**, 369.

Beardsley, R. C. & Festa, J. F. 1972 A numerical model of convection driven by a surface stress and non-uniform horizontal heating. *J. Phys. Ocean.* **2**, 444.

Birch, F. 1952 Elasticity and constitution of the Earth's Interior. *J. Geophys. Res.* **57**, 227–289.

Brindley, J. 1967 Thermal convection in horizontal fluid layers. *J. Inst. Maths. Applics.* **3**, 313–343.

BRUNE, J. & DORMAN, J. 1963 Surface waves and earth structure in the Canadian Shield. *Bull. Seism. Soc. Am.* **53**, 167–200.

BULLARD, E. C., EVERETT, J. E. & SMITH, A. G. 1965 The fit of the Continents around the Atlantic. *Phil. Trans. Roy. Soc.* A **258**, 41.

BUSSE, F. H. 1967 On the stability of two-dimensional convection in a layer heated from below. *J. Math. & Phys.* **46**, 140.

BUSSE, F. H. & SCHUBERT, G. 1971 Convection in a fluid with two phases. *J. Fluid Mech.* **46**, 801.

BUSSE, F. H. & WHITEHEAD, J. A. 1971 Instabilities of convection rolls in a high Prandtl number fluid. *J. Fluid Mech.* **47**, 305.

CARTER, N. L. & AVE'LALLEMANT, H. G. 1970 High temperature flow of Dunite and Peridotite. *Bull. Geol. Soc. Am.* **81**, 2181–2202.

CHANDRASEKHAR, S. 1961 *Hydrodynamic and Hydromagnetic Stability*, chap. 2. Clarendon Press.

CHASE, C. G. 1972 The N plate problem of plate tectonics. *Geophys. J. Roy. Astr. Soc.* **29**, 117.

CLEARY, J. R. 1967 Azimuthal variation to the Longshot source term. *Earth. Planet. Sci. Lett.* **3**, 29–37.

DAVIES, D. & JULIAN, B. R. 1972 A study of short period P-wave signals from Longshot. *Geophys. J. Roy. Astr. Soc.* **29**, 185.

DAVIES, D. & MCKENZIE, D. P. 1969 Seismic travel-time residuals and plates. *Geophys. J. Roy. Astr. Soc.* **18**, 51–63.

DEWEY, J. F. & BIRD, J. M. 1971 Origin and emplacement of the Ophiolite suite: Appalachian Ophiolites in Newfoundland. *J. Geophys. Res.* **76**, 3179–3206.

ELSASSER, W. M. 1969 Convection and stress propagation in the Upper Mantle. In *The Applications of Modern Physics to the Earth and Planetary Interiors* (ed. S. K. Runcorn), p. 223. Interscience.

ENGEL, A. E. J. & ENGEL, C. G. 1970 Mafic and Ultramafic rocks. In *The Sea*, vol. 4 (ed. A. E. Maxwell), p. 465. Interscience.

FOSTER, T. D. 1969 The effect of initial conditions and lateral boundaries on convection. *J. Fluid Mech.* **37**, 81.

FOSTER, T. D. 1971 Intermittent convection. *Geophys. Fluid Dyn.* **2**, 201.

FROMM, J. E. 1965 Numerical solution of the nonlinear equations for a heated fluid layer. *Phys. Fluids*, **8**, 1757.

FUJISAWA, H., FUJII, N., MIZUTANI, H., KANAMORI, H. & AKIMOTO, S. 1968 Thermal diffusivity of Mg_2SiO_4, Fe_2SiO_4, and NaCl at high pressures and temperatures. *J. Geophys. Res.* **73**, 4727–4733.

FUKAO, Y. 1969 On the radiative heat transfer and the thermal conductivity in the Upper Mantle. *Bull. Earth. Res. Inst.* **47**, 549–69.

FUKAO, Y., MIZUTANI, H. & UYEDA, S. 1968 Optical absorption spectra at high temperatures and radiative thermal conductivity of Olivines. *Phys. Earth Planet. Interiors*, **1**, 57–62.

GAPOSCHKIN, E. M. & LAMBECK, K. 1971 Earth's gravity field to sixteenth degree and station coordinates from satellite and terrestrial data. *J. Geophys. Res.* **76**, 4844–4883.

GAST, P. W. 1968 Trace element fractionation and the origin of tholeiitic and alkaline magma types. *Geoch. Cosmochim. Acta*, **32**, 1057.

GAST, P. W. 1972 The chemical composition of the Earth, the Moon and Chondritic meteorites. In *The Nature of the Solid Earth* (ed. E. C. Robertson), p. 19. McGraw-Hill.

GILBERT, F. 1972 Inverse problems for the Earth's normal modes. In *The Nature of the Solid Earth* (ed. E. C. Robertson), p. 125. McGraw-Hill.

GOETZE, C. 1971 High temperature rheology of westerly granite. *J. Geophys. Res.* **76**, 1223.

GOLDREICH, P. & TOOMRE, A. 1969 Some remarks on polar wandering. *J. Geophys. Res.* **74**, 2555.

GOLDSTEIN, H. 1950 *Classical Mechanics*. Addison-Wesley.

GOLDSTEIN, R. J. & GRAHAM, D. J. 1969 Stability of a fluid layer with zero shear boundaries. *Phys. Fluids*, **12**, 1133.

GORDON, R. B. 1965 Diffusion creep in the Earth's Mantle. *J. Geophys. Res.* **70**, 2413–2417.

GORDON, R. B. 1971 Observations of crystal plasticity under high pressure with applications to the earth's mantle. *J. Geophys. Res.* **76**, 1248–1254.

GRIGGS, D. T. 1972 The sinking lithosphere and the focal mechanism of deep earthquakes. In *The Nature of the Solid Earth* (ed. E. C. Robertson), p. 361. McGraw-Hill.

GUTENBERG, B. 1959 *Physics of the Earth's Interior*. Academic.

HALES, A. L. 1936 Convection currents in the Earth. *Mon. Not. Roy. Astr. Soc., Geophys. Suppl.* **3**, 372.

HALES, A. L. & HERRIN, E. 1972 Travel times of seismic waves. In *The Nature of the Solid Earth* (ed. E. C. Robertson), p. 172. McGraw-Hill.

HANKS, T. C. 1971 The Kuril Trench – Hokkaido Rise system: large shallow earthquakes and simple models of deformation. *Geophys. J. Roy. Astr. Soc.* **23**, 173.

HENDERSHOTT, M. C. 1972 The effects of solid Earth deformation on global ocean tides. *Geophys. J. Roy. Astr. Soc.* **29**, 389.

HENDERSHOTT, M. C. & MUNK, W. 1970 Tides. *Ann. Rev. Fluid Mech.* **2**, 205–224.

HESS, H. H. 1962 History of the ocean basins. *Petrologic Studies: Buddington Memorial Volume*, pp. 599–620. Geol. Soc. Am.

HOWARD, L. N. 1966 Convection at high Rayleigh numbers. In *Proc. 11th Int. Congr. Appl. Mech. Munich*, 1964 (ed. H. Görtler), p. 1109. Springer.

HOWARD, L. N., MALKUS, W. V. R. & WHITEHEAD, J. A. 1970 Self-convection of floating heat sources: a model for Continental Drift. *Geophys. Fluid Dyn.* **1**, 123–142.

HOYLE, F. 1972 The history of the Earth. *Quart. J. Roy. Astr. Soc.* **13**, 328.

HOYLE, F. & NARLIKAR, J. V. 1972 Cosmological models in a conformably invariant gravitational theory. II. A new model. *Mon. Not. Roy. Astr. Soc.* **155**, 323.

HSUI, A. T., TURCOTTE, D. L. & TORRANCE, K. E. 1972 Finite-amplitude thermal convection within a self-gravitating fluid sphere. *Geophys. Fluid Dyn.* **3**, 35–44.

HUPPERT, H. E. 1971 A note on the Howard–Malkus–Whitehead floating heat sources. *Geophys. Fluid Dyn.* **2**, 317–322.

ISACKS, B. L. & MOLNAR, P. 1969 Mantle earthquake mechanisms and the sinking of the Lithosphere. *Nature*, **223**, 1121.

ISACKS, B. L. & MOLNAR, P. 1971 Distribution of stresses in the descending lithosphere from a global survey of focal-mechanism solutions of Mantle earthquakes. *Rev. Geophys.* **9**, 103–174.

ISACKS, B. L., OLIVER, J. & SYKES, L. R. 1968 Seismology and the new global tectonics. *J. geophys. Res.* **73**, 5855–5899.

JEFFREYS, H. 1963 On the hydrostatic theory of the figure of the Earth, *Geophys. J. Roy. Astr. Soc.* **8**, 196.

JEFFREYS, H. 1971 *The Earth*, 5th ed. Cambridge University Press.

JOHNSON, L. R. 1967 Array measurements of P velocities in the upper mantle. *J. Geophys. Res.* **72**, 6309–6325.

JOHNSON, L. R. 1969 Array measurements of P velocities in the lower mantle. *Bull. Seism. Soc. Am.* **59**, 973–1008.

JOLLEY, L. B. W. 1961 *Summation of Series*. Dover.

KANAMORI, H., FUJII, N. & MIZUTANI, H. 1968 Thermal diffusivity measurement of rock-forming minerals from 400 °K to 1100 °K. *J. Geophys. Res.* **73**, 595–605.

KAULA, W. M. 1971 Dynamical aspects of lunar origin. *Rev. Geophys. Space Phys.* **9**, 217–238.

KNOPOFF, L. 1964 The convection current hypothesis. *Rev. Geophys.* **2**, 89.

KRISHNAMURTI, R. 1968*a* Finite amplitude convection with changing mean temperature. Part 1. Theory. *J. Fluid Mech.* **33**, 445.

KRISHNAMURTI, R. 1968*b* Finite amplitude convection with changing mean temperature. Part 2. An experimental test of theory. *J. Fluid Mech.* **33**, 457.

KRISHNAMURTI, R. 1970*a* On the transition to turbulent convection. Part 1. The transition from two- to three-dimensional flow. *J. Fluid Mech.* **42**, 295.

KRISHNAMURTI, R. 1970*b* On the transition to turbulent convection. Part 2. The transition to time-dependent flow. *J. Fluid Mech.* **42**, 309.

KULACKI, F. A. & GOLDSTEIN, R. J. 1972 Thermal convection in a horizontal fluid layer with uniform volumetric energy sources. *J. Fluid Mech.* **55**, 271.

LAMBECK, K. 1972 Gravity anomalies over oceanic ridges. *Geophys. J. Roy. Astr. Soc.* **30**, 37.

LANGSETH, M. G., LE PICHON, X. & EWING, M. 1966 Crustal structure of the mid-ocean ridges, 5. Heat flow through the Atlantic Ocean floor and convection currents. *J. Geophys. Res.* **71**, 5321–5355.

LE PICHON, X. 1968 Sea-floor spreading and Continental Drift. *J. Geophys. Res.* **73**, 3661.

LIPPS, F. B. & SOMERVILLE, R. C. J. 1971 Dynamics of variable wavelength in finite-amplitude Bénard convection. *Phys. Fluids*, **14**, 759–765.

LLIBOUTRY, L. 1969 Sea floor spreading, Continental drift and lithosphere sinking with an asthenosphere at melting point. *J. Geophys. Res.* **74**, 6525.

MACDONALD, G. J. F. 1963 The deep structure of oceans and continents. *Rev. Geophys.* **1**, 587–665.

MCKENZIE, D. P. 1966 The viscosity of the Lower Mantle. *J. Geophys. Res.* **71**, 3995–4010.

MCKENZIE, D. P. 1967*a* Some remarks on heat flow and gravity anomalies. *J. Geophys. Res.* **72**, 61–71.

MCKENZIE, D. P. 1967*b* The viscosity of the Mantle. *Geophys. J. Roy. Astr. Soc.* **14**, 297.

MCKENZIE, D. P. 1968*a* The influence of the boundary conditions and rotation on convection in the Earth's Mantle. *Geophys. J. Roy. Astr. Soc.* **15**, 457–500.

MCKENZIE, D. P. 1968*b* The geophysical importance of high temperature creep. In *The History of the Earth's Crust, Proc. NASA Conf.*, p. 28. Princeton University Press.

MCKENZIE, D. P. 1969 Speculations on the causes and consequences of plate motions. *Geophys. J. Roy. Astr. Soc.* **18**, 1.

MCKENZIE, D. P. 1970 Temperature and potential temperature beneath island arcs. *Tectonophys.* **10**, 357.

MCKENZIE, D. P. 1972 Plate tectonics. In *The Nature of the Solid Earth* (ed. E. C. Robertson), p. 323. McGraw-Hill.

MCKENZIE, D. P. & PARKER, R. L. 1967 The North Pacific: an example of tectonics on a sphere. *Nature*, **216**, 1276–1280.

MCKENZIE, D. P. & SCLATER, J. G. 1969 Heat flow in the Eastern Pacific and sea floor spreading. *Bull. Volcanologique*, **33**, 101–118.

MCKENZIE, D. P. & SCLATER, J. G. 1971 The evolution of the Indian Ocean since the late Cretaceous. *Geophys. J. Roy. Astr. Soc.* **25**, 437–528.

MALKUS, W. V. R. 1954 Discrete transitions in turbulent convection. *Proc. Roy. Soc.* A **225**, 185.

MELSON, W. G. & THOMPSON, G. 1971 Petrology of a transform fault zone and adjacent ridge segments. *Phil. Trans. Roy. Soc.* A **268**, 423–441.

MITRONOVAS, W., ISACKS, B. & SEEBER, L. 1969 Earthquake locations and seismic wave propagation in the upper 250 km of the Tonga island arc. *Bull. Seism. Soc. Am.* **59**, 1115–1135.

MIZUTANI, H., HAMANO, Y., IDA, Y. & AKIMOTO, S. 1970 Compressional wave velocities of Fayalite, Fe_2SiO_4 Spinel, and Coesite. *J. Geophys. Res.* **75**, 2741–2747.

MOORE, D. R., PECKOVER, R. S. & WEISS, N. O. 1974 Difference methods for time-dependent two-dimensional convection. *Comp. Phys. Comm.* **7**, in press.

MOORE, D. R. & WEISS, N. O. 1973 Two-dimensional Rayleigh–Bénard convection. *J. Fluid Mech.* **58**, 289–312.

MORGAN, W. J. 1968 Rises, trenches, great faults and crustal blocks. *J. Geophys. Res.* **73**, 1959–1982.

MORGAN, W. J. 1971 Convection plumes in the lower mantle. *Nature*, **230**, 42.

MUNK, W. 1968 Once again – tidal friction. *Quart. J. Roy. Astr. Soc.* **9**, 352–375.

MUNK, W. H. & MACDONALD, G. J. F. 1960 *The Rotation of the Earth*. Cambridge University Press.

O'CONNELL, R. J. 1971 Pleistocene glaciation and the viscosity of the lower mantle. *Geophys. J. Roy. Astr. Soc.* **23**, 299–327.

OLDENBURG, D. W. & BRUNE, J. N. 1972 Ridge transform fault spreading pattern in freezing wax. *Science*, **178**, 301.

OLIVER, J. & ISACKS, B. 1967 Deep earthquake zones, anomalous structures in the upper mantle and the lithosphere. *J. Geophys. Res.* **72**, 4259–4275.

OXBURGH, E. R. & TURCOTTE, D. L. 1968 Mid ocean ridges and geotherm distribution during mantle convection. *J. Geophys. Res.* **73**, 2643.

PARKER, R. L. 1971 The inverse problem of electrical conductivity in the mantle. *Geophys. J. Roy. Astr. Soc.* **22**, 121–138.

PECKOVER, R. S. 1972 Convection in the presence of magnetic fields. Ph.D. thesis, University of Cambridge.

PEKERIS, C. L. 1935 Thermal convection in the interior of the Earth. *Mon. Not. Roy. Astr. Soc., Geophys. Suppl.* **3**, 343.

PLOWS, W. H. 1968 Some numerical results for two-dimensional steady laminar Bénard convection. *Phys. Fluids*, **11**, 1593.

PRAGER, W. 1961 *Introduction to Mechanics of Continua*. Ginn.

RAYLEIGH, C. B. & KIRBY, S. H. 1970 Creep in the Upper Mantle. *Am. Mineral., Spec. Pap.* **3**, 113.

READ, W. T. 1953 *Dislocations in Crystals*. McGraw-Hill.

RINGWOOD, A. E. 1972*a* Mineralogy of the deep mantle: current status and future developments. In *The Nature of the Solid Earth* (ed. E. C. Robertson), p. 67. McGraw-Hill.

RINGWOOD, A. E. 1972*b* Phase transformations and mantle dynamics. *Earth. Planet. Sci. Lett.* **14**, 233.

RINGWOOD, A. E. & MAJOR, A. 1970 The system Mg_2SiO_4–Fe_2SiO_4 at high pressures and temperatures. *Phys. Earth. Planet. Interiors*, **3**, 89–108.

ROBERTS, K. V. & WEISS, N. O. 1966 Convective difference schemes. *Math. Comp.* **20**, 272.

ROBERTS, P. H. 1967 Convection in horizontal layers with internal heat generation. Theory. *J. Fluid Mech.* **30**, 33.

ROSSBY, H. T. 1969 A study of Bénard convection with and without rotation. *J. Fluid Mech.* **36**, 309–335.

RUNCORN, S. K. 1965 Changes in the convection pattern in the Earth's mantle and continental drift: evidence for a cold origin of the Earth. *Phil Trans. Roy. Soc.* A **258**, 228.

SCHILLING, J. G. 1971 Sea-floor evolution: rare-earth evidence. *Phil. Trans. Roy. Soc.* A **268**, 661–706.

SCHLÜTER, A., LORTZ, D. & BUSSE, F. 1965 On the stability of steady finite amplitude convection *J. Fluid Mech.* **23**, 129.

SCHUBERT, G. & TURCOTTE, D. L. 1971 Phase changes and Mantle convection. *J. Geophys. Res.* **76**, 1424.

SCHWIDERSKI, E. W. & SCHWAB, H. J. A. 1971 Convection experiments with electrolytically heated fluid layers. *J. Fluid Mech.* **48**, 703.

SCLATER, J. G., ANDERSON, R. N. & BELL, M. L. 1971 The elevation of ridges and the evolution of the central eastern Pacific. *J. Geophys. Res.* **76**, 7888–7915.

SCLATER, J. G. & FRANCHETEAU, J. 1970 The implications of terrestrial heat flow observations on current tectonic and geochemical models of the crust and upper Mantle of the Earth. *Geophys. J. Roy. Astr. Soc.* **20**, 509.

SHERBY, O. D. & BURKE, P. M. 1968 Mechanical behaviour of crystalline solids at elevated temperatures. In *Progress in Materials Science* (ed. B. Chalmers & W. Hume-Rothery), p. 325. Pergamon.

SKINNER, B. J. 1966 Thermal expansion. In *Handbook of Physical Constants* (ed. S. P. Clark), p. 75. Geol. Soc. Am. Memoir no. 97.

SLATER, J. C. 1939 *Introduction to Chemical Physics*. McGraw-Hill.

SOMERVILLE, R. C. J. 1967 A nonlinear spectral model of convection in a fluid unevenly heated from below. *J. Atmos. Sci.* **24**, 665–676.

SPARROW, E. M., GOLDSTEIN, R. J. & JONSSON, V. K. 1964 Thermal instability in a horizontal fluid layer: effect of boundary conditions and nonlinear temperature profile. *J. Fluid Mech.* **18**, 513.

SPIEGEL, E. A. 1971 Convection in Stars. I. Basic Boussinesq convection. *Ann. Rev. Astron. Astrophys.* **9**, 323.

STRAUS, J. M. 1972 Finite amplitude doubly diffusive convection. *J. Fluid Mech.* **56**, 353.

SYKES, L. R. 1966 The seismicity and deep structure of island arcs. *J. Geophys. Res.* **71**, 2981–3006.

TALWANI, M. & LE PICHON, X. 1969 Gravity field over the Atlantic Ocean. In *The Earth's Crust and Upper Mantle* (ed. P. J. Hart), p. 341. Am. Geophys. Un. Monograph 13.

TALWANI, M., WINDISCH, C. C. & LANGSETH, M. G. 1971 Rekyjanes Ridge crest: a detailed geophysical study. *J. Geophys. Res.* **76**, 473–517.

THIRLBY, R. 1970 Convection in an internally heated layer. *J. Fluid Mech.* **44**, 673.

TOKSÖZ, M. N., MINEAR, J. W. & JULIAN, B. R. 1971 Temperature field and geophysical effects of a downgoing slab. *J. Geophys. Res.* **76**, 1113–1138.

TORRANCE, K. E. & TURCOTTE, D. L. 1971 Thermal convection with large viscosity variations. *J. Fluid Mech.* **47**, 113.

TOZER, D. C. 1965 Heat transfer and convection currents. *Phil. Trans. Roy. Soc.* A **258**, 252–271.

TRITTON, D. J. & ZARRAGA, M. N. 1967 Convection in horizontal layers with internal heat generation. Experiments. *J. Fluid Mech.* **30**, 21.

TURCOTTE, D. L. & OXBURGH, E. R. 1967 Finite amplitude convection cells and continental drift. *J. Fluid Mech.* **28**, 29–42.

TURCOTTE, D. L. & OXBURGH, E. R. 1969 Convection in a mantle with variable physical properties. *J. Geophys. Res.* **74**, 1458.

TURCOTTE, D. L. & OXBURGH, E. R. 1972 Mantle convection and the new global tectonics. *Ann. Rev. Fluid Mech.* **4**, 33.

TURNER, J. S. 1973 Convection in the mantle: a laboratory model with temperature-dependent viscosity. *Earth Planet. Sci. Lett.* **17**, 369.

VENING MEINESZ, F. A. 1962 Thermal convection in the Earth's Mantle. In *Continental Drift*, (ed. S. K. Runcorn), pp. 145–176. Academic.

VERHOOGEN, J. 1965 Phase changes and convection in the Earth's Mantle. *Phil. Trans. Roy. Soc.* A **258**, 276–283.

VERONIS, G. 1966 Large amplitude Bénard convection. *J. Fluid Mech.* **26**, 49.

VON HERZEN, R. P. & LEE, W. H. K. 1969 Heat flow in oceanic regions. In *The Earth's Crust and Upper Mantle* (ed. P. J. Hart), p. 88. Am. Geophys. Un. Monograph 13.

WEERTMAN, J. 1970 Creep strength in the Earth's Mantle. *Rev. Geophys.* **8**, 145–168.

WETHERILL, G. W. 1966 Radioactive decay constants and energies. In *Handbook of Physical Constants* (ed. S. P. Clark), p. 513. Geol. Soc. Am. Memoir no. 97.

WHITEHEAD, J. A. 1972 Moving heaters as a model of continental drift. *Phys. Earth Planet. Interiors*, **5**, 199–212.

WILLIS, G. E. & DEARDORFF, J. W. 1970 The oscillatory motions of Rayleigh convection. *J. Fluid Mech.* **44**, 661.

WILLIS, G. E., DEARDORFF, J. W. & SOMERVILLE, R. C. J. 1972 Roll-diameter dependence in Rayleigh convection and its effect upon heat flux. *J. Fluid Mech.* **54**, 351.

WILSON, J. T. 1963 A possible origin of the Hawaiian Islands. *Can. J. Phys.* **41**, 863.

WILSON, J. T. 1965 A new class of faults and their bearing on continental drift. *Nature*, **207**, 343–347.

WOOLLARD, G. P. 1969 Regional variations in gravity. In *The Earth's Crust and Upper Mantle* (ed. P. J. Hart), p. 320. Geophys. Un. Monograph no. 13.

ZHIVAGO, A. V. 1966 Bathymetric chart (Indian sector of the southern ocean). *Atlas of the Antarctic*, p. 190. Moscow: Akad. Nauk.